UNIVERSIDAD DE VIGO
DEPARTAMENTO DE FÍSICA APLICADA

CARACTERIZACIÓN OCEANOGRÁFICA DE LA COSTA NORTE GALLEGA

José Luís Gómez Gesteira
Febrero, 2010

Dra. María Teresa de Castro Rodríguez y **Dra. Maria Inés Álvarez Fernández** profesoras del Departamento de Física Aplicada de la Universidad de Vigo,

CERTIFICAN:

Que la presente memoria titulada *"Caracterización oceanográfica de la costa norte gallega"*, ha sido realizada bajo su dirección por José Luis Gómez Gesteira en el Departamento de Física Aplicada de la Universidad de Vigo para optar al grado de Doctor en Física.

Y para que así conste, firma la presente en Ourense a 18 de noviembre de 2009.

Dra. María Teresa de Castro Rodríguez

Dra. Maria Inés Álvarez Fernández

Resumen

La costa norte de Galicia ha atraído muchos menos estudios que la adyacente costa oeste. Posiblemente a esto contribuya la falta de grandes concentraciones de población, la existencia de una menor presión turística y la menor extensión de los estuarios. El presente estudio pretende, dentro de lo posible, paliar esa carencia de datos oceanográficos.

En el estudio se abordarán varios contenidos:

1) La evolución de la temperatura superficial del mar (SST). Para ello se considerarán diferente escalas espaciales (costa y océano) y temporales (diarias, semanales y mensuales). En particular, se considerarán dos estudios diferentes pero complementarios:
   a) Estudio de la evolución de la SST costera desde 1985. Se ha elegido esta fecha debido a que sólo existen datos con la suficiente resolución espacial a partir de las medidas de satélite. El estudio no se circunscribirá a la costa norte gallega, sino que se comparará con la evolución de la SST costera a lo largo del Arco Atlántico.
   b) Estudio histórico de la evolución de la SST oceánica desde mediados del siglo XIX para poner en contexto el cambio climático observado en la actualidad. Esta evolución se pondrá en el contexto de los cambios observados en el Golfo de Vizcaya.

2) Caracterización del afloramiento. Este fenómeno no había sido caracterizado en las rías del norte en el pasado, por lo que se hará especial hincapié en su comparación con el mismo fenómeno observado en la costa oeste gallega. Se caracterizarán dos tipos de afloramiento, dependiendo de la estación del año:
   a) Afloramiento de invierno. Este tipo de afloramiento nunca había sido observado anteriormente en la costa norte gallega y raramente en la costa oeste, por lo que se prestará especial atención en analizar el tipo de agua aflorada, así como sus características biogeoquímicas. También se analizará la periodicidad, persistencia temporal e intensidad de estos eventos.
   b) Afloramiento de verano. Además del análisis de periodicidad, persistencia temporal, variación a lo largo del tiempo e intensidad, se prestará especial atención al desfase temporal entre las condiciones de forzamiento (vientos de componente este) y la reacción del estuario caracterizada por una bajada intensa de temperatura.

Índice de Contenidos

Chapter 1

Introducción

1.1. Circulación oceánica

Una característica importante de la circulación en la superficie de los océanos es que en el hemisferio norte tiene sentido horario y en el hemisferio sur tiene sentido antihorario.

Tanto la conducción por el viento, como los efectos de cambios en la densidad son importantes para explicar la circulación general en los océanos, pero el primero probablemente domina en más o menos los primeros 1000 m de profundidad en la mayoría de las regiones del océano.

En 1898 Nansen, un biólogo, explicó cualitativamente porque las corrientes conducidas por el viento no fluyen en la dirección del viento, sino entre 20º y 40º a su derecha (en el hemisferio norte), cosa que observó al ver como los icebergs del Ártico en lugar de desplazarse en la dirección del viento, como sería de esperar, lo hacían unos grados hacia su derecha.

Para explicar esto, en la Figura 1.1 se representa un cubo de agua en la capa superficial del océano, el cual se ve sometido a una fuerza de fricción debida al viento. La fricción del viento ejercerá sobre la superficie del cubo una fuerza tangencial, $F_{t,}$ haciendo que éste tienda a moverse en su dirección.

Tan pronto como el cubo comience a moverse, la fuerza de Coriolis, F_c, entra en acción desplazando el cubo hacia la derecha.

De este modo el movimiento resultante será en alguna dirección entre la de F_t y F_c. Además, como el agua de superficie se mueve con relación al agua

que tiene bajo ella, habrá una fuerza de resistencia debida a la fricción, $F_{b,}$ en la base del cubo en dirección contraria al movimiento del mismo. Así, la combinación de F_t y F_c hace que el cubo se acelere y mientras lo hace, la fuerza F_b aumenta. Finalmente se alcanza un estado de equilibrio en el cual F_t, F_c y F_b están compensadas y el cubo continúa moviéndose a una velocidad constante, V_0, en una dirección entre la de F_t y la de F_c, es decir, a la derecha de la dirección del viento (en el hemisferio norte). Para determinar la dirección exacta con relación a la del viento habrá que aplicar argumentos cuantitativos usando las ecuaciones del movimiento como hizo Ekman.

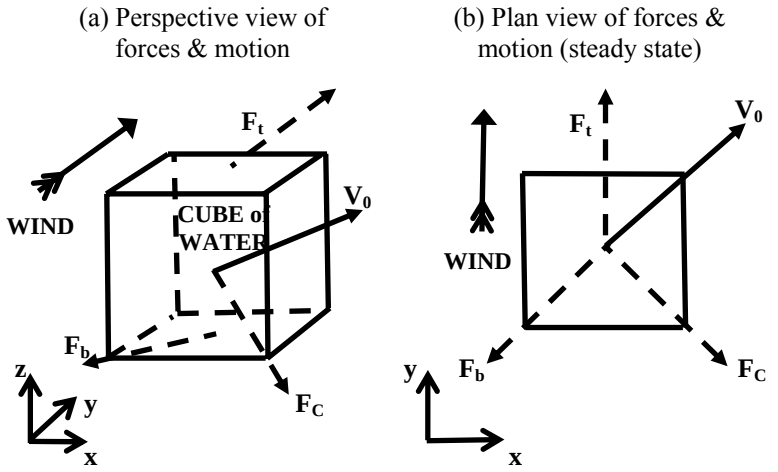

Figura 1.1. Fuerzas en un cubo de agua en la capa superficial. (Imagen reproducida de *Pond & Pickard*, *Introductory Dynamical Oceanography*).

1.1.1. Corrientes superficiales

Las ecuaciones del movimiento horizontal, incluyendo el rozamiento y omitiendo el término de Coriolis que implica a *w* (velocidad vertical) son (Pond & Pickard, 1983),

$$\frac{du}{dt} = fv - \alpha \frac{\partial p}{\partial x} + F_x$$
$$\frac{dv}{dt} = -fu - \alpha \frac{\partial p}{\partial y} + F_y \qquad (1.1)$$

Donde f es el parámetro de Coriolis, α es la inversa de la densidad, F_x y F_y son las componentes de la fuerza de rozamiento por unidad de masa.

Como no hay aceleraciones, tanto $\frac{du}{dt}$ como $\frac{dv}{dt}$ serán iguales a cero. Por lo tanto las ecuaciones 1.1 quedan

$$fv - \alpha \frac{\partial p}{\partial x} + F_x = 0$$
$$-fu - \alpha \frac{\partial p}{\partial y} + F_y = 0 \qquad (1.2)$$

Es decir,

Coriolis + Presión + Rozamiento = 0

De este modo el diagrama de fuerzas será el siguiente

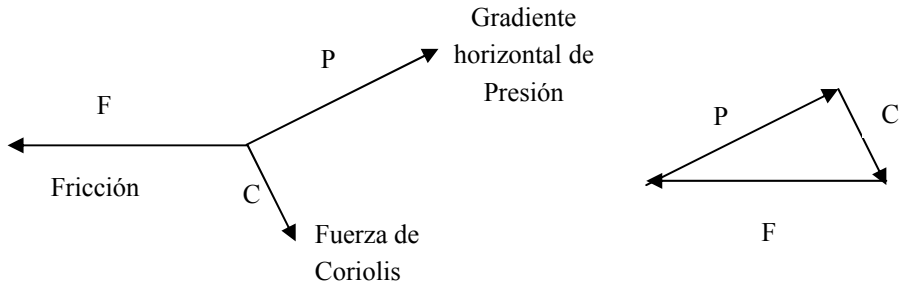

Antes de poder encontrar una solución a estas ecuaciones se debe encontrar una expresión para F_x y F_y.

La fricción o rozamiento es una fuerza que aparece cuando se tiene movimiento relativo entre dos cuerpos y aunque la más conocida es aquella que sucede cuando los dos cuerpos son sólidos, cuando en un fluido dos partes están en movimiento relativo también se produce fricción. A la velocidad relativa entre las partes del fluido se le denomina velocidad de cizalla y la fricción se debe a ella. A medida que se profundiza en el océano la velocidad de cizalla se va haciendo cero. Para un fluido Newtoniano como es el agua del mar, la tensión de fricción τ, que es la fuerza por unidad de área en un plano paralelo al flujo, es

$$\tau = \mu \frac{\partial u}{\partial z} = \rho \nu \frac{\partial u}{\partial z} \tag{1.3}$$

Donde μ es la denominada viscosidad dinámica (molecular), y $\nu = \mu / \rho$ es la viscosidad cinemática (molecular). Para agua de mar a 20º C, μ tiene un valor de aproximadamente 10^{-3} kg m^{-1} s^{-1}, por lo que ν vale aproximadamente 10^{-6} m^2 s^{-1}. Los valores reales de las viscosidades en los océanos oscilan entre 0.8 y 1.8 veces estos valores, siendo la temperatura la principal responsable de ello, aunque también hay una leve influencia de la salinidad.

En el océano, donde el movimiento es generalmente turbulento, la viscosidad cinemática es la viscosidad *eddy* por lo que la expresión de τ queda (Pond & Pickard, 1983)

$$\tau = \rho A_z \frac{\partial u}{\partial z} \tag{1.4}$$

Siendo A_z la cizalla vertical que para el agua del mar toma valores hasta 10^{-1} m^2 s^{-1}.

Esta expresión representa la fuerza que ejerce una capa de fluido sobre un área de su capa vecina situada por encima o por debajo, pero para la ecuación del movimiento se necesita una expresión de la fuerza de fricción en términos de masa de fluido. Así pues la expresión que se obtiene es (Pond & Pickard, 1983)

$$\text{Fuerza de fricción por unidad de masa} = A_z \frac{\partial^2 u}{\partial^2 z} \tag{1.5}$$

De este modo las ecuaciones del movimiento quedarán de la siguiente manera

$$\begin{aligned} fv + \alpha \frac{\partial \tau_x}{\partial z} &= fv + A_z \frac{\partial^2 u}{\partial z^2} = \alpha \frac{\partial p}{\partial x} \\ -fu + \alpha \frac{\partial \tau_y}{\partial z} &= -fu + A_z \frac{\partial^2 v}{\partial z^2} = \alpha \frac{\partial p}{\partial y} \end{aligned} \tag{1.6}$$

1.1.2. La solución de Ekman a las ecuaciones del movimiento

La dificultad con la que se encontró Ekman a la hora de tratar con las ecuaciones del movimiento (1.6) fue que hay dos causas diferentes que generan las corrientes, la distribución de la masa (cambios en la densidad), que viene representada por el término del gradiente horizontal de presión, y la fricción del viento. Así pues se puede pensar en la velocidad como la suma de dos vectores, uno asociado con el gradiente horizontal de presión y otro con la fricción vertical. Cada parte se puede solucionar por separado y posteriormente sumar las dos soluciones de manera que se obtendrá,

$$fv = f\left(v_g + v_E\right) = \alpha \frac{\partial p}{\partial x} - A_z \frac{\partial^2}{\partial z^2}\left(u_g + u_E\right) \tag{1.7}$$

Las dos partes en las que se divide la ecuación son

$fv_g = \alpha \dfrac{\partial p}{\partial x}, \qquad u_g, v_g$ las componentes de la velocidad geostrófica,

$fv_E = -A_z \dfrac{\partial^2 u_E}{\partial z^2}, \quad u_E, v_E$ las componentes de la velocidad de Ekman asociadas con la fricción vertical (no geostrófica).

El término $-A_z \dfrac{\partial^2 u_g}{\partial z^2}$ se puede despreciar ya que es $\leq 10^{-3} \alpha \dfrac{\partial p}{\partial x}$ (Pond & Pickard, 1983).

Esta separación es posible debido a que las ecuaciones son lineales. Esto proporciona un ejemplo del principio de superposición; para un sistema lineal la suma de dos soluciones es también una solución.

Para simplificar el problema, Ekman (1905) asumió que el término del gradiente horizontal de presión apenas contribuía en la capa superficial, por lo que sólo busco solución para v_E y u_E. Además también asumió que

1. No hay fronteras
2. Profundidad del mar infinita
3. A_z constante
4. Un viento constante y que sopla durante un largo periodo de tiempo
5. Densidad del agua y nivel del mar constante
6. f constante

De este modo las ecuaciones del movimiento quedan

$$\left.\begin{aligned} fv_E + A_z \frac{\partial^2 u_E}{\partial z^2} &= 0, \\ -fu_E + A_z \frac{\partial^2 v_E}{\partial z^2} &= 0, \end{aligned}\right\} \text{Ecuaciones de Ekman} \qquad (1.8)$$

Así la fuerza de Coriolis y la de fricción se anulan ente ellas y la corriente de superficie tendrá una dirección perpendicular a ambas.

Si por simplicidad se escoge que el viento sople en la dirección del eje *y*, la solución a las ecuaciones de Ekman será

$$u_E = \pm V_0 \cos\left(\frac{\pi}{4} + \frac{\pi}{D_E} z\right) \exp\left(\frac{\pi}{D_E} z\right), \qquad \text{(+ para el hemisferio norte y – para el sur)}$$

$$v_E = V_0 \sin\left(\frac{\pi}{4} + \frac{\pi}{D_E} z\right) \exp\left(\frac{\pi}{D_E} z\right), \qquad (1.9)$$

Donde

$V_0 = \dfrac{\sqrt{2}\pi\tau_{y\eta}}{D_E \rho |f|}$ es el módulo de la corriente superficial de Ekman

$\tau_{y\eta}$ = es la tensión que provoca el viento en la superficie del mar

$\mathrm{D_E} = \pi\left(\dfrac{2A_z}{|f|}\right)^{1/2}$ es la llamada profundidad de Ekman o profundidad de influencia de la fricción

Estudiando estas soluciones para u_E y v_E se llega a que

1. En la superficie del mar ($z = 0$) las soluciones son

$$u_E = \pm V_0 \cos\left(\frac{\pi}{4}\right), \quad v_E = \pm V_0 \sin\left(\frac{\pi}{4}\right)$$

Lo cual significa que la corriente fluye 45º a la derecha de la dirección del viento si se trata del hemisferio norte y a la izquierda si se trata del hemisferio sur.

2. Bajo la superficie *z* ya no es cero, por lo tanto la velocidad total de la corriente será $V_0 \exp\left(\dfrac{\pi}{D_E} z\right)$, de manera que a medida que aumenta la

profundidad, la corriente cae exponencialmente. Al mismo tiempo, el ángulo que forma la corriente con la dirección del viento, $\left(\frac{\pi}{4}+\frac{\pi}{D_E}z\right)$, aumenta de manera que su dirección girará en sentido horario (antihorario) en el hemisferio norte (sur). La Figura 1.2 muestra estos dos cambios con la profundidad.

3. La dirección del flujo toma sentido contrario al que tenía en superficie al alcanzar la profundidad de $z = -D_E$, donde la velocidad cae a $\exp(-\pi) = 0.04$ veces la de la superficie. La profundidad D_E se toma arbitrariamente como la profundidad efectiva de la corriente producida por el arrastre del viento, es decir, la profundidad hasta la cual se considera que hay corriente inducida por el viento. La capa de Ekman se considera desde la superficie hasta esta profundidad D_E.

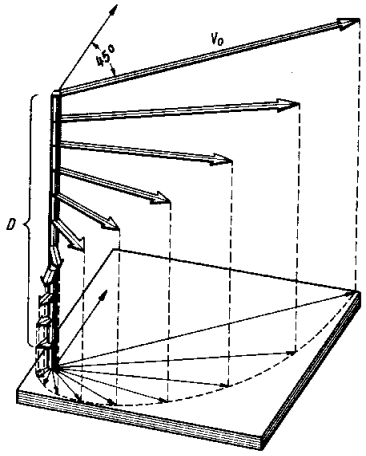

Figura 1.2. Vista en perspectiva de la disminución de la velocidad de la corriente y giro en sentido horario con el aumento de la profundidad.

1.1.3. Transporte por viento

1.1.3.1. Conceptos generales

La corriente producida por el viento tiene su máxima velocidad en la superficie y disminuye a medida que aumenta la profundidad. Debido a que las mayores corrientes ocurren hacia la derecha (izquierda en el hemisferio sur) de la dirección del viento, el mayor transporte también será hacia la derecha (izquierda) de la dirección del viento. De hecho, se demostrará que este transporte se produce 90º a la derecha (izquierda) de la dirección del viento (Pond & Pickard, 1983).

Partiendo de las ecuaciones (1.6), si se asume una ausencia de gradiente horizontal de presión se tiene

$$\rho f v_E + \frac{\partial \tau_x}{\partial z} = 0$$
$$-\rho f u_E + \frac{\partial \tau_y}{\partial z} = 0$$

que se puede expresar de otro modo como

$$\begin{aligned} \rho f v_E dz &= -d\tau_x \\ \rho f u_E dz &= d\tau_y \end{aligned} \qquad (1.10)$$

donde $\rho v_E dz$ es la masa de agua que fluye por segundo en la dirección del eje *y* a través de una sección vertical de profundidad *dz* y anchura de un metro en la dirección *x*, y $\int_z^0 \rho v_E dz$ será la masa total que fluye en la dirección *y* desde la profundidad *z* hasta la superficie. Del mismo modo, $\int_z^0 \rho u_E dz$ será la masa total transportada por unidad de anchura en la dirección *x*. Si se escoge el nivel inferior lo suficientemente profundo, las integrales incluirán toda la corriente producida por el arrastre del viento. Escogiendo el valor $z = -2D_E$

donde la velocidad esperada será exp(-2π) = 0.002 veces la de la superficie, es decir, prácticamente nula, y llamando M_{xE} y M_{yE} a los transportes de masa debidos al viento (transporte de masa de Ekman) en las direcciones x e y respectivamente, se puede escribir

$$\begin{aligned} fM_{yE} &= f\int_{-2D_E}^{0}\rho v_E dz = \int_{-2D_E}^{0} d\tau_x = -(\tau_x)_{\text{sup}} + (\tau_x)_{-2D_E} \\ fM_{xE} &= f\int_{-2D_E}^{0}\rho u_E dz = \int_{-2D_E}^{0} d\tau_y = (\tau_y)_{\text{sup}} - (\tau_y)_{-2D_E} \end{aligned} \tag{1.11}$$

Los valores de τ_x y τ_y a una profundidad de $2D_E$ se pueden considerar nulos ya que la velocidad debida al arrastre del viento es esencialmente cero. Por lo tanto, las ecuaciones (1.11) se pueden expresar

$$fM_{xE} = \tau_{y\eta} \qquad fM_{yE} = -\tau_{x\eta} \tag{1.12}$$

donde el subíndice η indica que son valores en la superficie.

Las variaciones de la densidad son pequeñas, por lo que ρ se puede sacar de la integral en las ecuaciones (1.11). El valor que se tomará para la densidad será uno típico, como por ejemplo una media vertical sobre $2D_E$ en la región considerada.

El volumen de agua transportado $Q_y = \int_{z}^{0} v_E dz$ se puede usar como una alternativa a la masa transportada de manera que $M_{yE} = \rho Q_{yE}$ y $M_{xE} = \rho Q_{xE}$. Por lo tanto las ecuaciones (1.12) se pueden escribir

$$fQ_{xE} = \alpha\tau_{y\eta} \qquad fQ_{yE} = -\alpha\tau_{x\eta} \tag{1.13}$$

Por simplicidad se considera el eje y como la dirección en la que sopla el viento, por lo que $\tau_{x\eta}$ será nulo (no habrá cizalla en dirección x) y por consiguiente M_{yE} también lo será. Sin embargo, M_{xE} será positivo debido a que $\tau_{y\eta}$ también lo es, con lo cual se demuestra que el transporte se produce

en ángulos de 90º a la derecha (izquierda) de la dirección del viento cuando se trata del hemisferio norte (sur).

1.1.3.2. Afloramiento lejos de la costa

Sobre el océano el viento no es uniforme como asumió Ekman, sino que varía según la posición. Por ejemplo si el viento permanece constante en dirección pero varía en velocidad, entonces el transporte de Ekman perpendicular al viento también variará y las aguas de las capas superiores se desplazarán unas hacia otras o se alejarán creándose así convergencias y divergencias. Por continuidad se requiere que una convergencia esté acompañada de un movimiento de las aguas superficiales hacia el fondo (hundimiento o *downwelling*) mientras que una divergencia vendrá acompañada de un movimiento de las aguas del fondo hacia la superficie (afloramiento o *upwelling*).

En el Atlántico norte, la dirección del viento suele ser hacia el este en latitudes altas y hacia el oeste en latitudes bajas. En el siguiente diagrama (Figura 1.3) se muestra el viento en el Atlántico norte de una forma simplificada.

Se puede observar que el transporte de Ekman debido al viento será hacia el sur para vientos del oeste (latitudes altas) y hacia el norte para vientos del este (latitudes bajas), además, cuanto mayor sea la velocidad del viento mayor será el transporte. Según este diagrama, el transporte de Ekman hacia el sur aumenta desde el punto A al punto B. Para reemplazar el agua transportada debido a este incremento en el transporte, es necesario que el agua aflore desde debajo de la capa de Ekman, por lo que habrá una zona de divergencia ente A y B.

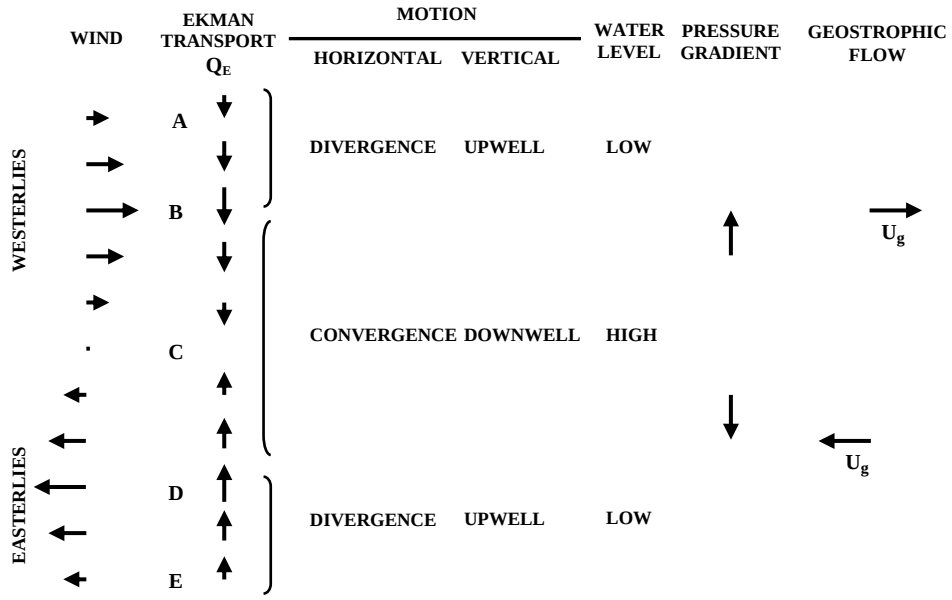

Figura 1.3. Convergencias y divergencias relacionadas con la cizalla del viento y el flujo geostrófico asociado, en el Atlántico norte. La longitud de las flechas del viento indica la velocidad. (Imagen reproducida de *Pond & Pickard*, *Introductory Dynamical Oceanography*).

Desde B hasta C sucede lo contrario con una disminución en el transporte hacia el sur hasta que se hace nulo, y de C a D el transporte empieza a crecer pero, en este caso, en dirección norte ya que es una zona de influencia de vientos del este. Como consecuencia la región alrededor de C será una zona de convergencia y se producirá entonces un hundimiento del agua de la superficie. Entre D y E habrá de nuevo una región de divergencia y por lo tanto afloramiento. En una región de convergencia el nivel de la superficie tiende a ser alto mientras que en una región de divergencia tiende a ser bajo.

Por lo tanto, se tendrá un gradiente de presión y flujos geostróficos (u_g) que también aparecen representados en la Figura 1.3.

1.1.3.3. Afloramiento cerca de la costa

El transporte de Ekman analizado en las secciones anteriores se complica si se asume que el viento sopla paralelo a una línea de costa de manera que ésta queda a su izquierda (en el hemisferio norte). Este viento causará un transporte hacia la derecha de su dirección, es decir, un movimiento del agua hacia fuera de la costa. Para un océano infinito como el que supuso Ekman, esto no supone un problema pero en un océano real sí. Esto se debe a que la ecuación de continuidad requiere que haya un flujo proveniente de la izquierda de la dirección del viento para reemplazar el flujo que sale hacia la derecha. Como a la izquierda de la dirección del viento no hay agua, lo que sucede es que agua proveniente del fondo asciende para reemplazar el agua transportada. Este fenómeno es conocido como afloramiento costero y sucede en varias regiones de las zonas orientales de los océanos. En las costas este del hemisferio norte para que esto suceda el viento debe soplar hacia el sur, lo cual ocurre normalmente en verano. Para generalizar, se puede decir que los fenómenos de afloramiento ocurren a lo largo de las costas orientales de los océanos, cuando el viento sopla hacia el ecuador y a lo largo de las costas occidentales cuando sopla en dirección al polo, aunque está última situación es menos común.

En la Figura 1.4 se muestra un esquema de desarrollo del afloramiento costero. En general, el agua aflorada no proviene de grandes profundidades. Estudiando las propiedades de esta agua se ha llegado a la conclusión que proviene de profundidades no mayores que 200-300 m (Pond & Pickard, 1983).

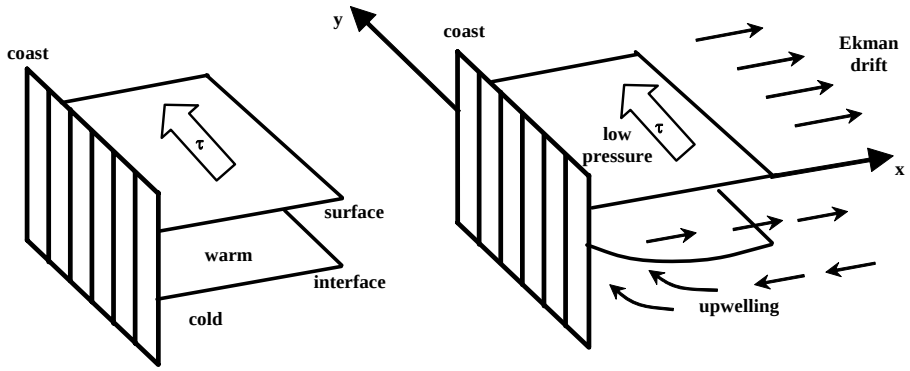

Figura 1.4. Esquema del desarrollo del afloramiento costero. (Imagen reproducida de *Cushing & Walsh, The ecology of the seas).*

Los procesos de afloramiento en zonas próximas a la costa pueden tener una implicación biológica muy importante, ya que normalmente el agua aflorada tiene mayor concentración de nutrientes (nitratos, silicatos, etc.) que el agua superficial original que ha sido desplazada, los cuales son indispensables para la producción biológica. Al aflorar a la superficie esta agua cargada de nutrientes, el fitoplancton se sirve de ellos junto con la acción de la luz solar para realizar la fotosíntesis. De este modo, el fitoplancton en estas zonas será abundante y rico atrayendo así a una gran cantidad de peces que se alimentan de él.

Debido a la importancia que tienen los fenómenos de afloramiento, éstos han sido ampliamente estudiados a lo largo de todo el planeta. Los cinco mayores afloramientos que se producen en las costas del planeta son, el que tiene lugar en las costas occidentales de EEUU (Di Lorenzo, 2003; Hickey & Banas, 2003); el de la costa sudoccidental de África (Monteiro & Largier, 1999; Shannon et al., 2003); el de la costa noroeste africana (Pelegrí et al., 2005); el que ocurre frente al cuerno de África en el Océano Indico (Conan

& Brumer, 2000) y el que se produce a lo largo de las costas Peruanas y Chilenas (Nixon & Thomas, 2001; Rutllant et al., 2004). También hay estudios realizados en otras zonas donde se dan fenómenos de afloramiento no tan relevantes como los cinco mencionados anteriormente como los que ocurren en la costa de Irlanda (Edwards et al., 1994); en la costa australiana (Roughan & Middleton, 2002); en la costa canadiense (Ianson et al., 2003); etc.

1.2. Temperatura Superficial del Océano (SST)

La temperatura superficial del océano (SST) tiene una gran influencia en el clima. Por ejemplo, cada 3-7 años una franja del Océano Pacífico situada a lo largo del ecuador se calienta entre 2-3ºC. Este calentamiento es un distintivo del patrón climático de El Niño, el cual modifica los patrones de lluvia alrededor de la tierra, causando fuertes lluvias en el sur de Estados Unidos e importantes sequías en Australia, Indonesia y el sur de Asia. En una escala menor, la temperatura del océano influye en el desarrollo de ciclones tropicales que obtienen energía de las aguas calientes del océano para formarse e intensificarse.

Desde los años 80 los satélites se han convertido en la herramienta más útil para medir la temperatura superficial del océano proporcionando una gran ventaja para ver la variación espacial y temporal de la SST. Las medidas de satélite de SST son mucho más constantes y, en algunos casos, más precisas que las medidas in situ obtenidas de boyas o barcos.

La SST medida por satélite proporciona un rango de visión sinóptico del océano y una alta frecuencia de repetición de las medidas, permitiendo un análisis de la dinámica superficial del océano que no es posible utilizando solamente datos de boyas o barcos. Por ejemplo, un barco navegando a 10

nudos (20 km/h) necesitaría 10 años para cubrir la misma área que un satélite cubre en 2 minutos.

Debido a la alta resolución temporal y espacial, las observaciones de SST mediante satélite son una buena herramienta para analizar diversos fenómenos oceánicos como la variabilidad del afloramiento. La disminución de la SST en un evento de afloramiento costero puede ser de hasta 6-8ºC, haciendo que los datos medidos por satélites sean particularmente útiles en el estudio de la distribución del afloramiento costero a larga escala. Así, las imágenes de SST obtenidas de los satélites se han utilizado en numerosos estudios para analizar los procesos sinópticos del afloramiento a lo largo del planeta (Nykjaer & Van Camp, 1994 en el sistema de afloramiento de las Canarias; Tang et al., 2004 en el estrecho de Taiwán; Zavala-Hidalgo et al., 2006 en el Golfo de Mejico).

Además de estudiar fenómenos oceánicos como el afloramiento, los análisis de la variación de SST también permiten determinar los cambios en el clima relacionados con el calentamiento oceánico. Por este motivo, durante las últimas décadas se ha hecho un importante esfuerzo para desarrollar series de SST con cobertura global de manera que además de los datos de satélite, se han considerado datos obtenidos por barcos de observación, pesqueros y boyas. Esto ha permitido reconstruir series de SST durante períodos muy largos que, aunque tienen una baja resolución espacial, proporcionan la posibilidad de analizar la tendencia temporal de la SST. Un ejemplo es la base de datos reconstruida ERSST de la NOAA/OAR/ESRL PSD (http://www.cdc.noaa.gov/) que dispone de datos desde 1854 con una periodicidad mensual en una malla de 2º x 2º.

En general, la tendencia de la SST depende en gran medida de las escalas temporal y espacial de manera que se pueden observar tendencias opuestas

cuando se consideran diferentes periodos de tiempo (Parker et al., 1994; Casey and Cornillom, 2001). A pesar de este hecho, la mayor parte de los estudios llevados a cabo durante las últimas décadas concluyen que durante el siglo pasado se ha producido un considerable calentamiento global de la SST independientemente de la base de datos utilizada que no muestra una tendencia uniforme temporalmente ni espacialmente (Folland et al., 1984; Parker et al., 1994; Casey and Cornillom, 2001). De acuerdo con el Intergovernmental Panel on Climate Change (IPCC, 2007) las series globales de SST muestran dos periodos de calentamiento distinto durante los últimos 100 años. El primero ocurrió durante el periodo 1910-1945 seguido de un periodo de enfriamiento y el segundo comenzó en los años 70.

Este calentamiento es también importante desde un punto de vista biológico ya que los ecosistemas costeros son vulnerables a los cambios climáticos. Un aumento general de la temperatura del agua puede producir un adelantamiento en el desove afectando a la producción y supervivencia de peces (atún, bacalao, etc.) y moluscos (Young et al., 1996; Honkoop et al., 1998).

1.3. Litoral gallego

Galicia cuenta con una línea costera muy amplia (más de 1600 km), bañada por el mar Cantábrico y el océano Atlántico. De acuerdo con Gomez-Gesteira et al (2006) y Alvarez et al. (2008), macroscópicamente, la costa gallega se puede dividir en 3 regiones (Figura 1.7), la costa oeste que se extiende desde el norte de Portugal hasta Cabo Finisterre, con un ángulo de aproximadamente 90º relativo al ecuador; la costa intermedia desde Cabo Finisterre a Estaca de Bares, con un ángulo aproximado de 55º; y la costa norte, aproximadamente paralela al ecuador.

Los campos de viento sobre esta región distan mucho de ser homogéneos, debido a la particular geometría costera (Torres et al., 2003; Herrera et al., 2005). El viento tanto en verano como en invierno presenta un pequeño número de patrones dominantes, los cuales no son necesariamente representativos ya que los patrones típicos de verano pueden dominar en invierno y viceversa dependiendo de la región costera, que se divide en tres partes bien diferenciadas. De este modo, las observaciones de viento en un sólo punto de la costa o mar adentro no son representativas de las condiciones de viento dominantes a lo largo de toda la línea de costa, sin embargo, las condiciones de viento dentro de cada región sí mantiene un comportamiento regular (Alvarez et al., 2005; Gomez-Gesteira et al., 2006; Alvarez et al., 2008).

El elemento más característico de la costa de Galicia son las rías. Se trata de profundas penetraciones del mar en la tierra sobre las que desembocan los numerosos ríos de la región.

A lo largo de la costa gallega se distinguen las Rías Baixas y las Rías Altas, separadas por el Cabo Finisterre. En la Ría de Ribadeo, que marca el límite con el Principado de Asturias y en la que desemboca el río Eo, se inician las Rías Altas, en general menos profundas y con un perfil menos recortado que las Rías Baixas, que se extienden desde la Ría de Muros hasta el estuario del Miño.

La costa en la zona de las Rías Altas se caracteriza por una fuerte pendiente hacia el mar, es dura, de abruptos e inaccesibles acantilados y peligrosas rompientes. En las Rías Baixas, al contrario que en las Rías Altas, la costa es baja por la existencia de una plataforma litoral que desciende suavemente hasta el mar.

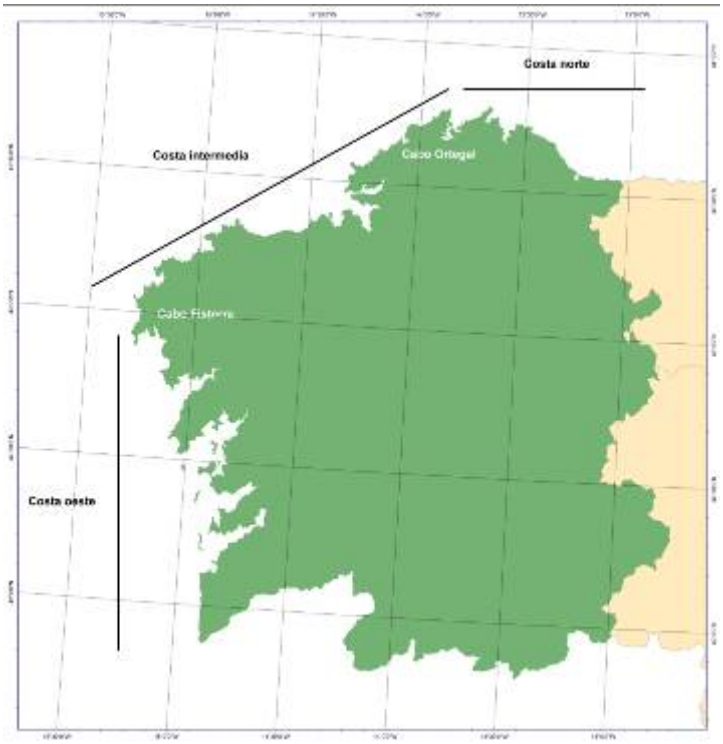

Figura 1.7. Imagen de la costa gallega.

1.3.1. Masas de agua oceánicas

Los tipos de masas de agua que bañan las costas gallegas son descritos por Fraga (1987), pudiéndose distinguir tres niveles en función de su profundidad:

- Aguas profundas: En la latitud en la que se encuentra la costa gallega, por debajo de los 3800 m hay un tipo de agua caracterizado por una temperatura de 2.2 ºC y salinidad de 34.91, que recibe el nombre de North Atlantic Deep Water (NADW). Su origen no es único, en su formación intervienen Antartic Bottom Water (AABW) y North-West Atlantic Bottom Water.
- Aguas intermedias, dentro de las que se distinguen dos capas:

♦ Existe una vena de Mediterranean Water (MW), que llega al litoral gallego con un núcleo situado a 1200 m de profundidad y con poca dilución. Este tipo de agua se forma en el Mar Mediterráneo y después de salir por el estrecho de Gibraltar se divide en dos venas: una superior que se considera secundaria, y una inferior que se denomina "Agua Mediterranea tipo", que fluye hacia el norte a lo largo de la costa oeste de la península Ibérica (Diaz del Río et al., 1998), y en su profundidad de equilibrio tiene unos valores de salinidad de 36.5 y una temperatura de 12 °C. Su distribución en la costa de Galicia no es muy regular, e incluso varía en el tiempo.

♦ Labrador Sea Water: forma una capa a unos 1900 m que penetra a modo de cuña horizontal entre la mezcla de North Atlantic Deep Water (NADW) y MW, y se desplaza en dirección contraria. Forma una capa de mínimo de salinidad y máximo de oxigeno, y sus características en la zona de formación son, salinidad de 34.89 y temperatura de 3.4 °C.

- Aguas de las capas subsuperfiales, dentro de las cuales se encuentran:

♦ Eastern North Atlantic Central Water (ENACW), una capa situada en un rango de profundidad entre 100 y 400 m, variando su límite superior en función de la situación geográfica, la época del año y las condiciones meteorológicas. Por debajo existe un intervalo entre 400 y 1000 m en el que se ubica una mezcla de esta agua central con MW. Las características de ENACW no son fijas sino que tienen un rango variable de temperatura y salinidad. En el caso de Galicia los límites se restringen debido a la mezcla con el MW en la parte inferior, y al enfriamiento invernal en su parte superior.

En la costa gallega existen dos ramas de procedencia distinta:

• La rama procedente del norte, se sitúa lejos de la costa en invierno y se acerca en verano desplazándose posteriormente al oeste. En invierno su mezcla en la vertical alcanza los 300 m de profundidad.

• La rama situada al suroeste, frente a la costa portuguesa, se desplaza en verano en dirección nordeste hasta alcanzar la costa, apareciendo ya a una profundidad de 60 m.

♦ El agua de la corriente que va hacia el polo (Poleward Current). Esta corriente hacia el polo (Frouin et al., 1990), es una corriente que se encuentra a una profundidad aproximada de 200 m y fluye aproximadamente a lo largo de 1500 km a través de la parte superior de la plataforma continental, desde el oeste de Portugal, noroeste de España y suroeste de Francia. Es decir, fluye hacia el norte, próxima al margen continental de la costa oeste de la Península Ibérica. Cuando alcanza la esquina noroeste de España, gira hacia el este y prosigue paralela a la costa. En el Golfo de Vizcaya, la corriente restablece su dirección hacia el norte a lo largo del margen continental Francés.

- En la capa superior existe un agua superficial cuyas características varían con las condiciones climáticas locales. En su parte inferior, entre los 30-50 m, se establece una termoclina que sólo desaparece en invierno, cuando no hay un calentamiento solar de las aguas más superficiales.

De todos los tipos de masas de agua que se localizan en la costa gallega, son particularmente interesantes las aguas de las capas subsuperficiales, ya que son las que se encuentran en la plataforma continental adyacente y pueden afectar a las rías. Por este motivo, a continuación se hará una descripción más detallada de las dos masas de agua subsuperficiales consideradas anteriormente.

1.3.1.1. Caracterización de ENACW

Como se ha dicho anteriormente, en la costa gallega existen dos ramas de ENACW de distinta procedencia. Estas ramas se denominan $ENACW_p$, cuando su origen es subpolar, y $ENACW_t$ cuando su origen es subtropical (Fiuza et al., 1984; Rios et al., 1992). La primera rama ($ENACW_P$) se define por una línea en un diagrama de temperatura-salinidad entre T = 10.00 ºC, S = 35.40 y T = 12.20 ºC, S = 35.66, y se forma en el este del Atlántico norte, más allá de los 46º N por un enfriamiento invernal y una convección profunda (McCartney & Talley, 1982). La segunda rama ($ENACW_T$), relativamente más cálida y salina, corresponde a una línea que se extiende entre T = 13.13 ºC, S = 35.80 y T = 18.50 ºC, S = 36.75. Se forma a lo largo del frente de Azores aproximadamente a 35º N, como resultado de la subducción de capas gruesas de aguas modales superficiales causadas localmente por una elevada evaporación y enfriamiento en invierno y por su posterior advección hacia el este por la Corriente de las Azores y luego por su prolongación hacia el ecuador y hacia el norte a lo largo del noroeste de África y oeste de la Península Ibérica.

Estas dos ramas se dirigen hacia el sur y el norte respectivamente, formando un frente subsuperficial al encontrarse (Figura 1.8).

Rios et al (1992) definen en esta zona un área subsuperficial de convergencia donde el agua de origen subpolar, modificada por el calor del verano, puede mezclarse con el agua de origen tropical. Esta convergencia está muy marcada en Finisterre, que marca el abrupto cambio entre la costa oeste y el resto de la zona costera y es normalmente una zona de un máximo estacionario de afloramiento (Blanton et al., 1984; Castro et al., 1994) y un repetido filamento de afloramiento (Haynes et al., 1993).

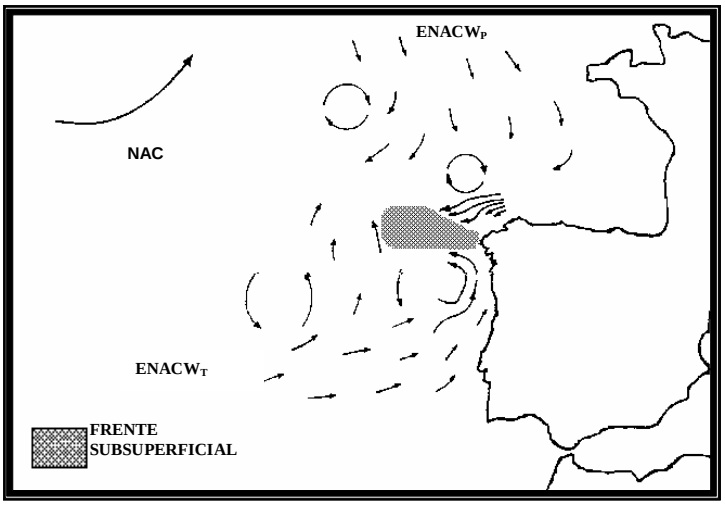

Figura 1.8. Esquema general de la distribución de ENACW en el norte del Océano Atlántico (Rios et al., 1992).

De este modo, se establecen diferencias importantes entre las aguas de la zona litoral. En la costa oeste el viento predominante en verano, de dirección norte, desplaza el agua superficial permitiendo que se eleve ENACW cargada de sales nutrientes, esta ascensión será más fácil cuanto más delgada sea la capa de agua superficial. El fértil carácter de las Rías Baixas está provocado por este aporte de nutrientes, tres veces superior al normal, que penetra por el fondo y se transforma en materia orgánica que entra a formar parte del ciclo biológico (Fraga y Margalef, 1979).

En el resto de la zona costera el afloramiento se produce con vientos del este, el agua que aflora desde profundidades de 200 m es agua de mezcla invernal y aunque es rica en sales nutrientes, su concentración es inferior a ENACW.

1.3.1.2 Caracterización de la corriente hacia el polo

Varios autores han observado y estudiado el agua transportada por la corriente hacia el polo. Frouin et al (1990) describieron su presencia a lo largo del margen continental de la Península Ibérica durante el invierno. Para caracterizar esta corriente, estos autores emplearon una secuencia de imágenes infrarrojas de satélite y datos hidrográficos medidos durante el invierno de 1983-1984. Los datos hidrográficos fueron tomados solamente a lo largo de la costa de Portugal entre noviembre y diciembre de 1983, sin embargo las imágenes de satélite que emplearon abarcaban una mayor zona y un mayor período de tiempo (noviembre de 1983 a enero de 1984).

De acuerdo con los datos hidrográficos obtenidos por esos autores, el agua transportada por la corriente hacia el polo cerca de la costa de Portugal es aproximadamente 0.2 más salina y 0.5 ºC más cálida que el agua de sus alrededores. Esta agua se caracteriza por valores de salinidad y temperatura de 35.9 y 15.2 ºC respectivamente, por lo que es más cálida y salina que ENACW. En la Figura 1.9 se muestran la distribución vertical de salinidad y temperatura medida por estos autores en varias estaciones en límite entre la costa portuguesa y la costa gallega.

En la Figura 1.9(a) se puede observar un centro de agua más salina aproximadamente a 200 m de profundidad, que caracteriza a las estaciones más próximas a la costa. Coincidiendo con este centro de agua salina, las isotermas adquieren una pendiente hacia abajo en dirección a la costa (Figura 1.9 (b)), indicando un incremento de temperatura a medida que se avanza hacia el margen continental. Por lo tanto, es posible identificar en esta zona la presencia de una masa de agua con valores de temperatura y salinidad mayor que los valores del agua que se encuentra en sus alrededores.

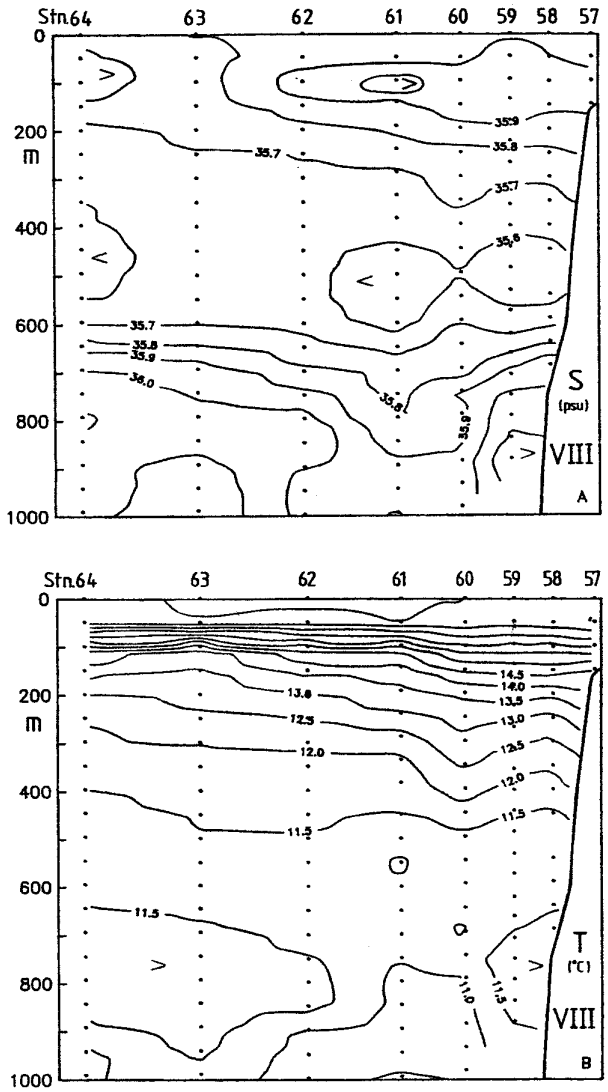

Figura 1.9. Distribución vertical de salinidad y temperatura medida por Frouin et al (1990) en varias estaciones situadas a lo largo de una sección perpendicular a la costa frente al río Lima (al sur del río Miño).

Según Frouin et al (1990), la corriente hacia el polo tiene una anchura entre 25-40 km, una profundidad aproximada de 200 m y se caracteriza por valores de velocidad de 0.2-0.3 m s^{-1}. Además, el transporte del volumen de agua asociado a esta corriente se incrementa hacia el norte desde aproximadamente 3.10^5 m^3 s^{-1} cerca de los 38º 3' N hasta 5-7.10^5 m^3 s^{-1} a 41º-42º N.

Wooster et al (1976) también observaron esta corriente durante todo un año entre el noroeste de España, a aproximadamente 43º N (Cabo Finisterre) y Sierra Leona a 7.5º N.

A lo largo de la costa de la Península Ibérica durante el verano, el viento sopla principalmente hacia el sur causando la aparición del afloramiento como resultado del transporte de Ekman hacia fuera de la costa. Durante el invierno, un cambio completo de la componente meridional del viento hacia el norte induce un transporte de Ekman hacia la costa, acompañado por un flujo superficial extremadamente débil a lo largo de la costa hacia el polo. Para estudiar el origen de la corriente hacia el polo, Frouin et al (1990) examinan diversos mecanismos como el transporte de Ekman hacia la costa generado por vientos del sur, gradientes de presión meridional a gran escala y *dam break*.

Arrastre del Viento:

El centro de altas presiones, anticiclón de las Azores, localizado en el noroeste de la Península Ibérica durante los meses de primavera y verano, se ve desplazado en invierno por una depresión a gran escala originada por la extensión hacia el sur del centro de bajas presiones situado en Islandia (ver figura 7 de Frouin et al (1990)). Como consecuencia de este desplazamiento la circulación atmosférica que previamente daba lugar a vientos del norte, durante el invierno produce vientos del sur bajo la influencia ciclónica del

centro de bajas presiones. Estos vientos dirigidos hacia el norte a lo largo de la costa causan un transporte de Ekman hacia la costa que provoca que el agua se apile en la región costera y que el campo de presiones cambie significativamente.

Gradientes meridionales de presión a gran escala:

Otro posible mecanismo que contribuye a la aparición de la corriente hacia el norte puede resultar del flujo a gran escala desde la parte interior del océano hacia el este, asociado con el gradiente de presión meridional baroclínico a lo largo de la costa oeste de la Península Ibérica. Este flujo fuerza un hundimiento local del agua y como consecuencia una corriente superficial hacia el norte.

"Dam Break":

La forma de cuña de la intrusión de agua salada y cálida a lo largo de la costa Ibérica sugiere que algún tipo de mecanismo de *dam break* puede estar asociado con su origen. Algunos de los resultados obtenidos concuerdan con las características observadas de la corriente hacia el polo como por ejemplo la orientación y la forma de cuña. Sin embargo, existen discrepancias considerables entre estas características observadas y otros resultados de los estudios de *dam breaks*. Una de estas diferencias es que en estos estudios se estiman velocidades de corrientes entre 1.4-2.0 m s^{-1}, las cuales son muy superiores a las observadas en la corriente hacia el polo (0.2 m s^{-1}). Esta diferencia, indica que el mecanismo de *dam break* no es probablemente quien genera y controla la corriente estudiada.

De acuerdo con estos autores la existencia de la corriente hacia el polo y el incremento en el volumen de agua hacia el norte que transporta, se explican por medio de una combinación del cambio geostrófico del flujo oceánico a gran escala que afecta al margen continental del oeste de la Península Ibérica

y el transporte de Ekman hacia la costa inducido por vientos del sur. Los cálculos realizados en su trabajo indican que el primer mecanismo es más importante que el segundo, pero se pueden dar situaciones en las que el segundo mecanismo contribuirá más a la descripción global.

Además de los datos hidrográficos medidos *in situ* y de las imágenes de satélite correspondientes al invierno de 1983-1984, estos autores analizaron un grupo de imágenes infrarrojas de satélite que abarcaban un período de seis años (1982-1988). En estas imágenes pudieron observar la presencia de una masa de agua cálida que se propagaba hacia el norte desde Portugal y noroeste de España durante todos los inviernos desde 1982-1983 hasta 1987-1988. Por lo tanto se puede concluir que la denominada corriente hacia el polo es una característica presente en la circulación oceánica de la costa del sudoeste de Europa durante el invierno.

Corrientes hacia el polo similares a la estudiada aquí han sido observadas a lo largo de la parte superior de la pendiente continental de la costa este de otros continentes. Ejemplos de estas corrientes son la Corriente Leeuwin del oeste de Australia (Cresswell & Golding, 1980; Thompson, 1984), la Corriente de Davison del oeste de los Estados Unidos (Hickey, 1979) y la Corriente de Haida del oeste de Canadá (Thomson & Emery, 1986). Estos ejemplos junto con el caso estudiado por Frouin et al (1990), sugieren que la ocurrencia de las corrientes superficiales hacia el polo es una característica universal de la circulación invernal en el límite este de los océanos a latitudes medias y subtropicales.

1.3.2. El afloramiento en la costa Gallega

El afloramiento en la costa gallega forma parte de un sistema general que se extiende a lo largo de la costa este del Atlántico norte desde

aproximadamente 7.5 hasta 44º N (Wooster *et al*., 1976). El Cabo Finisterre marca el abrupto cambio entre la costa oeste y el resto de la zona costera y es con frecuencia una zona de un máximo estacionario de afloramiento (Blanton *et al*., 1984) y un filamento recurrente (Haynes *et al*., 1993).

A lo largo de la costa oeste gallega, el fenómeno de afloramiento ocurre normalmente primavera-verano y ha sido ampliamente estudiado durante las últimas décadas (Fraga, 1981; Prego et al., 2001; Alvarez et al. 2005; Gomez-Gesteira et al., 2006; Alvarez et al., 2008). Este afloramiento introduce agua fría y rica en nutrientes procedente del este del Atlántico Norte (ENACW) en los estuarios, generando una gran productividad biológica.

Aunque este fenómeno es básicamente un proceso de primavera-verano relacionado con vientos del NE, también se ha observado en otoño-invierno. Alvarez et al. (2003) caracterizaron un evento de afloramiento en Enero de 1998 que introdujo agua transportada por la corriente hacia el polo en la Ria de Pontevedra. El mecanismo que generó este evento fue similar al observado en verano (vientos del NE), pero la intrusión del agua transportada por la corriente hacia el polo cambió las propiedades termohalinas y el tiempo de residencia del agua, disminuyendo la cantidad de nutrientes y aumento la salinidad. deCastro et al. (2006) también estudiaron un evento de afloramiento en el interior de la Ria de Vigo en Noviembre de 2001. Las propiedades termohalinas mostraron que el agua aflorada se correspondía con ENACW. deCastro et al. (2008) caracterizaron seis eventos de afloramiento en las Rias Baixas entre Noviembre y Febrero durante seis años (2000-2005) con características similares a los observados en verano.

Al norte de Cabo Finisterre, el afloramiento también está presente aunque no es un fenómeno común. Estudios previos mostraron que a lo largo de esta parte de la costa gallega el afloramiento es discontinuo y se observa cerca del borde de la plataforma continental (Prego & Bao 1997). Es también un hecho conocido que estos eventos con características similares pueden ocurrir a ambos lados de Cabo Finisterre pero con diferente probabilidad e intensidad. Torres et al. (2003) describieron la región de afloramiento de la costa gallega de Julio de 1999 a Mayo de 2001 usando datos de viento del satélite QuikSCAT. Encontraron que los patrones de viento se pueden alternar produciendo breves episodios de afloramiento al norte o al sur de Cabo Finisterre, o un patrón de viento combinado que puede producir afloramiento en ambas costas a la vez. Gomez-Gesteira et al. (2006) analizaron el transporte de Ekman cerca de la costa gallega usando datos de viento de predicciones meteorológicas de Noviembre de 2001 a Octubre de 2004 y encontraron que los eventos de afloramiento tienen una probabilidad de ocurrir del 60% a lo largo de la costa oeste gallega mientras en la costa norte esta probabilidad no supera el 30%. Estos resultados también fueron corroborados por Alvarez et al. (2008) usando datos de viento de QuikSCAT desde Noviembre de 1999 hasta Octubre de 2005.

1.4. Referencias

Alvarez, I., deCastro, M., Prego, R., Gomez-Gesteira, M., 2003. Hydrographic characterization of a winter-upwelling event in the Ria of Pontevedra (NW Spain). Estuarine Coastal and Shelf Science, 56, 869-876.

Alvarez, I., deCastro, M., Gomez-Gesteira, M., Prego, R., 2005. Inter- and intra-annual analysis of the salinity and temperatura evolution in the Galician Rías Baixas--ocean boundary (northwest Spain), Journal of Geophysical Research, 110, C04008, doi:10.1029/2004JC002504.

Alvarez, I., Gomez-Gesteira, M., deCastro, M., Novoa, E.M., 2008. Ekman Transport along the Galician Coast (NW, Spain) calculated from QuikSCAT winds. Journal of Marine Systems, 72, 101-115.

Blanton, J.O., Atkinson, L.P., Castillejo, F., Montero, A.L., 1984. Coastal upwelling of the Rias Bajas, Galicia, northwest Spain, I; hydrographic studies, Rapp.P.V. Reun. Cons. Int. Explor. Mer. 183, 179–190.

Casey, KS., Cornillon, P., 2001. Global and regional sea surface temperature trends. Journal of Climate, 14, 3801-3818.

Castro, C.G., Perez, F.F., Alvarez-Salgado, X.A., Roson, G., Rios, A.F., 1994. Hydrography conditions associated with the relaxation of a upwelling event off the Galcian coast (NW Spain). Journal of Geophysical Research, 99, 5135-5147.

Conan, S.M.H., Brummer, G.J.A., 2000. Fluxes of planktic foraminifera in response to monsoonal upwelling on the Somalia Basin margin. Deep Sea Research I, 47, 2207-2227.

Cresswell, G.R., Golding, T.J., 1980. Observations of a south-flowing current in the southeastern Indian Ocean. Deep Sea Research II, 27, 449-466.

deCastro, M., Dale, A.W., Gomez-Gesteira, M., Prego, R., Alvarez, I., 2006. Hydrographic and atmospheric analysis of an autumnal upwelling event in the Ria de Vigo (NW Iberian Península). Estuarine Coastal and Shelf Science, 68, 529-537.

deCastro, M., Gomez-Gesteira, M., Alvarez, I., Cabanas, J.M., Prego, R., 2008. Characterization of fall-winter upwelling recurrence along the Galician western coast (NW Spain) from 2000 to 2005: dependence on atmospheric forcing. Journal of Marine Systems, 72, 145-148, doi:10.1016/j.jmarsys.2007.04.005.

Di Lorenzo, E., 2003. Seasonal dynamics of the surface circulation in the Southern California Current System. Deep Sea Research II, 50, 2371-2388.

Diaz del Rio, G., Gonzalez, N., Marcote, D., 1998. The intermediate Mediterranean water inflow along the northern slope of the Iberian Peninsula. Ocanologica Acta, 21, 157-163.

Edwards, A., Jones, K. M., Graham, J., Grifftihs, C.R., MacDougall, N., Patching, J., Richard, J.M., 1994. Transient Coastal Upwelling and Water Circulation in Bantry Bay, a Ria on the South-West Coast of Ireland, Raine R. Estuarine Coastal and Shelf Science, 42, 213-230.

Fiuza, A.F.G., 1984. Hidrologia e dinamica das aguas costeiras de Portugal (Hydrology and dynamics of the Portuguese coastal water). Ph.D. Thesis, University of Lisboa, Lisboa. 294 pp.

Folland, C., Parker, D., Kates, F. 1984. Worldwide marine temperature fluctuations 1856–1981. Nature, 310**,** 670–673.

Fraga, F., 1981. Upwelling off the Galician Coast, Northwest Spain, in: Richardson, F.A. (Ed.), Coastal Upwelling. American Geophysical Union, Washington, pp. 176-182.

Fraga, F., 1987. Oceanografía de la plataforma gallega. Academia Galega de Ciencias. Santiago de Compostela. 48 pp.

Fraga, F., Margalef, R., 1979. Las Rias Gallegas. Estudio y explotación del mar en Galicia. Cursos y congresos, Universidad de Santiago, Santiago de Compostela, pp. 101-122.

Frouin, R., Fiuza, A.F.G., Ambar, I., Boyd, T.J., 1990. Observations of a poleward surface current off the coasts of Portugal and Spain during winter. Journal of Geophysical Research, 95, 679-691.

Gomez-Gesteira, M., Moreira, C., Alvarez, I., deCastro, M., 2006. Ekman transport along the Galician coast (NW, Spain) calculated from forecasted winds. Journal of Geophysical Research, 111, C10005, doi:10.1029/2005JC003331.

Haynes, R., Barton, E.D., Pilling, I., 1993. Development, persistence and variability of upwelling filaments off the Atlantic coast of the Iberian peninsula. Journal of Geophysical Research, 98, 22681-22692.

Herrera, J. L. Piedracoba, S., Varela, R. A. and Roson, G. 2005. Spatial analysis of the wind field on the western coast of Galicia (NW Spain) forn in situ measurements. Continental Shelf Research, 25: 1728-1748.

Hickey, B., 1979. The California Current system-Hypotheses and facts. Progress Oceanography, 8, 191-279.

Hickey, B.M., Banas, N., 2003. Oceanography of the U. S. Pacific Northwest Coastal Ocean and Estuaries with Application to Coastal Ecology. Estuaries, 26, 1010-1031.

Honkoop, P.J.C., Van der Meer, J., Beukema, J.J., Kwast, D., 1998. Does temperature-influenced egg production predict the recruitment in the bivalve Macoma balthica? Marine Ecology Progress Series, 164,

229–235.

Intergovernmental Panel on Climate Change. 2007. Climate Change 2007: The Physical Science Basis. Contribution of Working Group 1 to the Fourth Assessment Report of the Intergovernmental panel on Climate Change, Cambridge University Press, Cambridge.

McCartney, M.S., Talley, L.D., 1982. The Subpolar Mode Water of the North Atlantic Ocean. Journal of Physical Oceanography, 12, 1169-1188.

Monteiro, P.M.S., Largier, J.L., 1999. Thermal stratification in Saldhana Bay (South Africa) and subtidal, density-driven exchange with the coastal waters of the Benguela upwelling system. Estuarine Coastal and Shelf Science, 49, 877-890.

Nykjaer, L., Van Camp, L., 1994. Seasonal and interannual variability of coastal upwelling alongnorthwest Africa and Portugal from 1981 to 1991. Journal of Geophysical Research, 99, 14,197– 14,208.

Nixon, S., Thomas, A., 2001. On the size of the Peru upwelling ecosystem. Deep Sea Research I, 48, 2521-2528.

Parker, D.E., Jones, P., Folland, C., Bevan, A., 1994. Interdecadal changes of surface temperature since the late nineteenth century. Journal of Geophysical Research, 99, 14 373- 14 339.

Pelegrí, J.L., Arístegui, J., Cana, L., Gonzalez-Davila, M., Hernandez-Guerra, A., Hernandez-Leon, S., Marrero-Diaz, A., Montero, M. F., Sangrà, P., Santana-Casiano, M., 2005. Coupling between the open ocean and the coastal upwelling region off northwest Africa: water recirculation and offshore pumping of organic matter. Journal of Marine Systems, 54, 3-37.

Pond, S., Pickard, G.L., 1983. Introductory dynamical oceanography, Pergamon Press, Oxford, 329 pp.

Prego, R., Bao, R., 1997. Upwelling influence on the Galician coast: silicate in shelf water and underlying surface sediments. Continental Shelf Research, 17, 307-318.

Prego, R., Dale, A., deCastro, M., Gomez-Gesteira, M., Taboada, J.J., Montero, P., Perez-Villar, V., 2001. Hydrography of the Pontevedra Ria: Intra-annual spatial and temporal variability in a Galician coastal system (NW Spain). Journal of Geophysical Research, 106, 19845-19857.

Rios, A.F., Pérez, F.F., Álvarez- Salgado, X.A., Figueiras, F.G., 1992. Water masses in the upper and middle North Atlantic Ocean east of the Azores. Deep Sea Research I, 39, 645-658.

Roughan, M., Middleton, J.H., 2002. A comparison of observed upwelling mechanisms off the east coast of Australia. Continental Shelf Research, 22, 2551-2572.

Rutllant, J.A., Rosenblunth, B., Hormazabal, S., 2004. Intraseasonal variability of wind-forced coastal upwelling off central Chile (30ºS). Continental Shelf Research, 24, 789-804.

Tang, D.L., Kawamura, H., Guan, L., 2004. Long-time observation of annual variation of Taiwan Strait upwelling in summer season. Advances in Space Research, 33, 307–312

Thompson, R.O.R.Y., 1984. Observations of the Leeuwin Current off western Australia, Journal of Physical Oceanography, 14, 623-628.

Thomson, R.E., Emery, W.J., 1986. The Haida Current. Journal of Geophysical Research, 91, 845-861.

Torres, R., Barton, D., Miller, P., Fanjul, E., 2003. Spatial patterns of wind and sea surface temperature in the Galician upwelling region. Journal of Geophysical Research, *108*, 3130- 3143, doi:10.1029/2002JC001361.

Wooster, W.S., Bakun. A., McClain, D.R., 1976. The seasonal upwelling cycle along the eastern boundary of the north Atlantic, Journal of Marine Research ,34, 131-141.

Young, E., Bigg, G.R., Grant, A., 1996. A statistical study of environmental influences on bivalve recruitment in the Wash, England. Marine Ecology Progress Series, 143, 121-129.

Zavala-Hidalgo, J., Gallegos-García, A., Martínez-López, B., Morey, S.L., O'Brien, J.J., 2006. Seasonal upwelling on the western and southern shelves of the Gulf of Mexico. Ocean Dynamics, 56, 333–338

Chapter 2

Data Bases

Here a brief sumary of the different data bases used throughout the manuscript is presented.

2.1. Ekman transport: Pacific Fisheries Environmental Laboratory

The Pacific Fisheries Environmental Laboratory (PFEL). (http://www.pfeg.noaa.gov) distributes environmental index products and time series data bases to cooperating researchers, taking advantage of its long association with the U.S. Navy's Fleet Numerical Meteorology and Oceanography Centre (FNMOC). FNMOC produces operational forecasts of the state of the atmosphere and the ocean several times daily and maintains archives of several important parameters. These parameters are model derived products which are routinely distributed to researchers. Among others, six-hourly Ekman transport data model derived from Sea Level Pressure are provided.

2.2. Wind data from QuikSCAT satellite

QuikSCAT satellite data can be retrieved from the Jet Propulsion Laboratory web site (http://podaac.jpl.nasa.gov/DATA_CATALOG/quikscatinfo.html). The data set consists of global grid values of meridional and zonal components of wind measured twice daily on an approximately $0.25^{o}\times0.25^{o}$ grid with global coverage. Wind speed measurements range from 3 to 20 m

s^{-1}, with an accuracy of 2 m s^{-1} and 20º in direction. The reference height of wind data is 10 m. QuikSCAT data are given in an ascending and descending pass. Data corresponding to one pass present numerous shadow areas, therefore, an average between both passes was considered to increase the coverage. Wind data from the near-coastal zone with offshore distances of about 25 km are not available due to the applied coast mask. Nevertheless, a statistical comparison between QuikSCAT wind measurements and high resolution numerical models was carried out along the Galician coast (Penabad et al., 2008), revealing similar results between models and satellite data.

2.3. Teleconnection indices

The most representative teleconnection indices in the Northern Hemisphere (NAO, EA, SCA, EA/WR and POL) can be obtained from the Climate Prediction Center (CPC) at the National Center of Environmental Prediction (NCEP) at monthly time scales from 1950.

Although a detailed description of these teleconnection indices can be found on the web site from the NCEP (http://www.cpc.noaa.gov) a brief description will be given here. The North Atlantic Oscillation (NAO) consists of a north- south dipole of geopotential anomalies with one center located over Iceland and the other one spanning between 35ºN and 40ºN in the central North Atlantic. The East Atlantic (EA) pattern consists of a north-south dipole that spans the entire North Atlantic Ocean with the centers near 55ºN, 20-35ºW and 25-35ºN, 0-10ºW. The anomaly centers of the EA pattern are displaced southeastward to the centers of the NAO pattern. The Scandinavia pattern (SCA) consists of a primary circulation center over Scandinavia, with a weaker center of opposite sign over western Europe. The

East Atlantic/ West Russia (EA/WR) pattern (Barnston and Livezey 1987) is one of three prominent teleconnection patterns that affects Eurasia through the year. This pattern consists of four main anomaly centers. The Europe Polar/Eurasia pattern (POL) consists of one center over the polar region and centers of opposite sign over Europe and northeastern China.

2.4. High Resolution Sea Surface Temperature (SST) data

Sea Surface Temperature (SST) can be obtained from the NOAA/NASA Advanced Very High Resolution Radiometers (AVHRR) (http://poet.jpl.nasa.gov). Data are available from 1985, and they are distributed in a variety of resolutions and temporal averages. A spatial resolution of 4 km and a temporal average of 8 days were considered in the studies described throughout the text. Each data product is obtained as either an ascending (daytime) or descending (night-time) image. Only the night-time image is usually considered to avoid the solar heating effect.

2.5. Extended reconstructed SST data

The extended reconstructed SST (ERSST) version 3 (ERSST.v3) data is provided by the NOAA/OAR/ESRL PSD, Boulder, Colorado from their Web site at http://www.cdc.noaa.gov/. The first extended reconstruction of global SST (ERSST) (Smith and Reynolds, 2003) was initially produced based on Comprehensive Ocean Data Set (COADS) as an outgrowth of Smith et al. (1996). Data covered the period 1854-2007 with monthly periodicity on a $2^{o}\times2^{o}$ grid with global coverage. In spite of the updated COADS observations and new quality control procedures were added to the database, the analyzed signal was heavily damped before 1880 due to data

sparseness. Afterwards the strength of the signal was more consistent over time.

ERSST.v2 (Smith and Reynolds, 2004; Smith and Reynolds, 2005) was an improved extended reconstruction of ERSST. In this version, the high-frequency SST anomalies were reconstructed by an improved fitting to a set of spatial modes better analyzing the anomalies in regions where the variance is low. In addition, version 2 also used sea-ice concentrations to improve the high-latitude SST analysis, and a modified historical bias correction for the 1939-1941 period. Finally, version 2 also included an improved error estimate.

ERSST.v3 (Smith et al., 2008) is an improved extended reconstruction over version 2 with the same period of record (ICOADS). Both versions use the same bias adjustment (Smith and Reynolds, 2002). Most of the improvements are justified by testing with simulated data. The biggest change occurs due to the improved low-frequency (LF) tuning of ERSST.v3 which reduces the SST anomaly damping before 1930 using the optimized parameters. Other improvements as changes in the sea-ice to SST analysis produce minor changes. Beginning in 1985, ERSST.v3 is also improved by explicitly including bias-adjusted satellite infrared data from AVHRR. In most of the regions, except south of 45º S, the influence of satellite data is small due to the sufficient sampling, at least in a monthly scale, in the present period. Overall, ERSST.v3 resolves more variance than ERSST.v2.

2.6. References

Penabad, E., Alvarez, I., Balseiro, C.F., deCastro, M., Gomez, B., Perez-Muñuzuri, V., Gomez-Gesteira, M., 2008. Comparative analysis between operational weather prediction models and QuikSCAT wind

data near the Galician coast. Journal of Marine Systems, 72, 256- 270.

Smith, T.M., Reynolds, R.W., Livezey, R.E., Stokes, D.C. 1996. Reconstruction of of historical sea surface temperatures using empirical orthogonal functions. Journal of Climate, 9, 1403- 1420.

Smith, T.M., Reynolds, R.W. 2002. Bias corrections for historic sea surface temperatures based on marine air temperatures. Journal of Climate, 15, 73- 87.

Smith, T.M., Reynolds, R.W. 2003. Extended reconstruction of global sea surface temperatures based on COADS data (1854- 1997). Journal of Climate, 16, 1495- 1510.

Smith, T.M., Reynolds, R.W. 2004. Improved extended reconstruction of SST (1854- 1997). Journal of Climate, 17, 2466- 2477.

Smith, T.M., Reynolds, R.W. 2005. A global merged land- air- sea surface temperature reconstruction based on historical observations (1880- 1997). Journal of Climate, 18, 2021- 2036.

Smith, T.M., Reynolds, R.W., Peterson, T.C., Lawrimore, J., 2008. Improvements to NOAA's Historical Merged Land- Ocean Surface Temperature Analysis (1880- 2006). Journal of Climate, 21, 2283- 2296.

Chapter 3

Summer upwelling frequency along the western Cantabrian coast

Abstract

Upwelling events have been analyzed along the western part of the Cantabrian coast from 1967 to 2007. This analysis shows that the highest number of days under upwelling favorable conditions was observed from June to September (12-14 days per month) with a probability of finding consecutive days under upwelling favorable conditions decreasing from 47% to 17% when events between 1 and 5 consecutive days were considered respectively. This situation was also corroborated by Sea Surface Temperature data which revealed the presence of cold water over the continental shelf, near coast, associated to upwelling favorable winds. This cold water was also observed inside the estuaries located in this area. The water temperature signal measured at the inner part of the Ria de O Barqueiro (NW Iberian Peninsula) from June to September 2008 showed to be negatively correlated with the Upwelling Index calculated in front of the northern Galician coast. This correlation tends to increase as the number of lag days between both variables increases. The maximum value of -0.8 corresponds to a lag of 5 days.

3.1. Introduction

The understanding of the vulnerability and adaptation of some marine species to environmental changes constitutes and arduous task due to presence of different factors that can affect both positively and negatively the spreading of those species. In the particular case of the northwestern part

of Iberian Peninsula (Figure 3.1), differences in coastal temperatures between the Atlantic and Cantabrian coastline during summer (Fraga, 1981; Prego and Bao, 1997; Bode et al., 2002; Garcia- Soto et al., 2002; Torres et at., 2003; Alvarez et al., 2005) can provide different development conditions for many invasive alien species (IAS) from warmer waters. This is the case of the Pacific oyster (*Crassostrea gigas*) that although is cultured in the western Galician rias (south of Cape Finisterre) and spawning has been described in this area (Ruiz, et al., 1992), there is not evidence of natural settlement of larvae stage. On the contrary, naturalized populations of this species have been located in different areas of the Cantabrian shoreline. According to different authors (Mann et al., 1991; Shatkin et al., 1997) larval survival of Pacific oyster needs temperatures above 18º during at least two weeks in July and August. Thus, coastal upwelling can play a dual role since it provides the nutrients necessary for the development of marine species but, at the same time, it is responsible for sudden decreases in water temperature that can be potentially harmful for those species.

Several facts can be summarized from previous upwelling studies on both coasts. First, upwelling is mainly a spring-summer process, although some authors have also detected upwelling events in autumn-winter (Santos et al., 2001; Alvarez et al., 2003; Borges et al., 2003; Santos et al., 2004; deCastro et al., 2006a; Prego et al., 2007; deCastro et al., 2008a; Alvarez et al., 2009). Second, upwelled water is generally Eastern North Atlantic Central Water (ENACW; T-S definition can be found in Fiuza, 1984 and Rios et al., 1992) which is a cold and salty water mass. However, some authors have detected different upwelled waters associated with the Iberian Poleward Current (Alvarez et al., 2003; Prego et al., 2007) and with shelf bottom seawater (Alvarez et al., 2009). Third, upwelling frequency and intensity are

influenced by coastal orientation (Torres et al., 2003; Gomez-Gesteira et al., 2006; Alvarez et al., 2008a) which modulates wind direction and intensity. As a result of this different coastal orientation, upwelling favourable conditions are prevalent in the spring- summer along the western coast but not along the northern one. Possibly, this is the reason why upwelling research has been mainly focused on the western coast. Thus, different features of northern coastal upwelling remain unknown and need to be answered, for example, to determine the commercial viability of invasive alien species. In particular, the historical frequency and intensity have not been studied so far using long term data series. As far as we know, only Llope et al. (2006) have analyzed the long term behaviour of upwelling processes around Cape Peñas (~ 5º 51' W, 43º 39' N). Finally, the entrance of upwelled water into the inner part of the estuaries, especially the intertidal area, and its dependence on atmospheric forcing has still to be analyzed.

The aim of this manuscript is to analyze the influence of upwelling events along the western part of the Cantabrian coast. This study focuses on different spatio-temporal scale. On the one hand, the frequency and intensity of upwelling events will be described at shelf locations from 1967-2007 by means of Ekman volume transport and Sea Surface Temperature (SST). On the other hand, the dependence of SST on upwelling conditions will be studied in the inter-tidal area of a northern Galician ria for a continuous period (June-September 2008).

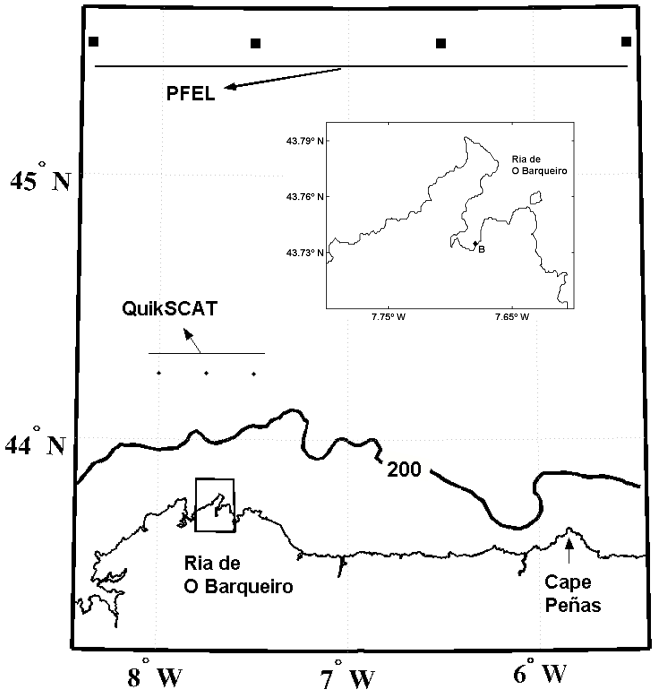

Figure 3.1. (a) Map of the western Cantabrian coast. Black circles represent the 3 control points considered to analyze wind data provided by the QuikSCAT satellite and black squares represent the 4 points where Ekman transport data from the PFEL were obtained. (b) Map of the Ria de O Barqueiro showing the sampling hydrographic station (black diamond, st. B).

3.2. Data and methods

To analyze the occurrence of summer upwelling events over the last 41 years (1967-2007), Ekman transport data provided by the Pacific Fisheries Environmental Laboratory (PFEL) (see Chapter 2). For our purposes six-hourly Ekman transport data were considered at 4 selected longitudes (8.5ºW, 7.5ºW, 6.5ºW, 5.5ºW) along 45.5ºN located in front of the area

under study (Figure 3.1(a), black squares) on an approximately 1º×1º grid. These data sets were averaged to obtain daily series.

To analyze the wind patterns measured from June to September 2008, surface wind fields provided by the QuikSCAT satellite (see Chapter 2) were used. Ekman transport was calculated using the wind speed from the QuikSCAT satellite at 3 control points located along the northern Galician coast at latitude 44.25ºN and from 7.5ºW to 8ºW (Figure 3.1(a), black circles).

A practicable upwelling index (UI) results from the meridional component of the Ekman volume transport per unit length $Q_y = -\frac{\rho_a C_d}{\rho_w f}\left(W_x^2 + W_y^2\right)^{1/2} W_x$ where W_x, W_y are the zonal and meridional components of wind data, ρ_a= 1.22 kg m^{-3} is the air density, C_d=1.4×10^{-3} is a dimensionless drag coefficient, ρ_w= 1025 kg m^{-3} is the sea water density and f is the local Coriolis frequency (Bakun, 1973; Nykjaer and Van Camp, 1994; Gomez-Gesteira et al., 2006). The latter will be considered to be constant along the Cantabrian coast because it only slightly deviates from the pure west-east orientation. In fact, only along the northern Galician coast it is possible to observe an irregular coastline due to the presence of the northern Galician rias (Figure 3.1(a)). Nevertheless, a recent study carried out by Gomez-Gesteira et al. (2006) using modeled wind data around the Galician coast, showed that along the northern Galician coast (~7.5-8.5º W) the wind direction presents the same behavior with some small differences in amplitude values. Thus, macroscopically the Cantabrian coast can be considered approximately parallel to the equator and the Q_y component can

be considered as the UI. Positive (negative) UI values mean upwelling favorable (unfavorable) conditions.

The most representative teleconnection indices in the Northern Hemisphere (NAO, EA, SCA, EA/WR and POL) have been obtained from the Climate Prediction Center (CPC) at the National Center of Environmental Prediction (NCEP) at monthly time scales from 1950 to 2005 (see Chapter 2). These modes have shown to be the most prevalent patterns on the eastern North Atlantic region (Rodríguez- Puebla et al., 1998; Lorenzo and Taboada, 2005; deCastro et al., 2006b).

Sea Surface Temperature (SST) data were obtained from the NOAA/NASA Advanced Very High Resolution Radiometers (see Chapter 2). Only night-time data with a spatial resolution of 4 km and a temporal average of 8 days were considered.

Water temperature was measured at the inner part of the Ria de O Barqueiro (Figure 3.1(b), black diamond (st. B)) using a DST CTD (Data Storage Tag, Conductivity Temperature Depth) recorder. This is a compact microprocessor-controlled temperature, depth and conductivity with two conductivity cells, temperature and pressure sensors placed in the device cup. CTD is inserted into a plastic protective housing deployed approximately 0.5m above the sea bed by using a metal trestle of the commercial oyster bag culture. The constant sampling interval of T and S was one hour. Only temperature data will be considered in the present study due to the low accuracy of the conductivity cells to identify small changes in salinity. Note that the location of temperature recorder in the intertidal area (0.5m to 4m deep from low tide to high tide) was specially designed to identify upwelling induced changes in the area where commercial species as oysters are cultured.

3.3. Results and discussion

The study of upwelling effect on the northern coast of the Iberian Peninsula was carried out in terms of Upwelling Index from 1967 to 2007 and water temperature both at offshore locations and inside estuaries.

3.3.1. Upwelling Index analysis

The time evolution of the UI from 1967 to 2007 was calculated taking into account 4 control points shown in Figure 3.1(a) (black squares). The inter-annual evolution of UI (Figure 3.2(a)) shows a marked annual cycle, with maximum values (upwelling favorable conditions) in July-August and minimum values in December-January. The monthly behavior associated with the annual cycle can be determined by averaging UI for each month during the period 1967-2007. This monthly average of UI (Figure 3.2(b)) shows positive values from June to August at all points with the maximum values in July (~300 $m^3 s^{-1} km^{-1}$). For the rest of the year UI shows negative values. Taking into account the small changes among the points located along the coast observed in Figure 3.2(a, b) it is possible to consider a longitudinal average of UI. The inter-annual evolution of the longitudinal average of UI (Figure 3.2(c)) shows maximum values in July- August and minimum values in December- January. The longitudinal and time averaging of UI is represented in Figure 3.2(d). The highest positive values (~300 $m^3 s^{-1} km^{-1}$) are observed from June to August. Negative values can be observed for the rest of the year, showing unfavorable upwelling conditions during most of the year. The error bars were calculated using the standard deviation of the monthly data, $\sigma(UI^W)$. Error bars are observed to be negligible compared to the amplitude of the annual cycle, which ranges from -1200 $m^3 s^{-1} km^{-1}$ to 300 $m^3 s^{-1} km^{-1}$.

The observed seasonal cycle can be compared with that reported by Alvarez et al. (2008b) from the Iberian west coast (see Figure 7 in that reference). Resulting patterns are very similar and exhibit positive peak values in summer, but negative ones in winter. Nevertheless, there are several significant differences among them. For instance, upwelling favorable conditions can be observed from March to September along the western coast but only from June to August along the northern coast. In addition, the highest values are close to 800 $m^3 s^{-1} km^{-1}$ along the western coast and only close to 300 $m^3 s^{-1} km^{-1}$ along the northern one.

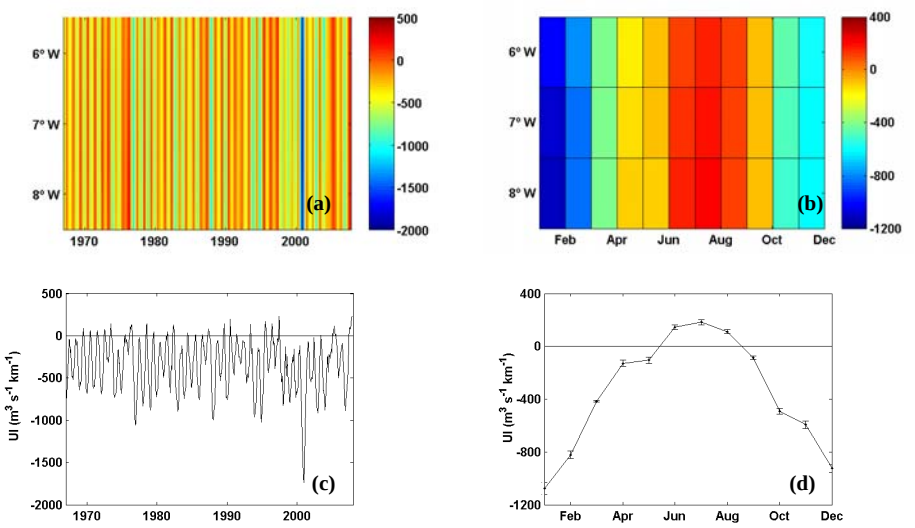

Figure 3.2. (a) Inter-annual evolution of the Upwelling Index (UI) [$m^3 s^{-1} km^{-1}$] from 1967 to 2007. (b) 41-year (1967-2007) mean of the annual evolution of UI. (c) Inter-annual evolution of the longitudinal average of UI from 1967 to 2007. (d) Annual cycle calculated by averaging UI in longitude and time from 1967 to 2007.

Interannual changes of UI can be also analyzed in terms of the most representative atmospheric modes in the North Atlantic. Teleconnection patterns reflect large-scale changes in the atmospheric wave and jet stream patterns, which can influence temperature, rainfall, storm tracks, and/or jet stream location/intensity over vast areas. Thus, they are often the phenomenon responsible for abnormal weather patterns occurring simultaneously over seemingly vast distances.

Previous studies (Rodríguez- Puebla et al., 1998; Lorenzo and Taboada, 2005; deCastro et al., 2006b) consider that the most representative regional patterns of atmospheric variation in the Northern Hemisphere with some influence on the eastern North Atlantic region are: NAO, EA, SCA, EA/WR and POL. The temporal variability of upwelling along the western Cantabrian coast can be analyzed taking into account the influence of these atmospheric patterns. Taking into account the observed behavior in Figure 3.2(d), the monthly indices and UI were correlated considering the winter season from December to February and the summer season from June to August at the 4 control points (Table 3.I).

In winter, UI shows the highest correlation coefficient value for the EA/WR pattern with a significant positive correlation along the entire area (close to 0.5). A negative correlation can be also observed for the EA and NAO patterns with a correlation coefficient around -0.4 and -0.3 respectively. UI and the rest of atmospheric indices are not significantly correlated. Taking into account these values it is possible to observe that EA/WR and EA are the most important teleconnection patterns on UI variability although the NAO pattern also shows some influence.

	8.5º W		7.5 º W		6.5 º W		5.5 º W	
	DJF	JJA	DJF	JJA	DJF	JJA	DJF	JJA
NAO	-0.35*	0.29*	-0.34*	0.30*	-0.34*	0.31*	-0.33*	0.31*
EA	-0.47*	-0.43*	-0.45*	-0.43*	-0.43*	-0.42*	-0.39*	-0.39*
EA/ WR	0.47*	---	0.48*	---	0.49*	---	0.51*	---

*significance level>95%

Table 3.I. Correlation coefficient between UI-winter (DJF) atmospheric patterns and UI-summer (JJA) atmospheric patterns from 1967 to 2007 at the 4 control points.

The correlations obtained in summer show that the EA pattern is the most important mode. UI shows a negative correlation with the highest correlation coefficient around -0.4 at the 4 control points. The NAO pattern also shows some influence on the UI with a positive correlation although the correlation coefficient value is on the order of 0.3. These results can be compared with that obtained by deCastro et al. (2008b) along the western coast of the Iberian Peninsula. They found that the main upwelling variability (considering the upwelling season as JASO) can be explained in terms of the EA pattern with a significant negative correlation (close to -0.4) along the entire coast. NAO pattern was the second atmospheric mode with some influence on upwelling variability showing a significant positive correlation.

Upwelling prevalence can be studied both in terms of the mean number of days under upwelling favorable conditions and the probability of finding consecutive days under these upwelling favorable conditions. Actually, previous studies carried out at the western coast of the Iberian Peninsula proved that upwelled water can be easily identified when upwelling favorable conditions persist for more than 3-4 days (Alvarez-Salgado et al., 2000; Alvarez et al., 2005; Alvarez-Salgado et al., 2006). In addition, a

recent study at the northern Galician coast (Alvarez et al., 2009) also characterized a winter upwelling event observed after 9 consecutive days of upwelling favorable conditions.

The mean number of days per month under favorable wind conditions (UI>16 $m^3 s^{-1} km^{-1}$) was calculated from 1967 to 2007 at the 4 control points located along the Cantabrian coast (Figure 3.1(a), black squares). For the sake of clarity only the 2 points (6.5ºW and 7.5ºW) located in the central part of the area were represented (Figure 3.3(a)). Note that the threshold (16 $m^3 s^{-1} km^{-1}$) corresponds to weak winds (<1 m s^{-1}) as well as to calms. The highest number of days was observed during the spring-summer months with 12-14 days per month, while during the autumn-winter period the number of days was lower (8-10 days per month) although not negligible (Alvarez et al., 2009). This situation can be also compared with the one observed at the western coast of the Iberian Peninsula (Cabanas and Alvarez, 2005; deCastro et al. 2008a).

The highest number of days under upwelling favorable conditions along the western coast is also observed during the summer months although with higher values (~22-25 days per month) than along the northern coast. During the winter period it is also possible to observe a number of days under favorable conditions along the western coast (~10-12 days per month) higher than along the northern one.

Taking into account the previous results it is possible to conclude that the summer season is characterized by exceptionally favored coastal upwelling conditions. Upwelling duration was also analyzed at the same control points from June to September. Figure 3.3(b) shows the probability of finding consecutive days under upwelling favorable conditions (UI>16 $m^3 s^{-1} km^{-1}$)

from 1967 to 2007. The highest probabilities can be found between 1 and 5 consecutive days reaching values of 47% and 17% respectively.

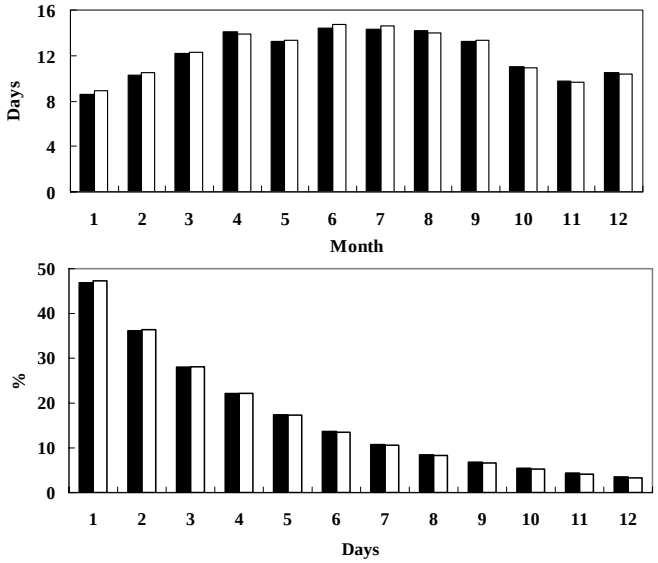

Figure 3.3. (a) Number of days with UI>16 m^3 s^{-1} km^{-1} per month averaged from 1967 to 2007 and (b) Probability of finding consecutive days under upwelling favorable conditions (UI>16 m^3 s^{-1} km^{-1}) in summer (Jun-Sep) from 1967 to 2007 at the control points 45.5ºN, 7.5ºW (dark bars) and 45.5ºN, 6.5ºW (light bars). The positions of the points correspond to the black squares depicted in Figure 3.1(a)).

In addition to the upwelling duration, the mean intensity of UI was also analyzed during these months taking into account the intensity values corresponding to the days under upwelling favorable conditions. Figure 3.4(a) shows $\langle UI \rangle^F$ average calculated from June to September for each year at the 2 control points, where the superscript *F* refers to the fact that averaging was performed considering only the days under upwelling favorable conditions (UI>16 m^3 s^{-1} km^{-1} as shown above). A 2-year running average was considered for each point to better show the overall behavior.

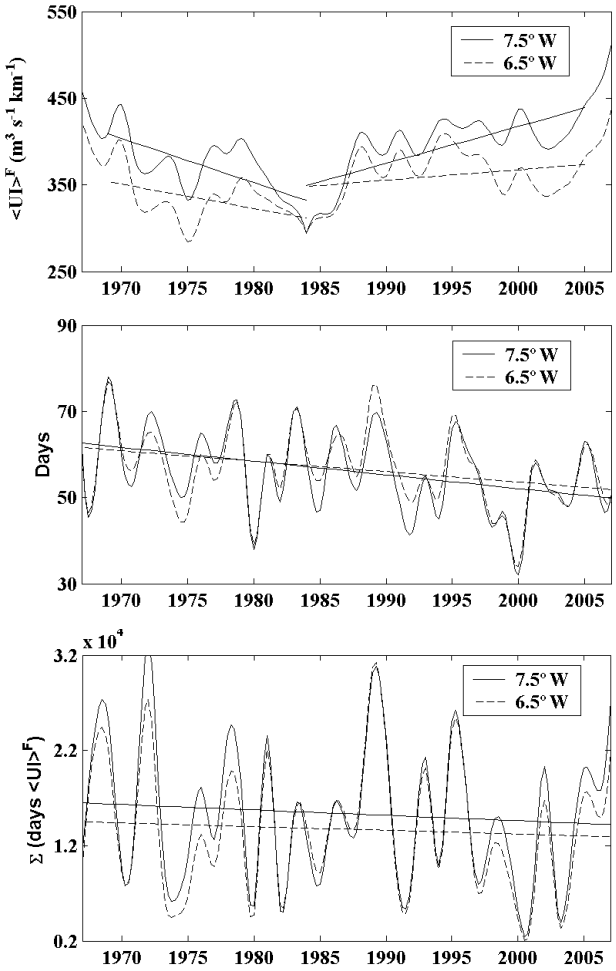

Figure 3.4. (a) Annual upwelling intensity (m^3 s^{-1} km^{-1}) averaged from June to September (1967-2007). (b) Number of days per year under upwelling favorable conditions from June to September (1967-2007). (c) $\sum_{i=1}^{N} n_i < UI >_i^F$ where n_i is the number of consecutive days under upwelling favorable conditions with $n_i \geq 3$, $<UI>_i^F$ is the mean intensity of UI during these days and N is the number of events per year. Straight lines in each frame show the linear fit at the two control points.

UI has a similar pattern at both control points although the westernmost point (7.5ºW, solid line) presents intensity values slightly higher than the other point throughout the whole period. Straight lines represent a liner fit to better observe the general trends. The upwelling intensity tends to decrease from the beginning of the period to 1984 and increases from 1984 on at both points. To analyze trends the original data were considered instead of the 2-year running average. During the decrease period (1969-1984) the upwelling intensity at each point shows a negative trend with values of -6 m^3 s^{-1} km^{-1} yr^{-1} at 7.5ºW and -4 m^3 s^{-1} km^{-1} yr^{-1} at 6.5ºW. From 1984 to 2005, intensity shows a positive trend with values of 6 m^3 s^{-1} km^{-1} yr^{-1} at 7.5ºW and 3 m^3 s^{-1} km^{-1} yr^{-1} at 6.5ºW. Considering the whole time period (1967-2007), the upwelling intensity suggests a positive trend with values around 1 m^3 s^{-1} km^{-1} yr^{-1} at both points. Figure 3.4(b) shows the variation in the number of days per year under upwelling favorable conditions (UI>16 m^3 s^{-1} km^{-1}) from June to September at the 2 control points. Both points show a negative trend with values around -0.3 d yr^{-1}. From these figures it is possible to observe the existence of interdecadal variations in upwelling conditions although the low statistical significance obtained (significance level<90%) shows that the trend is not clear. The upwelling intensity and duration was also analyzed by means of the expression $\sum_{i=1}^{N} n_i < UI >_i^F$ where n_i is the number of consecutive days under upwelling favorable conditions considering $n_i \geq 3$, $<UI>_i^F$ is the mean intensity of UI during these days and N is the number of events per year. Both control points show a negative trend although with a significance level<90%. These results are in contradiction with those of Llope et al. (2006) who found a decreasing trend of -1.75 m^3 s^{-1} km^{-1} yr^{-1} in upwelling intensity and no change in the number of days under upwelling

favorable conditions using an average of wind records from April to September, at the Asturias airport meteorological station from 1968 to 2003. This discrepancy can be due to the different period considered, the different position of the measurement point and the different source of wind data. It is necessary to take into account that wind data used by Llope et al. (2006) were measured at a land station where wind can be deflected by topographic features, while in the present work wind data are obtained from Sea Level Pressure fields over the ocean.

3.3.2. Water temperature analysis

Although the probability of upwelling events along the Cantabrian coast is considerably lower than along the Atlantic coast, upwelling events are still possible during summer months, being reflected in temperature changes both on the shelf and inside the estuaries.

3.3.2.1. Offshore Sea Surface Temperature

The presence of upwelled water at shelf can be analyzed in terms of $\nabla SST = SST^{coast} - SST^{ocean}$ (Figure 3.5), where the coastal region corresponds to the area between coast and 200m isobath (black line shown in Figure 3.1(a)) and the ocean region to the area between 44.5-45.5ºN and 5.5-8.5ºW. SST values were spatially averaged for the points inside these regions for every summer month (June-September) from 1985 to 2007. This gradient is similar to the Upwelling Index obtained using SST data (Nykjaer and Van Camp, 1994; Santos et al., 2005; deCastro et al., 2008b), which can be calculated as the SST gradient between coastal and oceanic locations at the same latitude. In the present study, this gradient cannot be considered as an absolute Upwelling Index since temperature also changes with latitude

due to differences in solar heating. However, it can provide an estimation of the presence of cold water near coast which can be related to upwelling events.

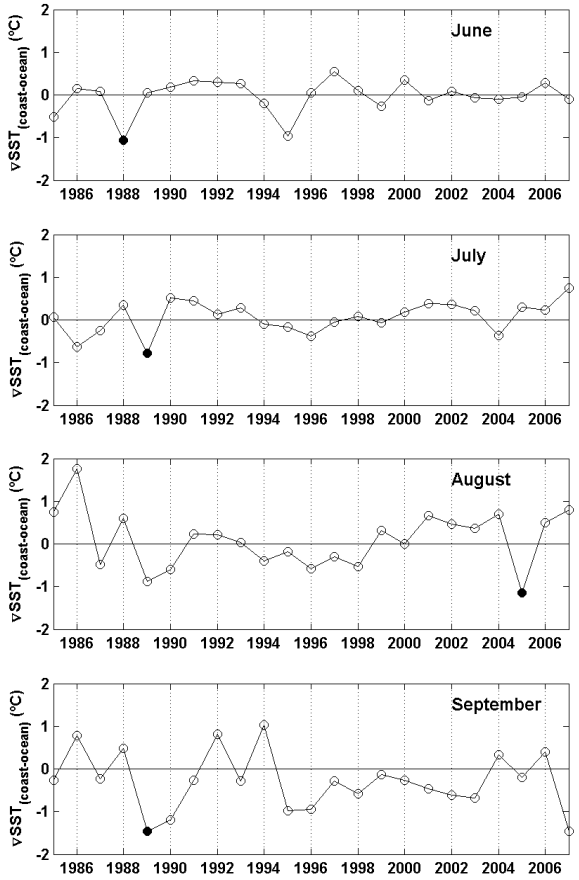

Figure 3.5. Monthly SST difference between a coastal and ocean region spatially averaged in June, July, August and September. The coastal region corresponds to the area between the shoreline and the 200m isobath (black line shown in Figure 3.1(a)) and the ocean region to the area between 44.5-45.5ºN and 5.5-8.5ºW. Full circles refer to the extreme values observed for each summer month.

In general, ∇SST is close to zero (Figure 3.5), which corresponds to neutral conditions without important upwelling events. Sharp negative peaks on the order of 1ºC correspond to years under strong upwelling favorable conditions. In particular, these events have been observed in June (1988 and 1995), July (1986 and 1989), August (1989 and 2005) and September (1989, 1990 and 2007). The full circles refer to the extreme values observed for each summer month.

The ∇SST images shown in Figure 3.6 correspond to those particular months (June 1988, July 1989, August 2005 and September 1989). Temperature gradients were calculated as the difference between SST at the month under study and the SST average calculated using the previous and following 2 years. Thus, for example Figure 3.6(a) corresponds to the SST gradient between the situation observed in June 1988 and the average situation observed during the same month from 1986 to 1990. Voids correspond to cloud coverage. This procedure allows analyzing the behavior of the month under study with regard to the same month during the previous and following years in such a way that negative values near coast are linked to upwelling events. The observed results are independent of the averaging period although the chosen period (± 2 years in this particular case) should be long enough to remove interannual oscillations and short enough to prevent the overlap of close negative peaks. In all frames, the most negative ∇SST values, which range from -0.5 to -1.5 ºC, are observed over the shelf (the 200m isobath is depicted in Figure 3.1(a)) showing the existence of well developed upwelling events in the area. The spatial distribution of the upwelled water significantly differs between the four months under study. This could be due to the different wind conditions. Nevertheless, the

atmospheric conditions observed for the particular months analyzed in this figure correspond to extreme positive upwelling indices ranging from 200 to 300 $m^3\ s^{-1}\ km^{-1}$ (Table 3.II). In addition, the upwelling favorable conditions (positive indices) were observed to last for more than 10 consecutive days during each month under study. This might indicate a complexity of upwelling events that is not resolved by the UI.

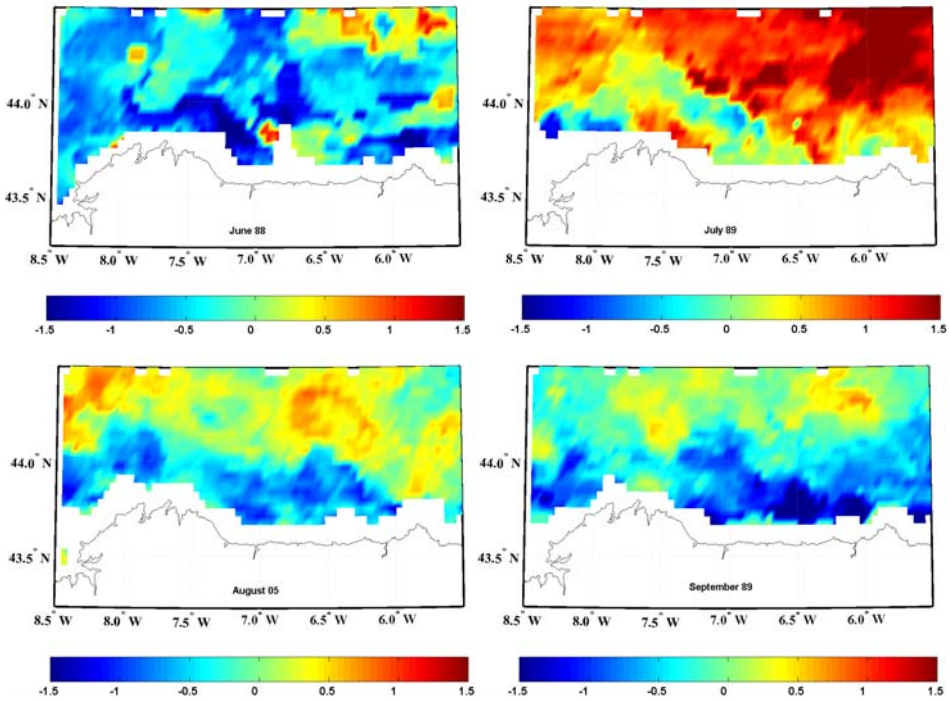

Figure 3.6. Monthly SST images corresponding to the difference calculated between (a) June 1988 and the average situation observed in June from 1986 to 1990, (b) July 1989 and the average situation observed in July from 1987 to 1991, (c) August 2005 and the average situation observed in August from 2003 to 2007, (d) September 1989 and the average situation observed in September from 1987 to 1991.

Punctual upwelling events have been depicted by other authors (Garcia- Soto et al., 2002) along the Cantabrian coast using AVHRR SST data. Here we have shown some of the most extreme events, which are characterized both by high intensity and long duration. Thus, a permanent SST decrease on the order of 1ºC has been observed to spread along the entire coastal area.

	∇SST$_{(coast-ocean)}$ (ºC)	UI (m^3 s^{-1} km^{-1})	
Jun-88	-1.07	326 (6.5º W)	335 (7.5º W)
Jul-89	-0.78	284	262
Aug-05	-1.14	196	226
Sep-89	-1.45	302	304

Table 3.II. ∇SST calculated by $SST^{coast} - SST^{ocean}$ corresponding to the particular months analyzed in Figure 3.6 and UI averaged for these months at the 2 control points (6.5ºW and 7.5ºW) located in the central part of the area under study.

3.3.2.2. Estuarine Temperature

Upwelling events along the Cantabrian coast have been studied by different authors (Botas et al., 1990; Prego and Bao, 1997) showing a temperature decrease at shelf. However, there is little evidence of upwelling inside the estuaries located in this area. Actually, only Alvarez et al. (2009) have shown the existence of upwelled water inside the northern Galician rias in winter.

Water temperature was measured at the inner part of one of the northern Galician rias (Ria de O Barqueiro) from June to September 2008 (Figure 3.1(b), black diamond (st. B)).

The northern Galician rias are funnel-like incised valleys characteristic of a relatively submergent coastline with 30-35 m depth at their open mouths and

around 0.1 km^3 of water content. The Ria de O Barqueiro, as the rest of the northern Galician rias, lies on a mesotidal coast with a tidal range of 2-4 m and is dominated by marine processes except at the inner estuarine zone which is partially enclosed with well-developed beach barriers (Alvarez et al., 2009). The temperature recorder was placed in the intertidal part of the estuary in order to identify temperature changes induced by possible upwelling events where commercial species as oysters are cultured.

This monitoring has shown evidence of recurrent upwelling events in the area. The time evolution of the water temperature daily measured inside the ria is depicted in Figure 3.7(a) (black solid line). Temperature signal shows a sequence between maxima and minima ranging from 17ºC to 21ºC. Note that the temperature axis range in the figure has been applied to easily identify the occurrence of the negative temperature peaks with regard to the positive UI peaks. UI was calculated at 3 control points located in front of the ria (Figure 3.1(a), black circles) using QuikSCAT data to characterize the origin of this temperature variation. The average of the 3 points was calculated and represented in Figure 3.7(a) (black dashed line). The UI signal also shows a sequence between maxima and minima. Maxima are related to easterly winds (upwelling favorable conditions) and minima to westerly winds. Taking into account the temporal evolution of temperature and UI signals, it is possible to observe that when a maximum occurs in UI, water temperature inside the ria shows a decrease a few days later. This behavior can be observed over the whole period showing evidence of different upwelling events which inject cold water from the ocean inside the ria. The correlation between UI and water temperature was calculated taking into account different lags between both variables (Figure 3.7(b)).

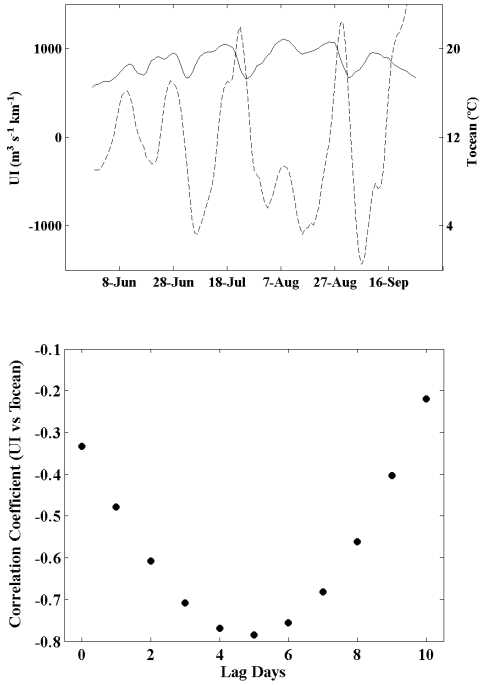

Figure 3.7. (a) Temporal evolution of water temperature daily measured inside the Ria de O Barqueiro (Figure 3.1(b), black diamond (st. B)) (black solid line) and temporal evolution of UI averaged at the 3 control points located in front of the northern Galician coast (Figure 3.1(a), black circles) (black dashed line) from June to September 2008. (b) Lag correlation between the UI series and that of the water temperature shown in Figure 3.7(a).

This correlation is negative because an increasing in UI implies a decreasing in water temperature. In addition, the correlation tends to increase as the number of lag days increases with the maximum value of -0.8 (significance level>95%) corresponding to a lag of 5 days.

The detected 5 days lag between the UI and the SST reaction shows that the effect of the wind pushing on the ocean surface has not an immediate

response observable at the measuring point. It is a known fact that atmosphere-ocean interactions take place on a wide range of spatial and temporal scales. Nevertheless, taking into account that the control station was located at the inner part of the Ria de O Barqueiro (Figure 3.1), the high lag could be due to the distance that the ocean upwelled water needs to cover to enter the ria until this point.

3.4. Summary and conclusions

The occurrence and intensity of upwelling events have been characterized along the western part of the Cantabrian coast from 1967 to 2007. The UI showed a marked annual cycle with maximum values (upwelling favorable) in July-August and minimum ones in December- January. During the winter season, EA/WR and EA patterns explain the main variance of UI while during summer the UI variability can be explained in terms of the EA pattern. The NAO pattern also shows some influence on UI.

The mean number of days under upwelling favorable conditions from June to September was around 12-14 days per month with a probability of finding these favorable conditions of ~17% when events of at least 5 consecutive days were considered. SST data also revealed the presence of cold water near coast associated to upwelling favorable winds.

In addition, the analysis of the water temperature dependence on upwelling conditions in the inter-tidal area of the Ria de O Barqueiro from June to September 2008 showed that when a maximum UI occurs, water temperature inside the ria decreases a few days later. Both variables presented a negative correlation which the maximum value of -0.8 corresponding to a lag of 5 days between them. The overall vertical velocity within the top layer results to be $<w>=Q_y/R_d$ where R_d is the Rossby radius. Taking into account that at

this region R_d is about 12 km (Gil and Gomis, 2008) and considering Q_y=0.3 m^2s^{-1} (see Figure 3.2(b), section 3.1), it results <w>~2.5 10^{-5} ms^{-1}. The typical SST response time was estimated to be about 5 days, consequently the overall mixing (stirring) depth-scale results to be 5d*<w>~11 m, a quite plausible value for the study area.

Finally, the present study has shown that intense and long lasting upwelling events can be observed over the western Cantabrian continental shelf although they are not as common as along the Atlantic coastline. This fact could provide favorable development conditions inside the estuaries for larval survival of IAS from warmer waters.

3.5. References

Alvarez, I., deCastro, M., Prego, R., Gomez-Gesteira, M., 2003. Hydrographic characterization of a winter-upwelling event in the Ria of Pontevedra (NW Spain). Estuarine Coastal and Shelf Science, 56, 869-876.

Alvarez, I., deCastro, M., Gomez-Gesteira, M., Prego, R., 2005. Inter- and intra-annual analysis of the salinity and temperature evolution in the Galician Rías Baixas-ocean boundary (northwest Spain). Journal of Geophysical Research, 110, C04008, doi:10.1029/2004JC002504.

Alvarez, I., Gomez-Gesteira, M., deCastro, M., Novoa, E.M., 2008a. Ekman Transport along the Galician Coast (NW, Spain) calculated from QuikSCAT winds. Journal of Marine Systems, 72, 101-115.

Alvarez, I., Gomez-Gesteira, M., deCastro, M., Dias, J.M., 2008b. Spatio-temporal evoltion of upwelling regime along the western coast of the

Iberian Península. Journal of Geophysical Research, 113, C07020, doi:10.1029/2008JC004744.

Alvarez, I., Ospina-Alvarez, N., Pazos, Y., deCastro, M., Bernardez, P., Campor, M.J., Gomez-Gesteira, J.L., Alvarez-Ossorio, M.T., Varela, M. Gomez-Gesteira, M., Prego, R., 2009. A winter upwelling event in the Northern Galician Rias: Frequency and oceanographic implications. Estuarine Coastal and Shelf Science, 82, 573-582, doi:10.1016/j.ecss.2009.02.023.

Alvarez- Salgado, X.A., Gago, J., Miguez, B.M., Gilcoto, M, Perez, F.F., 2000. Surface waters of the NW Iberian Margin: Upwelling on the shelf versus outwelling of upwelled waters from the Rias Baixas. Estuarine Coastal and Shelf Science, 51, 821-837.

Alvarez- Salgado, X.A., Nieto-Cid, M., Gago, Brea, S., Castro, C.G., Doval, M.D., Perez, F.F., 2006. Stoichiometry of the degradation of dissolved and particulate biogenic organic matter in the NW Iberian upwelling. Journal of Geophysical Research, 111(C07017), doi:10.1029/2004JC002473.

Bakun, A., 1973. Coastal Upwelling Indexes, west coast of North America, 1946–71. NOAA Technical Report, vol. 671. NMF, p. 103.

Bode, A., Varela, M., Casas, B., Gonzalez, N., 2002. Intrusions of eastern North Atlantic central waters and phytoplankton in the north na dnorthwesttern Iberian shelf during spring. Journal of Mairne Systems 36, 197-218.

Borges, M.F., Santos, A.M.P., Crato, N., Mendes, H., Mota, B., 2003. Sardine Regime shifts off Portugal: a time series analysis of catches and wind conditions. Scientia Marina, 67, 235-244.

Botas, J., Fernandez, E., Bode, A., Anadon, R., 1990. A persistent upwelling off the Central Cantabrian Coast (Bay of Biscay). Estuarine Coastal and Shelf Science, 30, 185–199.

Cabanas, J.M., Alvarez, I., 2005. Ekman transport patterns in the area close to the Galician coast (NW, Spain). Journal of Atmospheric and Oceanographic Science, 10, 325-341.

deCastro, M., Dale, A.W., Gomez-Gesteira, M., Prego, R., Alvarez, I., 2006a. Hydrographic and atmospheric analysis of an autumnal upwelling event in the Ria of Vigo (NW Iberian Peninsula). Estuarine Coastal and Shelf Science, 68, 529-537, doi:10.1016/j.ecss.2006.03.004.

deCastro, M., Lorenzo, N., Taboada, J.J., Sarmiento, M., Alvarez, I., Gomez-Gesteira, M., 2006b. Teleconnection patterns influence on precipitation variability and on river flow regimes in the Miño River basin (NW Iberian Peninsula). Climate Research, 32, 63- 73.

deCastro, M., Gomez-Gesteira, M., Alvarez, I., Cabanas, J.M., Prego, R., 2008a. Characterization of fall-winter upwelling recurrence along the Galician western coast (NW Spain) from 2000 to 2005: dependence on atmospheric forcing. Journal of Marine Systems, 72, 145-148, doi:10.1016/j.jmarsys.2007.04.005.

deCastro, M., Gomez-Gesteira, M., Lorenzo, M.N., Alvarez, I., Crespo, A.J.C., 2008b. Influence of atmospheric modes on coastal upwelling along the western coast of the Iberian Península, 1985 to 2005. Climate Research, 36, 169-179, doi:10.3354/cr00742.

Fiuza, A.F.G., 1984. Hidrologia e dinamica das aguas costeiras de Portugal (Hydrology and dynamics of the Portuguese coastal water). Ph.D. Thesis, University of Lisboa, Lisboa. 294 pp.

Fraga, F., 1981. Upwelling off the Galician Coast, Northwest Spain, in: Richardson, F.A. (Ed.), Coastal Upwelling. American Geophysical Union, Washington, pp. 176-182.

Garcia-Soto, C., Pingree, R. D., Valdes, L., 2002. Navidad development in the southern Bay of Biscay: climate change and swoddy structure from remote sensing and in situ measurements. Journal of Geophysical Research, 107 (C8), doi: 10.1029/2001JC001012.

Gil, J., Gomis, D., 2008. The secondary ageostrophic circulation in the Iberian Poleward Current along the Cantabrian Sea (Bay of Biscay). Journal of Marine Systems, 74, 60-73.

Gomez-Gesteira, M., Moreira, C., Alvarez, I., deCastro, M., 2006. Ekman transport along the Galician coast (NW, Spain) calculated from forecasted winds, Journal of Geophysical Research, 111(C10005), doi: 10.1029/2005JC003331.

Lorenzo, M.N., Taboada, J.J., 2005. Influences of atmospheric variability on freshwater input in Galician Rias in winter. Journal of Atmosphere and Ocean Sciences, 10, 377-387.

Llope, M., Anadon, R., Viesca, L., Quevedo, M., Gonzalez-Quiros, R., Stenseth, N.C., 2006. Hydrography of the southern Bay of Biscay shelf-break region: Integrating the multiscale physical variability over the period 1993-2003. Journal of Geophysical Research, 111(C09021), doi: 10.1029/2005JC002963.

Mann, R., Burreson, E.M., Baker, P.K., 1991. The decline of the Virginia oyster fishery in Chesapeake Bay: Considerations for introduction of a non-endemic species, Crassostrea gigas (Thunberg, 1793). Journal of Shellfish Research, 10, 379-388.

Nykjaer, L., Van Camp, L., 1994. Seasonal and Interannual variability of coastal upwelling along northwest Africa and Portugal from 1981 to 1991. Journal of Geophysical Research, 99(C7), 14197-14207

Prego, R., Bao, R., 1997. Upwelling influence on the Galician coast: silicate in shelf water and underlying surface sediments. Continental Shelf Research, 17, 307-318.

Prego, R. Guzmán-Zuñiga, D., Varela, M., deCastro, M., Gomez-Gesteira, M., 2007. Consequences of winter upwelling events on biogeochemical and phytoplankton patterns in a western Galician ria (NW Iberian peninsula). Estuarine Coastal and Shelf Science, 73, 409-422.

Ríos, A.F., Pérez, F.F., Alvarez-Salgado, X.A., Figueiras, F.G., 1992. Water masses in the upper and middle North Atlantic Ocean east of the Azores. Deep-Sea Research I, 39, 645–658.

Rodríguez-Puebla, C., Encinas, A.H., Nieto, S., Garmendia, J., 1998. Spatial and temporal patterns of annual precipitation variability over the Iberian Peninsula. International Journal of Climatology, 18, 299-316.

Ruiz, C., Abad, M., Sedano, F., García-Martín, L.O., Sánchez López, J.L., 1992. Influence of seasonal environmental changes on the gamete production and biochemical composition of Crassostrea gigas (Thunberg) in suspended culture in El Grove, Galicia, Spain. Journal of Experimental Marine Biology and Ecology, 155, 249-262.

Santos, A.M., Borges, M.F., Groom, S., 2001. Sardine and horse mackerel recruitment and upwelling off Portugal. ICES Journal of Marine Science, 58, 589- 596.

Santos, A.M.P., Peliz, A., Dubert, J., Oliveira, P.B., Angelico, M.M., Re, R., 2004. Impact of a winter upwelling event on the distribution and transport of sardine (Sardina pilchardus) eggs and larvae off western Iberia: a retention mechanism. Continental Shelf Research, 24, 149-165, doi:10.1016/j.csr.2003.10.004.

Santos, A.M., Kazmin, A.S., Peliz, A., 2005. Decadal changes in the Canary upwelling system as revealed by satellite observations: Their impact on productivity. Journal of Marine Research, 63, 359- 379.

Shatkin, G., Shumway, S. E., Hawes, R., 1997. Considerations regarding the possible introduction of the Pacific oyster (*Crassostrea gigas*) to the Gulf of Maine: a review of global experience. Journal of Shellfish Research, 16, 463-477.

Torres, R., Barton, E.D., Miller, P., Fanjul, E., 2003. Spatial patterns of wind and sea surface temperature in the Galician upwelling region. Journal of Geophysical Research, 108, 3130- 3143, doi:10.1029/2002JC001361.

Chapter 4

Winter upwelling in the Northern Galician Rias

Abstract

A winter shelf-water upwelling evidence (February 2008) is described by first time in the Northern Galician Rias (NW Iberian Peninsula). On February 20, after 9 consecutive days of upwelling favorable conditions, inside the O Barqueiro Ria was observed the presence of seawater below 10 m depth which replaced the less saline water previously observed in January. This situation was in agreement with the analyzed Ekman transport close to the northern Galician coast. Salinity and temperature distribution revealed that the upwelled water inside the rias corresponds to shelf bottom seawater which is not associated with Eastern North Atlantic Central Water or the Iberian Poleward Current. In addition, TS diagram indicated a higher influence of upwelling eastward (Viveiro-Barqueiro-Ortigueira). Nutrient salts concentrations also suggested the presence of seawater from subsurface origin with a small variation with regard to the winter mixing in this marine area. Plankton showed the existence of spring conditions related to solar radiation increase associated to upwelling favorable winds. Some species also corroborated the intrusion of shelf water inside the ria. Results from the analysis of Ekman transport data from 1967 to 2007 revealed that this event cannot be considered an isolated episode. In fact, the number of days per month under upwelling favorable conditions in winter (January-March) was not negligible (8-10 days) showing that upwelling events along the northern Galician coast are also possible during winter.

4.1. Introduction

The western Galician coast, south of Cape Finisterre, is the northernmost limit of the Eastern North Atlantic Upwelling System (ENAUS), which extends from 10ºN to about 44ºN (Wooster et al., 1976). Upwelling has important biological implications due to the high input of nutrients that triggers the great primary productivity of this coast, supporting an intense mussel raft culture (Blanton et al., 1987). Coastal upwelling is commonly observed along the western Galician coast during spring-summer and has been extensively studied during the last decades (Fraga, 1981; Prego et al., 2001; Alvarez et al. 2005; Alvarez-Salgado et al., 2006; Gomez-Gesteira et al., 2006; Alvarez et al., 2008). Upwelling injects a colder nutrient-rich deeper water (Prego et al., 1999), known as Eastern North Atlantic Central Water mass (ENACW; Fiuza, 1984; Rios et al., 1992) into the Western Galician Rias (locally named Rias Baixas). Although this coastal upwelling is basically a spring–summer process linked to NE winds, it has also been observed in autumn-winter under some special conditions. Alvarez et al. (2003) characterized a winter upwelling event in January 1998, pumping seawater driven by the Iberian Poleward Current into the Pontevedra Ria. The mechanism driving this winter upwelling was similar to the one observed in summer, but the poleward intrusion varied the ria thermohaline properties and residence time, making it much more salty and rendering it poor in nutrient salts; nonetheless the taxonomic composition of the phytoplankton community did not change noticeably, changing only in relative proportions (Prego et al., 2007). deCastro et al. (2006) studied an autumnal upwelling event in November 2001 inside Vigo Ria. Thermohaline variables revealed that the upwelled water mass was ENACW. These studies are not isolated events because deCastro et al. (2008) found six upwelling

events in the Western Rias during the wet season (November to February) from 2000 to 2005 with features similar to the ones observed in summer.

North of Cape Finisterre is the northern Galician coast. Eastward of 8ºW (Cape Ortegal), approximately along the 43.6ºN parallel are located the Northern Galician Rias (locally named Rias Altas). This coastal zone can be considered as the westernmost limit of the Cantabrian littoral where easterly winds parallel to the coast generate occasional spring-summer coastal upwelling at the eastern and middle Cantabrian coast (Botas et al., 1990; Fontan et al., 2008), cooling and fertilizing surface waters resulting in a primary production increase (Fernandez and Bode, 1991; Llope et al., 2006). Nevertheless, these phytoplankton productive events are less important than those observed in the Western Rias, south of Cape Finisterre (Varela et al., 2005). At the northern Galician coast, upwelling is also present although is not a common event. Previous studies showed that north of Cape Finisterre, upwelling is discontinuous and remains near the edge of the continental shelf (Prego and Bao, 1997). It is already known that upwelling events with similar features can occur at both sides of Cape Finisterre but with different probability and intensity. Torres et al. (2003) described the Galician upwelling region from July 1999 to May 2001 using 2 years of wind data from the QuikSCAT satellite. They found that the wind patterns may alternate producing brief episodes of upwelling at the northern or western coast, or a combined pattern may occur producing weak upwelling on both coasts. In addition, Gomez-Gesteira et al. (2006) analyzed Ekman transport close to the Galician coast using forecasted winds from November 2001 to October 2004. They found that upwelling reaches a maximum probability of 60% at western coast during summer and a minimum probability of around 15% in December-January. On the other hand, the probability of upwelling

favorable conditions never surpasses 30% at the northern coast, with two maxima in March and September and a minimum in December-January. These results were corroborated by Alvarez et al. (2008) using QuikSCAT satellite data from November 1999 to October 2005. There are not studies involving upwelling events inside the Northern Galician Rias. Nevertheless, other type of studies have been developed focused on biological characteristics, as the mortality in populations of flat oyster (Montes et al., 1991; 1992) and the salt march and sedimentary characteristics (Otero et al., 2000; Delgado et al., 2002; Lorenzo et al., 2007). Clearly, there is a lack of knowledge about the upwelling development in this area and its influence on biological processes. Thus, the aim of this paper is (i) to characterize a winter shelf-water upwelling evidence (February, 2008) and its consequences on the biological and chemical patterns in the water column of the Northern Galician Rias, and (ii) to find out the recurrence of these winter events at the northern Galician coast over a long period (1967-2007).

4.2. Data and methods

4.2.1. Study area

The Northern Galician Rias of Ortigueira (38 km^2 of surface), O Barqueiro (10 km^2) and Viveiro (27 km^2) are funnel-like incised valleys characteristic of a relatively submergent coastline (Evans and Prego, 2003) with 30-35 m depth at their open mouths to the north, and around 0.1 km^3 of water content (Figure 4.1(a)). At the innermost area, these rias receive the fluvial discharges of the Mera (annual average flow: 6.3 $m^3 \cdot s^{-1}$), Sor (6.0 $m^3 \cdot s^{-1}$) and Landro (7.1 $m^3 \cdot s^{-1}$) Rivers (Río-Barja and Rodríguez-Lestegás, 1992) with a seasonal regime with higher flow in winter and lower flow in summer, in

accordance with the wet temperate climate (Cfb Köppen type) of this geographical area.

The Northern Rias lie on a mesotidal coast with a tidal range of 2-4 m and a NW swell, but waves are diffracted to the NE due to the rias morphology. They are dominated by marine processes except at the inner estuarine zone which is partially enclosed with well-developed beach barriers (Lorenzo et al., 2007).

4.2.2. Atmospheric variables

Surface wind fields from January to February 2008 were provided by the QuikSCAT satellite (see Chapter 2). Five control points were considered along the northern Galician coast at the latitude 44.25ºN. The obtained discrete series covers from 8.25ºW to 7.25ºW (Figure 4.1(b), black points). Previous studies have shown that QuikSCAT data are comparable to modeled data in this area (Gomez-Gesteira et al., 2006; Alvarez et al., 2008). Actually, a statistical comparison between satellite wind measurements and high resolution numerical models was carried out (Penabad et al., 2008), revealing similar results between models and satellite data.

Ekman transport was calculated using wind data from QuikSCAT satellite, W, the sea water density, ρ_w= 1025 kg m^{-3}, a dimensionless drag coefficient, C_d=1.4×10^{-3}, and the air density, ρ_a= 1.22 kg m^{-3}, by means of

$$Q_x = \frac{\rho_a C_d}{\rho_w f}\left(W_x^2 + W_y^2\right)^{1/2} W_y \text{ and } Q_y = -\frac{\rho_a C_d}{\rho_w f}\left(W_x^2 + W_y^2\right)^{1/2} W_x$$

f is the Coriolis parameter defined as twice the vertical component of the Earth's angular velocity, Ω, about the local vertical given by $f = 2\Omega\sin(\theta)$

at latitude θ. Finally, x subscript corresponds to the zonal component and y subscript to the meridional one.

Ekman transport data from January 1967 to December 2007 were provided by the Pacific Fisheries Environmental Laboratory (see Chapter 2). For our purposes six-hourly Ekman transport data were considered at the control point 45.5ºN, 7.5ºW located in front of the northern Galician coast (Figure 4.1(b), black square) on an approximately 1º×1º grid. These data lie on a coarser spatial grid than the QuikSCAT ones although with a longer temporal extent which allows analyzing the temporal variability of upwelling. Data were averaged to a daily timescale.

The daily Ekman transport calculated from both databases can be compared taking into account the common period between both databases (1999-2007) at the control point located in front of the northern Galician coast (45.5ºN, 7.5ºW). This comparison was made in terms of the correlation coefficient ($r_{a,b}$, a: QuikSCAT data, b: PFEL data), which was calculated by $r_{a,b} = Cov(a,b)/\sigma_a \cdot \sigma_b$. In addition, the amplitude difference was analyzed in terms of the dimensionless parameter $\alpha = \sqrt{\sum_{i=1}^{N} a_i^2 \Big/ \sum_{i=1}^{N} b_i^2}$. The obtained correlation coefficient for both components is around 0.8-0.9 (significance level >99%) showing a good correlation between both data bases. The amplitude parameter for the zonal component (1.01) shows that the PFEL data amplitude is slightly smaller than the QuikSCAT one, while for the meridional component this parameter (0.93) shows that the PFEL data amplitude is slightly higher than the QuikSCAT one.

Upwelling Index (UI) can be defined as the Ekman transport component in the direction perpendicular to the shoreline (Nykjaer and Van Camp, 1994;

Gomez- Gesteira et al., 2006). Although the shoreline angle along the northern Galician coast changes slightly from the eastern to the western limit, macroscopically it can be considered approximately parallel to the equator. Thus, the Q_y component can be directly considered as the UI. Positive (negative) UI values mean upwelling favorable (unfavorable) conditions.

4.2.3. Sea variables

Two cruises were carried out in the Northern Galician Rias onboard the R/V *Lura* in January 22-23 and February 20-21, 2008. Thermohaline variables were measured at five stations located along the main channel of the O Barqueiro Ria with depths increasing from 7 m inshore to 50 m offshore (Figure 4.1(a)). In addition, a control point was also considered near the mouth of Ortigueira Ria and Viveiro Ria (Figure 4.1(a), station 6). Temperature and salinity profiles were measured by means of a General Oceanic Rosette, including a CTD 25 SeaBird with PAR and Fluorescence sensors. The water column at each station was also sampled using General Oceanic Niskin bottles of 5 L. Aliquots were collected along the main channel of the O Barqueiro Ria at standard depths (0, 5, 10, 20, 30 and 40 m) from surface to near bed to analyze (i) dissolved oxygen concentration, using the Winkler method to calculate saturation percentages (Aminot, 1983); (ii) nutrient salts, following the methods of Hansen and Grasshoff (1983) in a Integral Futura (Alliance Instruments) autoanalyzer system with separate lines to nitrate, nitrite, ammonium, phosphate and silicate determinations; (iii) chlorophyll-*a*, which samples were filtered through Whatman GF/F filters and extracted with 90% acetone (Unesco, 1994) to determine its concentration by spectrofluorimetry (Neveux and Panouse, 1987).

At station 5, located at the central part of the main channel of the O Barqueiro Ria (Figure 4.1(a)), were also measured at the same standard depths: (i) particulate organic carbon (POC) and nitrogen (PON) after aliquot filtration through Whatman GF/F filters, using a FlashEA 11-12 Termoquesth CNH analyzer; (ii) primary production by the ^{14}C method using 2 h onboard incubations simulated under in situ conditions (Bode and Varela, 1994); after incubation, samples were filtered through GF/F filters and daily primary production rates calculated by multiplying hourly rates by the total number of hours during the day, excluding the first 2 h after sunrise and the last 2 h before sunset (Varela et al., 2005); (iii) phytoplankton abundances after preservation with Lugol's solution following the technique described by Utermöhl (1958); the nomenclature for species followed that of Tomas (1997).

Planktonic ciliates were sampled, identified and counted as in the case of phytoplankton. Microzooplankton (40-200 mμ) samples were obtained with vertical hauls of a bongo-type net of 40 μm mesh-size (20 cm diameter) equipped with a flowmeter from near bed to surface. The samples were screened through a nylon mesh of 200 μm and preserved with borate-buffered formalin (2% final concentration) until examination under the microscope. Specimens were grouped in broad taxonomic categories as described in Valdés et al. (1991). Samples of mesozooplankton were collected by means of double-oblique tows from bed to surface of a Juday-Bogorov type net of 200 μm mesh-size (50cm diameter) and equipped with flow and depth meters (Bode et al., 1998). Samples were preserved with a final concentration of 4%.

Suspended particulate matter fluxes to sediment were also measured at station 5 using a multitrap collector system deployed 5 m over the sea-bed

and anchored for a 24 h period. The trap system was described in Knauer et al. (1984), following the JGOFS protocols (Unesco, 1994) (for a complete description of the system see Varela et al. (2004)). Aliquots of the collected material were filtered through Whatman GF/F filters to determine POC (carbonate was not removed from filters, but its contribution may represent about 2% of total carbon flux (Fernandez et al., 1995; Palanques et al., 2002)), PON, chlorophyll-*a* and phytoplankton identification.

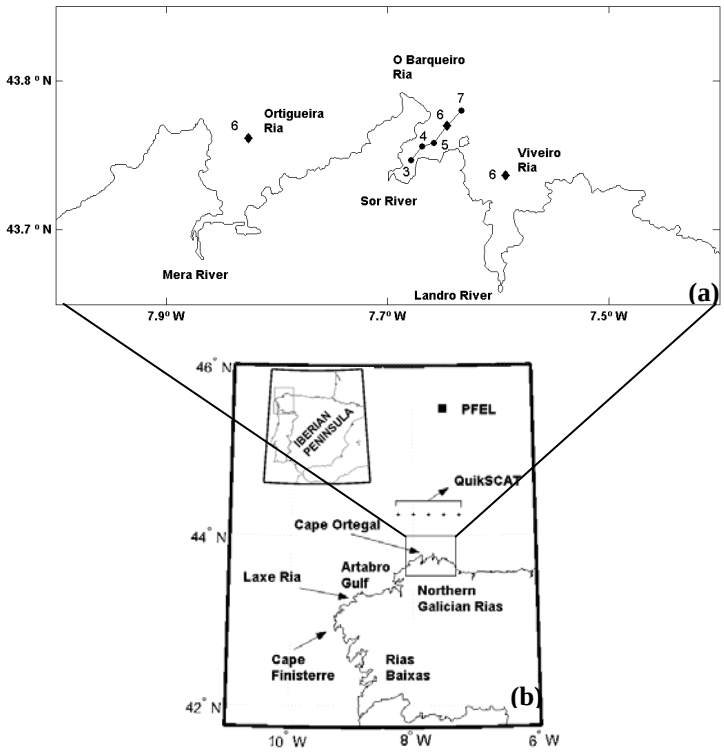

Figure 4.1. (a) Map of northern Galician Rias showing the sampling hydrographic stations (black circles). (b) Black square represent the point where data from the PFEL database were obtained and black points represent the 5 control points considered to analyze wind data provided by the QuikSCAT satellite.

In addition to the previous measured variables during these cruises, salinity and temperature CTD data (Sea-Bird 9/11) measured on 15 February 2008 (R/V *Cornide de Saavedra*) at six stations from 69 to 2,742 m depth along the 8ºW meridian (Cape Ortegal) were kindly supplied by the 'Instituto Español de Oceanografia' (project 'Radiales Profundos 02-08').

4.3. Results and Discussion

4.3.1. Atmospheric conditions

Figure 4.2 shows the Ekman transport behavior in the area of the Northern Galician Rias corresponding to the cruises carried out in January (a) and February (b) 2008. Ekman transport was calculated at 5 control points by means of wind data provided by the QuikSCAT satellite and was averaged for 4 days before each cruise. In January (Figure 4.2(a)), transport was mainly directed southward (upwelling unfavorable) showing approximately the same direction and amplitude at each point. In February (Figure 4.2(b)), the transport pattern was completely different pointing northward (upwelling favorable) along the coast and with the maximum intensity at the western area.

To analyze the temporal evolution of the Ekman transport, the Q_y component was represented at the 5 control points from January to February 2008 (Figure 4.2(c)). The 5 control points showed a similar behavior in direction and amplitude. During January and February, two periods of positive Q_y values were observed with maximum values on the order of 1500 $m^3 s^{-1} km^{-1}$. The first one covers from January 26 to February 5 and the second one from February 12-28. Thus, the cruise corresponding to February 20-21 was carried out after 9 consecutive days of upwelling favorable conditions. For the rest of the period under study, the meridional component showed

negative values with two important minima around -3800 m^3 s^{-1} km^{-1} on January 20 and -2300 m^3 s^{-1} km^{-1} on February 10.

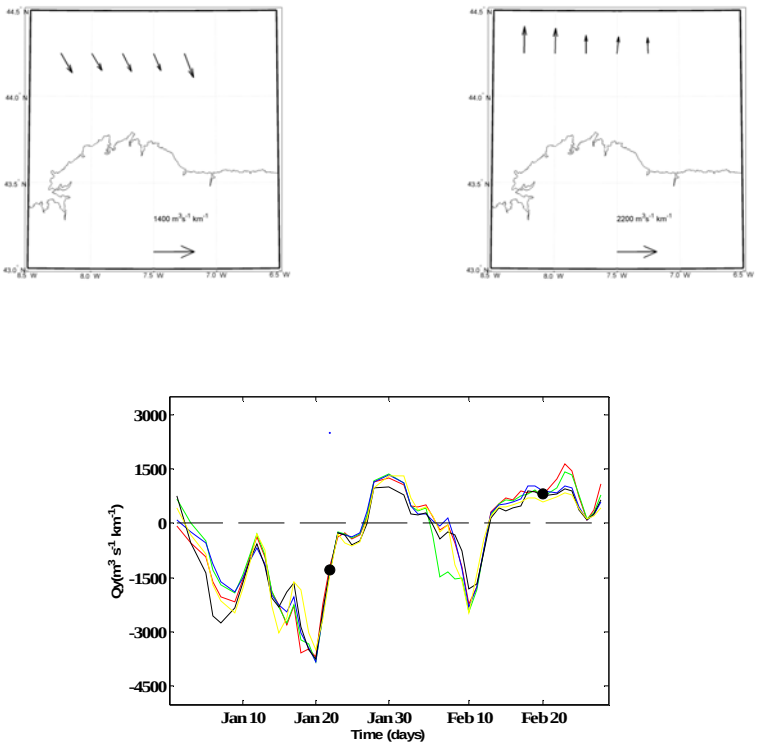

Figure 4.2. Ekman transport calculated at 5 control points (see Figure 4.1(b)) in the area of the northern Galician rias corresponding to the cruises carried out in January (a) and February (b) 2008. Data were averaged for 4 days before each cruise. (c) Temporal evolution of the meridional component of Ekman transport (Q_y) at the 5 control points from January to February 2008. Black points represent the date of each cruise.

4.3.2. Oceanographic conditions

To characterize the hydrographical, biogeochemical and phytoplankton patterns observed in the Northern Galician Rias during the two cruises under scope, the distribution of thermohaline variables, nutrient salts and planktonic material was studied along the main channel of the O Barqueiro Ria (see Figure 4.1(a)).

In January, the salinity distribution along the main channel of the O Barqueiro Ria (Figure 4.3, left panel) showed values between 35.0 near surface and 35.7 near bed with a higher stratification near surface. Temperature range throughout the water column (not shown) was small (13.2-13.7ºC) with a thermal inversion typical of winter weather conditions and density (not shown) was mainly the result of the salinity gradient showing isolines similar to the ones observed for salinity, with a small variation decreasing from 26.3 kg m^{-3} near surface to 26.8 kg m^{-3} near bed. Salinity values corresponding to February (Figure 4.3, right panel) ranged from 34.1 near surface to 35.8 near bed. This high salinity value was observed from around 10 m to near bed suggesting the presence of seawater. The lowest salinity values were measured near surface at the inner part of the ria due to the freshwater input (average flow of sampling date and the five previous days: 10.2±0.3 $m^3 \cdot s^{-1}$). In addition, the water column was more stratified near surface (~5 m) than near bed. Temperature distribution (not shown) displayed low vertical variations with a thermal inversion (13.5ºC near surface, 13.6ºC near bed) and density (not shown) was similar to the salinity distribution ranging from 25.7 kg m^{-3} near surface to 26.9 kg m^{-3} near bed. Thus, thermohaline properties under 10 m depth were practically homogeneous.

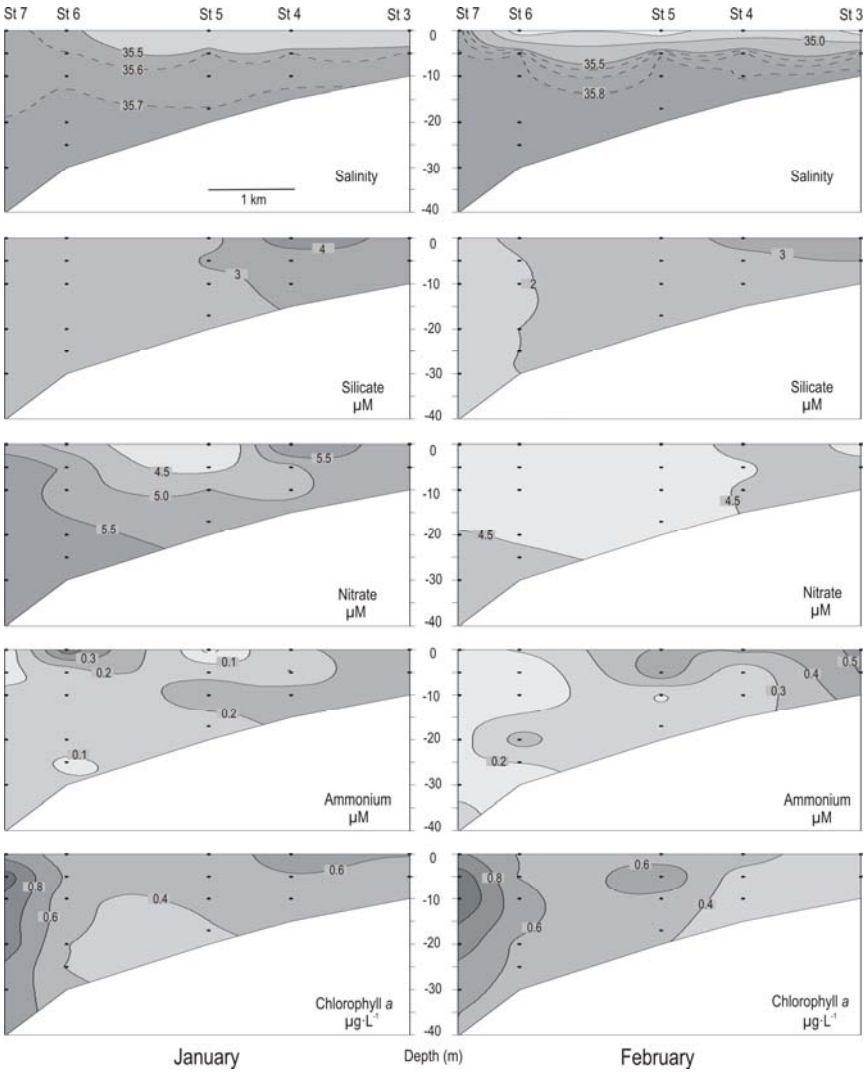

Figure 4.3. Contour maps of salinity, dissolved silicate, nitrate, ammonium and chlorophyll-*a* along the main channel of the Ria de O Barqueiro in January (left panel) and February (right panel) 2008. Station positions are indicated in Figure 4.1(a). Black points indicate sampling depths.

The TS diagram corresponding to data measured on 15 February 2008 along the 8ºW meridian (Figure 4.4) showed how the water column was vertically homogeneous west of Cape Ortegal (station A, B and C; Figure 4.4) due to winter cold conditions and to the lack of continental water supply. Note that the winter prevailing current is poleward in this area. East of Cape Ortegal, salinity and temperature values measured at the mouth of the northern rias showed that in February TS salinity profiles were not lineal. Surface seawater layer becomes heterogeneous due to the freshwater discharges from the rivers flowing into the rias and to a shelf-water intrusion, which reached the sub-surface layer. As well, TS diagram indicates a higher influence of upwelling eastward (Viveiro-Barqueiro-Ortigueira) when TS profiles are compared with the values of ENACW (station D, E and F; Figure 4.4).

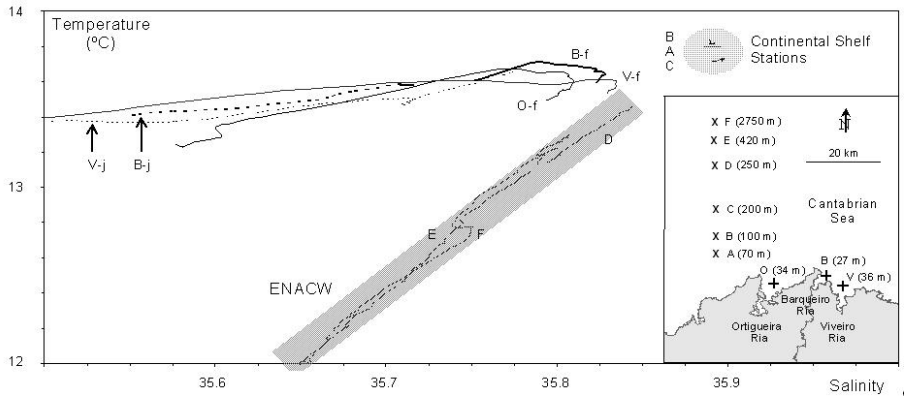

Figure 4.4. TS diagram corresponding to the stations located at the mouth of the northern rias (station 6 in Figure 4.1(a)) of Ortigueira (O), O Barqueiro (B) and Viveiro (V) in January (-j) and February (-f). Stations along the 8º W meridian (A-F) are also included to show the Eastern North Atlantic Central Water (ENACW grey band using D-F data from 150 to 300 m depth) and the continental shelf pattern (A-C). The stations position is shown in the map of lower-right corner with depth indicated between brackets.

Taking into account temperature and salinity values of the upwelled seawater in February inside the northern rias it is possible to ensure that this water cannot be associated with ENACW (Figure 4.4) or IPC (water transported by the Iberian Poleward Current; Frouin et al., 1990; Alvarez et al., 2003; Gil, 2003; Prego et al., 2007), but to shelf bottom water. This situation is in agreement with previous studies which showed that north of Cape Finisterre these water bodies keep distant from the coast, near the shelf break (Prego and Bao, 1997; Bao et al., 1997). Thus, a stronger meteorological forcing would be necessary to observe ENACW (Botas et al., 1990) or IPC (Gonzalez-Pola et al., 2005) inside the Northern Galician Rias.

The salinity decrease observed near surface in January at the inner part of the ria due to river outflow (average flow of sampling date and the five previous days: 21.4±5.0 $m^3 \cdot s^{-1}$) showed a fluvial contribution of nutrients (station 3, 4; Figure 4.3). There was up to 4.9 μM of silicate, 5.6 μM of nitrate and 0.28 μM of ammonium inside the ria (Figure 4.3). A slight increase of nitrate was detected at the external part of the ria (station 7; Figure 4.3). Dissolved oxygen (not shown) showed a small variation ranging from 98% to 102 % of saturation percentage indicating well oxygenated waters. Phosphate and nitrite (not shown) presented homogeneous concentrations of 0.3 μM and 0.26 μM respectively all along the ria channel. Chlorophyll-*a* distribution (Figure 4.3) showed low values around 0.5 μgL^{-1} at the inner part increasing up to 1 μgL^{-1} at the external part of the ria (Figure 4.3).

In February, biogeochemical parameters (Figure 4.3) showed different patterns to the ones described for the previous cruise. Silicate and ammonium decreased seaward with maxima at the inner part of the ria near surface (station 3; Figure 4.3) (3.1 and 0.5 μM respectively), and minima at the external part (station 6; Figure 4.3) (2 and 0.2 μM respectively). Nitrate

displayed the opposite behavior with the lowest concentrations at the inner part near surface (3.9 μM) and the highest ones at the ria mouth near bed (4.6 μM). Dissolved oxygen percentage (not shown) was homogeneous throughout the whole water column, corresponding to 99-101% of saturation while phosphate and nitrite (not shown) presented nearly uniform concentrations (0.2-0.3 μM) all along the ria. Chlorophyll-a showed lower concentrations at the inner part of the ria near surface, around 0.3 μg L^{-1}, and higher ones at the external part (station 7) about 10 m depth, with values of 1.2 μg L^{-1} (Figure 4.3).

Nutrient salts distribution in the O Barqueiro Ria (Figure 4.3), with a January small-concentration increase in the inner ria as result of a higher river flow, also suggested the presence of seawater from subsurface origin because (i) the nutrient concentrations were the half of typical ENACW in the continental border (Fraga, 1981; Prego et al., 1999), and (ii) these concentrations did not varied significantly with regard to January levels (Figure 4.3), i.e. nitrate similar of the forecasted from water temperature of the winter mixing in this marine area (Prego et al., 1999). However, winter upwelling events have been observed to increase the ria-ocean exchange both in the western and in the Northern Galician Rias. As a result, the surface outflow caused in the O Barqueiro Ria a salinity vertical gradient and chlorophyll-*a* poverty in surface water, as previously observed in the Pontevedra Ria (Prego et al., 2007).

Values of particulate material throughout the water column were also analyzed in January (Table 4.I) at station 5 (Figure 4.1(a)). Integrated chlorophyll-*a* was low, around 8 mg m^{-2} as well as the primary production, about 0.3 gC m^{-2} d^{-1}. The sunny hours and solar radiation were 6.0±2.5 (h) and 820±200 (10kJ·m^{-2}), respectively (average of sampling date and the five

previous days, Viveiro Meteorological station). Particulate organic carbon (POC) and nitrogen (PON) were around 1100 and 130 mg m^{-2} respectively, with a C/N ratio of particulate organic matter (POM) of 10 (Table 4.I).

	January	February	Unit
Water column			
Chl *a*	7.8	9.8	$mg \cdot m^{-2}$
POC	1130	1355	$mgC \cdot m^{-2}$
PON	136	189	$mgN \cdot m^{-2}$
C/N	10.03	8.54	mol/mol
PP	0.31	0.14	$gC \cdot m^{-2} \cdot d^{-1}$
Sediment trap			
Chl *a*	0.96	0.67	$mg \cdot m^{2} \cdot d^{-1}$
POC	445	503	$mgC \cdot m^{2} \cdot d^{-1}$
PON	41	47	$mgN \cdot m^{2} \cdot d^{-1}$
C/N	12.63	12.48	mol/mol

Table 4.I. Values of particulate material throughout the water column and fluxes to sediment measured at station 5 (see Figure 4.1) in the Ria de O Barqueiro in January and February 2008. Chl *a*: chlorophyll-*a*; POC: particulate organic carbon; PON: particulate organic nitrogen; C/N: carbon/nitrogen ratio; PP: primary production.

The mean abundances of phytoplankton measured at station 5 (Table 4.II, January) were dominated by naked flagellates with mean abundances of 150 cells mL^{-1}. Larger phytoplankton showed a predominance of diatoms, with *Navicula cf transitans, Nitzschia longissima and Pseudonitzschia cf australis* as dominant species.

Phytoplankton group	**January**	**February**
(a) Dinoflagellate		
Amphidinium flagellans	0.4	2.8
Heterocapsa niei	0.0	1.3
Prorocentrum minimum	0.0	2.4
Scrippsiella trochoidea	0.0	1.6
Total dinoflagellate	0.6	9.6

(b) Diatoms		
Chaetoceros curvisetus	0.0	0.6
Chaetoceros dydimus	0.0	2.3
Chaetoceros gracilis	0.0	0.4
Chaetoceros spp	0.0	3.0
Chaetoeros debilis	0.0	1.1
Corethron hystrix	0.9	0.0
Lauderia annulata	0.0	0.7
Navicula cf *transitans*	3.7	0.4
Nitzschia longissima	1.7	3.3
Nitzschia longissima small	5.8	0.9
Pseudonitzschia cf *australis*	1.5	1.7
Rhizosolenia setigera	0.0	2.7
Thalassionema nitzschioides	0.0	0.7
Thalassiosira nana	1.1	0.0
Thalassiosira rotula	0.7	0.0
Thalassiosira subtilis	0.7	0.0
Total diatoms	18.0	19.0
(c) Flagellates		
Flagellates 3-10µm	151.5	348.8
(d) Chrysophyceans		
Dctyocha speculum	0.0	21.7
(e) Planktonic ciliates		
Lohmaniella ovalis	1.4	0.5
Lohmaniella oviformis	0.7	1.3
Myrionecta rubra	0.7	2.4
Srombidium epidemum	0.1	0.7
Strombidium acutum	0.3	0.4
Strombidium conicum	0.2	0.0
Strombidium dalum	0.1	0.4
Strombilidoium neptuni	0.0	0.2
Total ciliates	4.1	6.5
(f) Microzooplankton (40-200 µm)		
Bivalves larvae	446	48
Nauplii copepods larvae	110	2356
Apendicularia	9	785
Total microzooplankton	604	3590

(g) Mesozooplankton >200 µm		
Braquiura zoea	35	26
Acartia clausi	27	421
Acartia clausi juveniles	4	832
Acartia discaudata	0	308
Calocalanus stylimeris	0	3
Clausocalanus spp.	12	21
Ctenocalanus vanus	5	24
Copepodits	21	42
Isias clavipes	0	253
Oithona similis	9	82
Total mesozooplankton	130	2232

Table 4.II. Mean abundance of phytoplankton (cells mL^{-1}), planktonic ciliates (cells mL^{-1}), microzoo and mesozooplankton (in individuals m^{-3}) at station 5 (see Figure 4.1) in the Ria de O Barqueiro in January and February 2008.

Dinoflagellates were very scarce and *Amphidinium flagellans* was the characteristic species. Other groups displayed negligible abundances. Planktonic ciliates showed low abundances, around 4 cells m L^{-1}. Species of Genus *Lohmaniella* and *Myrionecta rubra* were the dominant taxa. Microzooplankton abundance was low, around 600 indiv m^{-3} and dominated by bivalve's larva. Mesozooplankton was also low with around 100 indiv m^{-3}, with Braquiura larva, *Acartia clausi* and copepodits as the main taxa (Table 4.II, January).

Taking into account the fluxes of particulate material collected in sediment traps (station 5), the flux of chlorophyll-*a* to near bed was around 1 mg Chl-*a* m^{-2} d^{-1} (Table 4.I, January) representing approximately 10 % of the water column stock. POC flux was higher than 400 mg C m^{-2} d^{-1} and accounted for 39 % of stock throughout the water column. The C/N ratio of the particulate material was about 12.

Fluxes of planktonic material showed that diatoms dominated the large phytoplankton in the trap samples (Table 4.III, January). Copepods fecal pellets were also frequent while dinoflagellates were extremely scarce and represented by small unidentified species.

In February, values of particulate material throughout the water column at station 5 (Table 4.I) showed that the integrated chlorophyll-*a* was around 10 mg m^{-2}. Primary production was low, about 0.15 gC m^{-2} d^{-1}. The sunny hours and solar radiation were 5.2±2.7 (h) and 940±310 (10kJ·m^{-2}), respectively (average of sampling date and the five previous days, Viveiro Meteorological station). POC and PON were around 1300 and 190 mg m^{-2} respectively, with a C/N ratio of particulate organic matter (POM) of 8.5 (Table 4.I).

Mean abundances of phytoplankton measured in February throughout the water column (Table 4.II) revealed that small flagellates were the most abundant component of phytoplankton, with abundances higher than 300 cells m L^{-1}. Phytoplankton species composition of larger phytoplankton showed a dominance of diatoms. In addition to the species found in January, *Chaetoceros* and *Rhizosolenia* species were the most representatives of this group. However, the dominant species of large phytoplankton was the Chrysophycean *Dictyocha speculum*, with abundances higher than 20 cells m L^{-1}. Dinoflagellates increased with regard to January, reaching abundances around 9 cells m L^{-1}. *Heterocapsa niei*, *Prorocentrum minimum* and *Scrippsiella trochoidea* were the dominant species. In any case, low phytoplankton abundances were observed both, in January and February. Planktonic ciliates were slightly higher than in January, with abundances around 6 cells m L^{-1}.

Phytoplankton group	January	February
(a) Dinoflagellates		
Heterocapsa niei	0.0	12.8
Prorocentrum minimum	0.0	12.8
Scrippsiella trochoidea	0.0	6.6
Total dinoflagellates	38.46	70.87
(b) Diatoms		
Chaetoceros curvisetus	0.00	6.19
Chaetoceros dyadema	0.00	3.09
Chaetoceros spp	3.09	3.09
Dimmerogramma spp	0.00	12.82
Navicula cf *transitans*	11.05	14.15
Nitschia punctata	0.00	6.63
Nitzschia longissima	5.75	15.03
Nitzschia longissima small	12.82	9.73
Rhizosolenia pungens	0.00	7.96
Thalassiosira levanderi	3.27	0.00
Total diatoms	79.00	88.11
(c) Flagellates		
Flagellates 3-10 µm	239.62	416.01
(d) Chrysophyceae		
Dictyocha speculum	0.00	3.09
(e) Other components		
Fecal pellets Copepods	4.86	26.97
Total planktonic components	**443.42**	**632.86**

Table 4.III. Fluxes of planktonic material (cells or particles 10^6 m^{-2} d^{-1}) collected in sediment traps in the Ria de O Barqueiro in January and February 2008.

In addition to the taxa present in January, several species of *Strombidium* appeared as dominant in this date. Microzooplankton abundance highly increased with reference to the January sampling reaching more than 3500 indiv m^{-3}, with copepods nauplii larva as dominants. Mesozooplankton dramatically increased compared to values observed in January, with mean abundances higher than 2000 indiv m^{-3}. Two species of genus *Acartia*

dominated with values of 70% in the zooplankton community (Table 4.II, February).

The analysis of sediment traps at station 5 in February (Table 4.I) demonstrated that the flux of chlorophyll-*a* to near bed was 0.67 mg Chl-*a* m^{-2} d^{-1}, representing approximately the 7% of the water column stock. POC flux was 500 mg C m^{-2} d^{-1} and accounted for 37% of water stock, with a C/N ratio for the trap (POM) of about 12.

Fluxes of planktonic material collected in sediment traps showed that in February small flagellates were the more abundant taxa (Table 4.III). Diatoms dominated the larger phytoplankton. Dinoflagellates and Chrysophyceans also showed significant fluxes to near bed, and fecal pellets accounted for an important fraction of the collected material in the traps.

Taking into account the previous obtained distribution of planktonic material it is possible to observe that phytoplankton biomass (chlorophyll-*a*), like the solar radiation, did not show any relevant change from January to February (Figure 4.3, Table 4.I), however taxonomic composition gave a new insight of the situation (Table 4.II). Small flagellates doubled their abundances in February and dinoflagellates increased one order of magnitude. *Chrysophycean* appeared in relatively high abundance, with *Dictyocha speculum* being the dominant species of large phytoplankton. Diatoms did not displayed changes in abundances, although there was a clear shift from typical winter species to those characteristics of spring blooms in Galician coast as *Lauderia annulata or Chaetoceros* spp. There is some evidence of the relationship between that increase in dinoflagellates in Galician Rias and the existence of allocthonous transport from neighboring shelf (Crespo et al., 2006; Varela et al., 2005). Thus, the high increase of this group from January to February in the O Barqueiro Ria seems to indicate the existence of

intrusion of shelf waters into the ria. These facts suggest qualitative changes related to the development of spring conditions in February. Moreover, changes in water column are also reflected in the composition of particulate material recovered in the traps. Planktonic ciliates abundances also support the idea of environmental changes in February with a 50% increase of abundances and a shift in species composition (Table 4.II). However, the micro and zooplankton components were the best tracers of changing conditions in February with regard to January. Both increased their abundances in one order of magnitude. Most of organisms were copepods larva, suggesting active reproduction of zooplankton. In addition, copepods fecal pellets were an important component of particulate sedimented material. Most species observed in February were typical of spring (Valdés et al., 1991; Bode and Alvarez-Ossorio, 2004; Bode et al., 2005) and some of them as *Calocalanus styliremis* and *Pleuromamma gracilis* are indicative of deep shelf waters (Corral and Alvarez-Ossorio, 1978). In addition, *Ctenocalanus vanus* is a bathypelagic species of could waters (Corral, 1970) suggesting the intrusion of allocthonous material into the ria, as in the case of dinoflagellates. In summary, plankton showed the existence of spring conditions in February and an intrusion of shelf waters into the ria. In the Galician coast, both events are related to north-eastern upwelling favorable winds, which, in turn, are coincident with sunny days, characteristics of spring. What we found is the so called "Prebloom" or winter bloom, a phenomenon already reported in other Galician Rias (Varela et al., 2008).

4.3.3. Winter induced-upwelling conditions

At the western coast, south of Cape Finisterre, there is a high probability of upwelling events during summer which have been extensively studied

(Fraga, 1981; Blanton et al., 1987; Alvarez- Salgado et al., 2000; Prego et al., 2001; Alvarez et al., 2005; Alvarez- Salgado et al., 2006; Gomez-Gesteira et al., 2006; Prego et al., 2007; Alvarez et al., 2008), although recent studies have also shown the existence of upwelling events during winter (Alvarez et al., 2003; deCastro et al., 2006; deCastro et al., 2008). At the north-western coast, a summer upwelling event has been described in the Laxe Ria (Varela et al., 2005), north of Cape Finisterre. This summer upwelling do not reach the Rias of the Artabro Gulf due to the presence of the Gulf which generates an 'upwelling shadow' (Prego and Varela, 1998). Note that the coast orientation changes abruptly between Cape Finisterre and Cape Ortegal (Figure 4.1(b)), which has a double effect on the upwelling patterns. On the one hand, wind intensity and magnitude are modulated by changes in coastal orientation, especially for areas placed in the lee of the coast. On the other hand, the upwelling favorable conditions change with the coastal orientation, since northerly winds are upwelling favorable along the western coast and easterly winds along the northern coast.

To characterize the winter upwelling recurrence at the northern Galician coast, upwelling favorable conditions were analyzed by means of the number of days with UI>16 m^3 s^{-1} km^{-1} per month from 1967 to 2007 at the control point (45.5º N, 7.5º W) using data from the PFEL (Figure 4.5). Note that the threshold (16 m^3 s^{-1} km^{-1}) correspond to winds with intensity less than 1 m/s to discard calms. The highest number of days under favorable conditions was observed during the spring-summer months with 12-14 days per month. During autumn-winter, the number of days under favorable conditions was between 8-10 days per month making not negligible (~ 30%) the possibility of observing upwelling events in winter. This behavior was also observed in previous studies. Gomez-Gesteira et al. (2006), analyzed Ekman transport

close to the northern Galician coast using forecasted winds from November 2001 to October 2004 and they observed that the transport in northward direction is not negligible during the wet season. These results were corroborated by Alvarez et al. (2008) using QuikSCAT satellite data from November 1999 to October 2005.

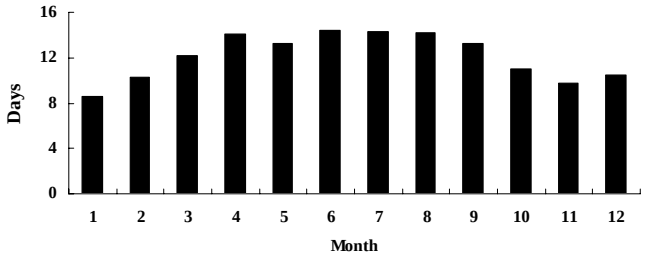

Figure 4.5. Number of days with UI>16 m^3 s^{-1} km^{-1} per month averaged from 1967 to 2007 at the control point 45.5º N, 7.5º W (black square in Figure 4.1(b)).

Upwelling duration was also studied at the same control point. Figure 4.6 shows the probability of finding consecutive days under upwelling favorable conditions (UI>16 m^3 s^{-1} km^{-1}) during the winter period (January-March) from 1967 to 2007. Obviously, the probability decreases when the number of consecutive days under favorable conditions increases. Upwelling favorable conditions with duration of at least 1 day was ~ 35%, decreasing to ~12% when events of at least 5 days were considered. Nevertheless, the probability of obtaining upwelling favorable conditions during at least three days was still on the order of 20%. Previous findings at the western Galician coast prove that upwelled water can be easily identified when upwelling favorable conditions persist for more than three days (Alvarez- Salgado et al., 2000; Alvarez et al., 2005; Alvarez- Salgado et al., 2006).

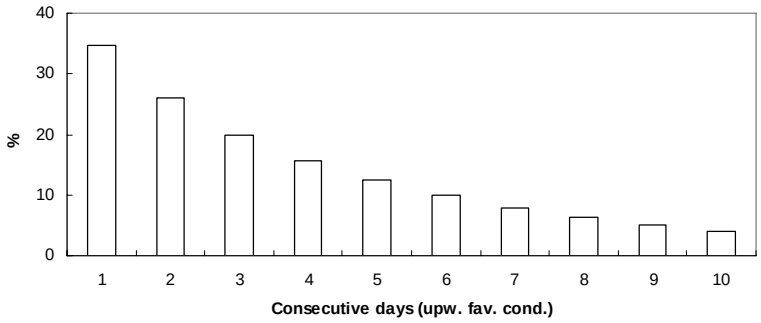

Figure 4.6. Probability of finding consecutive days under upwelling favourable conditions (UI>16 m^3 s^{-1} km^{-1}) during the winter period (January-March) from 1967 to 2007 at the control point 45.5º N, 7.5º W (black square in Figure 4.1(b)).

4.4. Summary and conclusions

Winter upwelling events are not a particular characteristic of the Western Galician Rias because, after favorable meteorological conditions, a similar event was detected in the O Barqueiro Ria, situated in the northern Galician coast. However, salinity and temperature distribution revealed that the upwelled water body corresponded to subsurface shelf seawater in opposite to the observed in the Western Galician coast where upwelling was associated with Eastern North Atlantic Central Water or the Iberian Poleward Current. This significant hydrographical difference involved no changes in the nutrient salts concentrations and nitrate levels were mainly the result of winter mixing throughout the water column. Phytoplankton biomass did not presented any relevant change but small flagellates and planktonic ciliates doubled their abundances and dinoflagellates increased one order of magnitude suggesting the existence of shelf-water intrusion into the ria.

From the Ekman transport analysis during the last forty years it was possible to calculate the number of days per month under upwelling favorable conditions in winter around the area (8-10 days) showing how the possibility of observing upwelling events in winter is not negligible and how the observed event cannot be considered an isolated episode.

4.5. References

Alvarez, I., deCastro, M., Prego, R., Gomez-Gesteira, M., 2003. Hydrographic characterization of a winter-upwelling event in the Ria of Pontevedra (NW Spain). Estuarine Coastal and Shelf Science, 56, 869-876.

Alvarez, I., deCastro, M., Gomez-Gesteira, M., Prego, R., 2005. Inter- and intra-annual analysis of the salinity and temperature evolution in the Galician Rías Baixas-ocean boundary (northwest Spain). Journal of Geophysical Research, 110, C04008, doi:10.1029/2004JC002504.

Alvarez, I., Gomez-Gesteira, M., deCastro, M., Novoa, E.M., 2008. Ekman Transport along the Galician Coast (NW, Spain) calculated from QuikSCAT winds. Journal of Marine Systems, 72, 101-115, doi:10.1016/j.jmarsys.2007.01.013.

Alvarez- Salgado, X.A., Gago, J., Miguez, B.M., Gilcoto, M, Perez, F.F., 2000. Surface waters of the NW Iberian Margin: Upwelling on the shelf versus outwelling of upwelled waters from the Rias Baixas. Estuarine Coastal and Shelf Science, 51, 821-837.

Alvarez- Salgado, X.A., Nieto-Cid, M., Gago, Brea, S., Castro, C.G., Doval, M.D., Perez, F.F., 2006. Stoichiometry of the degradation of dissolved and particulate biogenic organic matter in the NW Iberian

upwelling. Journal of Geophysical Research, 111(C07017), doi:10.1029/2004JC002473.

Aminot, A., 1983. Dosage de l'oxygène dissous, in: Aminot, A., Chaussepied, M., (Eds.), Manuel des Analysses Chimiques en Milieu Marin. CNEXO, Brest, pp. 75-92.

Bao, R. Varela, M., Prego, R., 1997. Mesoscale distribution patterns of diatoms in surface sediments as tracers of coastal upwelling of the Galician shelf (NW Iberian Peninsula). Marine Geology, 144, 117-130.

Blanton, J.O., Tenore, K.R., Castillejo, F., Atkinson, L.P., Schwing, F.B., Lavín, A., 1987. The relationship of upwelling to mussel production in the rias of the western coast of Spain. Journal of Marine Research, 45, 497- 511.

Bode, A., Varela, M., 1994. Planktonic carbon and nitrogen budgets for the N-NW Spanish shelf: the role of pelagic nutrient regeneration during upwelling events. Scientia Marina, 58, 221-231.

Bode, A., Alvarez-Ossorio, M.T., González, N, 1998. Estimations of mesozooplankton biomass in a coastal upwelling area off NW Spain. Journal of Plankton Research, 20, 1005-1014.

Bode, A., Álvarez-Ossorio, M.T., 2004. Taxonomic versus trophic structure of mesozooplankton: a seasonal study of species succession and stable carbon and nitrogen isotopes in a coastal upwelling ecosystem. ICES Journal of Marine Science, 61, 563-571.

Bode, A., Álvarez- Ossorio, M., Gonzalez, N., Lorenzo, J., Rodriguez, C., Varela, M., Varela, M.M., 2005. Seasonal variability of plankton blooms in the Ria de Ferrol (NW Spain): II. Plankton abundance,

composition and biomass. Estuarine Coastal and Shelf Science, 63, 285-300.

Botas, J., Fernandez, E., Bode, A., Anadon, R., 1990. A persistent upwelling off the Central Cantabrian Coast (Bay of Biscay). Estuarine Coastal and Shelf Science, 30, 185-199.

Corral, J., 1970. Contribución al conocimiento del plancton de Canarias. Estudio cuantitativo, sistemático y observaciones ecológicas de las Copépodos epipelágicos en la zona de Santa Cruz de Tenerife en el curso de un ciclo anual. Ph.D. Thesis, University of Madrid, Madrid. 266 pp.

Corral, J., Alvarez-Ossorio, M.T., 1978. El zooplancton de la ría de Arosa (NW de España). I Composición y distribución de las comunidades en un ciclo anual. Boletín del Instituto Español de Oceanografía, 265, 133-163.

Crespo, B.G., Figueiras, F.G., Porras, P., Teixeira, I.G., 2006. Downwelling and dominance of autochthonous dinoflagellates in the NW Iberian margin: The example of the Ría de Vigo. Harmful Algae, 5, 770-781.

deCastro, M., Dale, A.W., Gomez-Gesteira, M., Prego, R., Alvarez, I., 2006. Hydrographic and atmospheric analysis of an autumnal upwelling event in the Ria de Vigo (NW Iberian Península). Estuarine Coastal and Shelf Science, 68, 529-537.

deCastro, M., Gomez-Gesteira, M., Alvarez, I., Cabanas, J.M., Prego, R., 2008. Characterization of fall-winter upwelling recurrence along the Galician western coast (NW Spain) from 2000 to 2005: dependence on atmospheric forcing. Journal of Marine Systems, 72, 145-148, doi:10.1016/j.jmarsys.2007.04.005.

Delgado, I., Alcantara-Carrio, J., Alejo, I., Alonso, I., Louzao, M., 2002. Influence of hydrodynamics and sedimentary characteristics of Barqueiro Ria on Arealonga Beaxh Dynamics. Journal of coastal Research, 36, 231-239.

Evans, G., Prego, R., 2003. Rias, estuaries and incised valleys: is a ria an estuary? Marine Geology, 196, 171-175.

Fernandez, E., Bode, A., 1991. Seasonal patterns of primary production in the Central Cantabrian Sea (Bay of Biscay). Scientia Marina, 55, 629-636.

Fernandez, E., Marañón, E., Cabal, J., Alvarez, F., Anadón, R., 1995. Vertical particle flux in outer shelf waters of the southern Bay of Biscay in summer 1993. Oceanological Acta, 18, 379-384.

Fiuza, A.F.G., 1984. Hidrologia e dinamica das aguas costeiras de Portugal (Hydrology and dynamics of the Portuguese coastal water). Ph.D. Thesis, University of Lisboa, Lisboa. 294 pp.

Fontán, A., Valencia, V., Borja, A., Goikoetxea, N., 2008. Oceano-meteorological conditions and coupling in the southeastern Bay of Biscay, for the period 2001–2005: A comparison with the past two decades. Journal of Marine Systems, 72, 167-177.

Fraga, F., 1981. Upwelling off the Galician Coast, Northwest Spain, in: Richardson, F.A. (Ed.), Coastal Upwelling. American Geophysical Union, Washington, pp. 176-182.

Frouin, R., Fiuza, A.F.G., Ambar, I., Boyd, T.J., 1990. Observations of a poleward surface current off the coasts of Portugal and Spain during winter. Journal of Geophysical Research, 95, 679-691.

Gil, J., 2003. Changes in the pattern of water masses resulting from a poleward slope current in the Cantabrian Sea (Bay of Biscay). Estuarine Coastal and Shelf Science, 57, 1139-1149.

Gonzalez-Pola, C., Ruiz-Villarreal, M., Lavín, A.,Cabanas, J.M., Alvarez-Fanjul, E., 2005. A subtropical water intrusion spring-event in the shelf-slope of the south-western Bay of Biscay after strong wind-forcing pulses. Journal of Atmospheric and Ocean Science, 10, 343-359.

Gomez-Gesteira, M., Moreira, C., Alvarez, I., deCastro, M., 2006. Ekman transport along the Galician coast (NW, Spain) calculated from forecasted winds, Journal of Geophysical Research, 111(C10005), doi:10.1029/2005JC003331.

Hansen, H.P., Grasshoff, K., 1983. Automated chemical analysis, in: K. Grasshoff, M. Ehrhardt, K. Kremling (Eds.), Methods of Seawater Analysis. Verlag Chemie, Weinhein. pp. 368-376.

Knauer, G.A., Martin, J.H., Karl, D.M., 1984. The flux of organic material out of the euphotic zone, in: Global Ocean Flux Study: Proceedings of a Workshop, Academy Press. Woods Hole, pp. 136-150.

Lorenzo, F., Alonso, A., Pages, J.L., 2007. Erosion and Accretion of Beach and Spit Systems in Northwest Spain: A Response to Human Activity. Journal of Coastal Research, 23, 834-845.

Llope, M., Anadon, R., Viesca, L., Quevedo, M., Gonzalez-Quiros, R., Stenseth, N.C., 2006. Hydrography of the southern Bay of Biscay shelf-break region: Integrating the multiscale physical variability over the period 1993-2003. Journal of Geophysical Research, 111, C09021, doi:10.1029/2005JC002963.

Montes, J., Villalba, A., Lopez, M.C., Carballal, M.J., Mourelle, S.G., 1991. Bonamiasis in native flat oysters (Ostrea edulis L.) from two intertidal beds of the Ortigueira estuary (Galicia, NW Spain) witn different histories of oyster culture. Aquaculture, 93, 213-224.

Montes, J., Carballal, M.J., Lopez, M.C., Mourelle, S.G., 1992. Incidence of bonamiasis in falt oyster, Ostrea edulis L., cultured in Galicia (NW Spain). Aquaculture, 107, 189-192.

Neveux, J., Panouse, M., 1987. Spectrofluorometric determination of chlorophylls and pheophytins. Archiv für Hydrobiologie, 109, 567-581.

Nykjaer, L., Van Camp, L., 1994. Seasonal and Interannual variability of coastal upwelling along northwest Africa and Portugal from 1981 to 1991. Journal of Geophysical Research, 99, 14197-14207

Otero, X.L., Huerta-Diaz, M.A., Macias, F., 2000. Heavy metal geochemistry of saltmarsh soils from the Ria of Ortigueira (mafia and ultramafic areas, NW Iberian Peninsula). Environmental Pollution, 110, 285-296.

Palanques, A., Isla, E., Puig, P., Sanchez-Cabeza, J.A., Masqué, P., 2002. Annual evolution of downward particle fluxes in the Western Bransfield Strait (Antarctica) during the FRUELA project. Deep Sea Research II, 49, 903-920.

Penabad, E., Alvarez, I., Balseiro, C.F., deCastro, M., Gómez, B., Pérez-Muñuzuri, V., Gomez-Gesteira, M., 2008. Comparative analysis between operational weather prediction models and QuikSCAT wind data near the Galician coast. Journal of Marine Systems, 72, 256-270, doi:10.1016/j.jmarsys.2007.07.008.

Prego, R., Bao, R., 1997. Upwelling influence on the Galician coast: silicate in shelf water and underlying surface sediments. Continental Shelf Research, 17, 307-318.

Prego, R., Varela, M., 1998. Hidrography of the Artabro Gulf in summer: western coastal limit of Cantabrian seawater and wind-induced upwelling at Prior Cape. Oceanologica Acta, 21, 145-155.

Prego, R., Barciela, C., Varela, M., 1999. Nutrient dynamics in the Galician coastal area (Northwestern Iberian Peninsula): Do the Rias Bajas receive more nutrient salts than the Rias Altas? Continental Shelf Research, 19, 317-334.

Prego, R., Dale, A., deCastro, M., Gomez-Gesteira, M., Taboada, J.J., Montero, P., Perez-Villar, V., 2001. Hydrography of the Pontevedra Ria: Intra-annual spatial and temporal variability in a Galician coastal system (NW Spain). Journal of Geophysical Research, 106, 19845-19857.

Prego, R., Guzman-Zuñiga, D., Varela, M., deCastro, M., 2007. Consequences of winter upwelling events on biogeochemical and phytoplankton patterns in a western Galician ria (NW Iberian Península). Estuarine Coastal and Shelf Science, 73, 409-422.

Río-Barja, F.J., Rodríguez-Lestegás, F., 1992. Os ríos galegos. Consello da Cultura Galega, Santiago, pp. 333.

Ríos, A.F., Pérez, F.F., Fraga, F., 1992. Water masses in the upper and middle North Atlantic Ocean east of the Azores. Deep Sea Research I, 39, 645-658.

Tomas, C., 1997. Identifying Marine Phytoplankton. Academic Press, New Cork, pp. 858.

Torres, R., Barton, E.D., Miller, P., Fanjul, E., 2003. Spatial patterns of wind and sea surface temperature in the Galician upwelling region. Journal of Geophysical Research, 108, 3130- 3143, doi:10.1029/2002JC001361.

Unesco, 1994. Protocols for the Joint Global Ocean Flux Study (JGOFS) core measurements. Manuals and Guides, 29, 1-70.

Utermöhl, H., 1958. Zur Vervollkommnung der quantitativen Phytoplankton-Methodik. Mitteilungen Internationale Vereinigung Theoretische und Angewandte Limnologie 9, 1-38.

Valdés, L., Álvarez-Ossorio, M.T., Lavín, A., Valera, M., Carballo, R., 1991. Ciclo anual de parámetros hidrográficos, nutrientes y plancton en la plataforma continental de La Coruña (NO España). Boletín del Instituto Español de Oceanografía, 7, 91-138.

Varela, M., Prego, R., Pazos, Y., 2004. Vertical biogenic particulate flux in a Galician Ria (NW Spain). Marine Ecology Progress Series, 269, 17-32.

Varela, M., Prego, R. Pazos, Y., Moroño, A., 2005. Influence of upwelling and river runoff interaction on phytoplankton assemblages in a Middle Galician Ria and Comparison with northern and southern rias (NW Iberian Peninsula). Estuarine Coastal and Shelf Science, 64, 721-737.

Varela, M., Prego, R., Pazos, Y., 2008. Spatial and temporal variability of phytoplankton biomass, primary production and community structure in the Pontevedra Ria (NW Iberian Peninsula): oceanographic periods and posible response to environmental changes. Marine Biology, 154, 483-499.

Wooster, W.S., Bakun, A., McClain, D.R., 1976. The seasonal upwelling cycle along the eastern boundary of the north Atlantic. Journal of Marine Research, 34, 131 - 141.

Chapter 5

Coastal SST warming trend along the continental part of the Atlantic Arc

Abstract

Coastal warming was analyzed by means of satellite derived sea surface temperature (SST) along the continental part of the Atlantic Arc extending from 37ºN to 48ºN for the period 1985-2005. Inter-annual SST variability calculated from anomalies shows an inhomogeneous warming trend in coastal SST (ΔSST). Coastal warming trend ranges from 3.5ºC century^{-1} at latitudes close to 48ºN to 1.2ºC century^{-1} at latitudes close to 37ºN. This warming is observed to reflect oceanic ΔSST which increases northward in the Atlantic area. In addition, a westward increase was also observed across the north Atlantic. Coastal warming is not constant all year long. It only occurs during spring and summer in the entire area under scope following a trend similar to the annual one. The mean spring ΔSST values are 5.1ºC century^{-1} in the French coast, 4.4 ºC century^{-1} in the Cantabrian coast and 3.8 ºC century^{-1} in the Western Iberian Peninsula coast. Similar values (5.0 ºC century^{-1}, 3.7 ºC century^{-1} and 2.7 ºC century^{-1}) are observed in summer.

5.1. Introduction

Understanding sea surface temperature (SST) changes is critical to determine scenarios and policies to mitigate anthropogenic effects on climate. Unfortunately, monitoring becomes an arduous task due to technical problems inherent to measurements at sea and to the vast extent of the area to be covered. In addition, long-term series can be biased not only by

changes in instrumentation but also by the reliability of the measurement techniques.

Despite these facts, numerous studies have attempted to quantify trends in SST over the last century (Paltridge and Woodruff, 1981; Folland et al., 1984; Strong, 1989; Folland et al., 1990). Different data sets have been created during the last decades in an attempt to provide better and more reliable data to the scientific community. Special mention should be given to the Comprehensive Ocean Atmosphere Data SET (COADS, Woodruff et al., 1987) and to the World Ocean Atlas (Levitus and Boyer, 1994).

In addition, developments in satellite technology have provided a valuable tool to calculate SST trends (Strong, 1989; Casey and Cornillon, 1999; Strong et al., 2000; Casey and Cornillon, 2001). Detailed analyses (Reynolds et al., 1989; Reynolds and Smith, 1995) have shown the consistency of these satellite data with the oceanographic data previously described.

All previous studies conclude that a considerable global warming in SST has occurred over the last century no matter the considered data set. This warming cannot be considered an isolated fact and similar trends towards increase in the heat content of the ocean have been reported by other authors (Levitus et al., 2000). In addition, SST trends also coincide with global trends in wind (Caires et al., 2003; Gillet and Thompson, 2003; Chelton et al., 2004), cloud coverage (Wiley et al., 2002; Roderick and Farquhar, 2002), and humidity (Flohn et al., 1990).

This global warming is far from being uniform during the 20th century. Global SST time series show two distinct warming periods during the past 100 years according to the Intergovernmental Panel on Climate Change (1996). The first occurred during the period 1920 to 1940 and was followed by a period of cooling; the second warming period began during the 1970s.

Levitus et al., (2000) observed a marked long term increase in the integrated heat content of the upper 3000 meters in all oceans from the mid-1950s to the mid-1990s.

In addition, global warming is not uniformly distributed all over the world's oceans. The Atlantic Ocean contributes most to the increase in the heat content. Nerem et al., (1999) observed a relative maximum in global SST at the beginning of 1998. Levitus et al., (2000) emphasized that the extreme warmth of the world ocean during mid-1990s was in part due to a multidecadal warming of the Atlantic and Indian oceans as well as a positive polarity in a possible bidecadal oscillation of Pacific Ocean heat content. Strong et al., (2000) showed a latitudinal pattern in SST increase, with greater warming in the Northern hemisphere than in the Southern one.

These differences among macroscopic areas (hemispheres and oceans) are even more marked at regional scales where some areas warm at higher or lower rates than others as shown in regional studies (Bell and Goring, 1998; Cole et al., 2000; Casey and Cornillon, 2001; Lemos and Pires, 2004; Ginzburg et al., 2004; Santos et al., 2005; Goreau et al., 2005). Thus, regional warming can be explained by changes in winds, cloudiness, ocean currents, thermocline depth and upwelling intensity. Actually, these factors can account for larger changes in regional SST than global average trends.

Changes in coastal areas are of large economic and ecologic importance. On the one hand, about 20% of global fish catch is obtained in near shore regions, especially in those areas affected by coastal upwelling events. On the other hand, coastal ecosystems have shown to be highly vulnerable to global climate changes (e.g. SST increase and sea level rise). Thus, warming can have profound impacts on biological production of coastal areas. A general increase of water temperature can produce an advancement of

bivalve spawning and the resulting mismatch with the phytoplankton bloom involve a reduction of food availability during the pelagic phase and an increase of mortality (Philippart et al., 2003). Other studies suggest that rising seawater temperatures affect eggs production and fecundity and increase the number of predators affecting survival of bivalve early life stage (Beukema, 1992; Honkoop et al., 1998; Young et al., 1996). Thermal tolerance is lower in early juveniles and suboptimal temperatures may be indirectly responsible for early juvenile mortality by aggravating the effects of other factors such as reduced salinity and desiccation (Goselin and Quian, 1997). Even, in more sensible species like cockles, dominant bivalve in European tidal flats, adults can also be subjected to extraordinary summer mortalities caused by water temperature stress (Thieltges, 2006). In addition, some authors (Occhipinti-Ambrogi, 2007), have linked climate change and biological invasions of non indigenous species (NIS). SST increase have facilitated the spawning and larval development of species characteristic of warmer regions in the European coast, (Walther et al., 2002; Diederich et al., 2005), which have been implicated in the decline and even collapse of several marine ecosystems (Harris and Tyrrell, 2001; Frank et al., 2005).

The aim of this paper is to analyze whether or not there was a significant warming trend along the coast of the Atlantic Arc extending from 37ºN to 48ºN for the period 1985- 2005. This study, which will be carried out using satellite derived SST, aims to highlight the dependence of coastal warming trends on spatial (shore position and orientation) and temporal (seasonal) constraints. As far as we know this study constitutes the first analysis on coastal warming, which is of special relevance due to its biological and economic implications.

5.2. Data processing

Weekly mean SST data is obtained from night-time measurements carried out by the Advanced Very-High Resolution Radiometer (AVHRR) onboard of NOAA series satellites (see Chapter 2).

For our purposes, the area 37ºN -52ºN corresponding to the eastern north Atlantic region was cut from the global data set for the period 1985-2005. Night-time data were used to avoid the solar heating effect. First, SST data were averaged to a monthly time scale. Then, voids due to cloud coverage or other malfunctions were interpolated from nearest neighbours by means of a weighted (Gaussian) average. The process was iterated from an initial square box of 3×3 neighbours (12×12 km) around the point up to a maximum distance of 25×25 neighbours (100×100 km). The process was automatically stopped when the number of neighbours with reliable values inside the box was higher than 5.

The continental limits of the area under scope coincide with the Region IV defined by the OSPAR commission (http://www.ospar.org). The region comprises almost the whole of the Bay of Biscay and the western Iberian margin and falls under the national jurisdiction of France, Portugal and Spain. The shore line can be macroscopically divided into three regions (Figure 5.1).

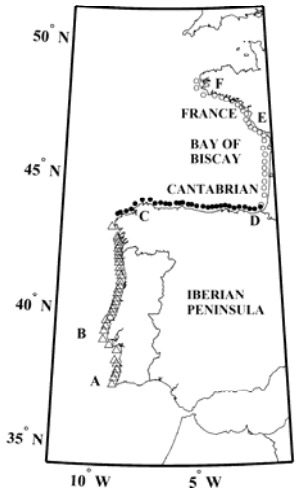

Figure 5.1. Area under scope. A discrete set of points placed at 20 km from coast were generated along the coast. Twenty-eight points were placed along the French coast (empty circles in Figure 5.1), 31 along the Cantabrian coast (full circles) and 35 along the WIP coast (empty triangles). Point A represents Cape San Vicente, point B Lisbon, point C the Artabrian Gulf, point D the mouth of the Bidasoa River, point E La Rochelle and point F represents the French Brittany.

The western part of the Iberian Peninsula (WIP from now on) extends from Cape SanVicente in Portugal (point A in Figure 5.1) to the Artabrian Gulf in Spain (point C) with N-S orientation. The Cantabrian coast extends from the Artabrian Gulf to the mouth of the Bidasoa River (point D), which constitutes the natural border between France and Spain. This coast has a marked E-W orientation. Finally, the Atlantic French coast extends from point D to the French Brittany (point F). The shore line has a marked N-S orientation till point E, with NW-SE orientation till point F. This region is particularly well suited to analyze geographic trends in coastal warming for

several reasons. On the one hand, the coast maintains an almost constant orientation for at least 500 km as described above, in such a way that warming changes slowly along the coast from point to point. On the other hand, there are not other land masses close to the coast under scope. Thus, coastal warming mainly depends on open ocean conditions, being independent of local conditions which can bias trends in semi-enclosed basins and in areas surrounded by islands or large peninsulas.

A discrete set of points corresponding to 94 positions placed at 20 km from the coast were generated along the coast (Figure. 5.1). Twenty-eight points were placed along the French coast (empty circles in Figure 5.1), 31 along the Cantabrian coast (full circles) and 35 along the WIP coast (empty triangles). Discretization effects were smoothed by calculating the SST monthly values at each point as the average of its nearest neighbours (separated by 4 km in the original data set) in latitude or longitude depending on coast orientation. The distance between adjacent points is approximately 20 km, considering the total number of points and the coastal extent. Finally, SST trends were analyzed using the anomalies from the annual cycle obtained from the 21 year (1985-2005) monthly means.

5.3. Results and Discussion

5.3.1. Seasonal variability of the SST

Seasonal SST was calculated from monthly SST for the four hydrological seasons: winter (January- March), spring (April- June), summer (July- September) and autumn (October- December). The 21-yearly mean seasonal SST fields are represented in Figure 5.2(a- d). Each SST field is characterized by a different pattern with longitudinal and latitudinal temperature gradients.

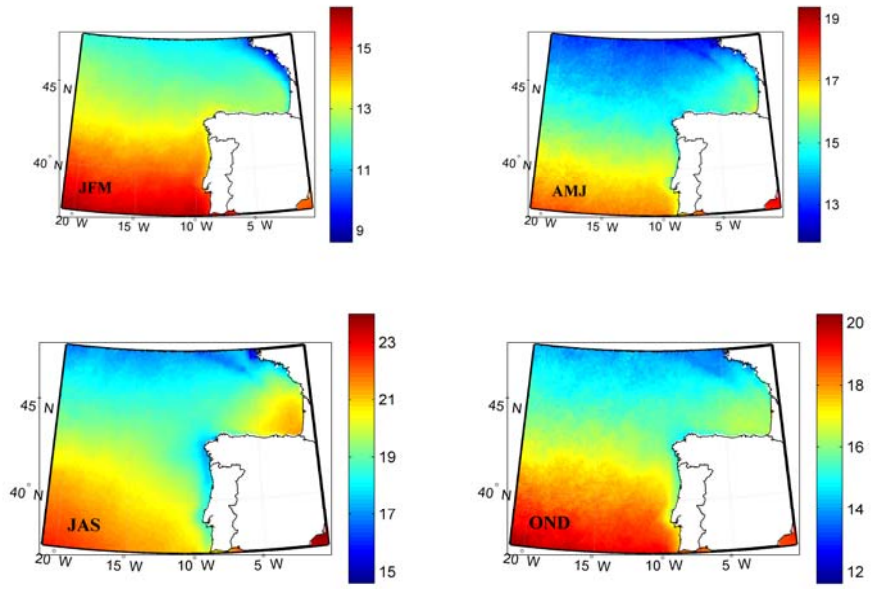

Figure 5.2. 21- year (1985-2005) mean SST (ºC) fields for the four hydrological seasons: winter (JFM), spring (AMJ), summer (JAS) and autumn (OND).

Winter (Figure 5.2(a)) shows a maximum latitudinal gradient of 4ºC, ranging from 17ºC at the southern coast of Portugal to 13ºC at the north of the Bay of Biscay. The longitudinal gradient is practically negligible in front of the WIP and south of the Bay of Biscay. In contrast, north of the Bay of Biscay the maximum longitudinal gradient is 4ºC ranging from 13ºC at 20ºW, 47ºN to 9ºC near the Atlantic French coast. Spring (Figure 5.2(b)) shows a stronger latitudinal gradient with a maximum value of 6ºC ranging from 17ºC at the southern coast of Portugal to 11ºC at the north of the Bay of Biscay. During this season the longitudinal gradient is practically negligible except along the Cantabrian Sea and at Lisbon (point B in Figure 5.1) where a longitudinal gradient between 1ºC and 1.5ºC is observed. SST fields change drastically

during summer (Figure 5.2(c)) where the entrance of colder water along the WIP coast and the existence of warmer water in the south-eastern corner of the Bay of Biscay can be observed. In this case the maximum latitudinal gradient (7ºC, ranging from 23ºC at 37ºN and 16ºC at 48ºN) decreases from the ocean to the coast (3ºC, ranging from 19ºC southern of Portugal to 16ºC at 48ºN). The maximum longitudinal gradient also decreases from 4ºC (from 37ºN to 43.5ºN) to 2ºC (from 43.5ºN to 46ºN) and it is negligible from 46ºN to 48ºN. The presence of cold water in front of the WIP coast is due to upwelling events which usually occur from April to October being more intense during July and August (Wooster et al., 1976; Nykjaer and Van Camp 1994; Santos et al., 2005; Cabanas and Alvarez, 2005; Gómez-Gesteira et al., 2006; deCastro et al., 2007). In fact, traces of these upwelling events can be observed in spring and autumn SST fields. The warmer water measured in the south-eastern corner of the Bay of Biscay can also be perceived in the spring SST pattern and it is consistent with studies carried out by Koutsikopoulos and Le Cann (1996) and Pingree and Le Cann (1989). Autumn (Figure 5.2(d)) shows the strongest maximum latitudinal gradient with a value of 8ºC (ranging from 20ºC at 37ºN to 12ºC at 48ºN). The longitudinal gradient is practically negligible except in front of the north part of the WIP where a maximum temperature gradient around 2ºC is observed.

5.3.2. Annual variability of coastal SST

The annual cycle of coastal SST for each coast is represented in Figure 5.3(a-c) by means of the 21-year average of SST.

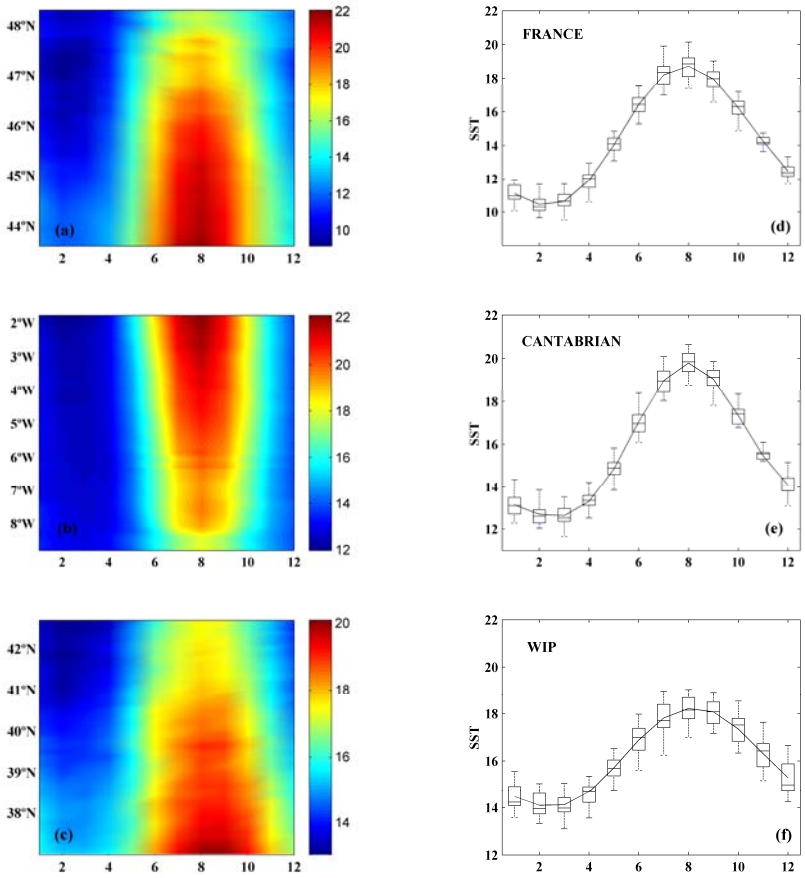

Figure 5.3. 21-year (1985-2005) mean of the annual evolution of: (a) the meridional SST (ºC) for the Atlantic French coast, (b) the zonal SST (ºC) for the Cantabrian coast, (c) the meridional SST (ºC) for the WIP coast, (d) the meridional average of coastal SST (ºC) for the Atlantic French coast, (e) the zonal average of coastal SST for the Cantabrian coast and (f) the meridional average of coastal SST (ºC) for the WIP coast

Practically, the entire area presents the lowest temperature values from January to March corresponding with winter time and the highest ones in August. The highest value along the Atlantic French (Figure 5.3(a)) and the Cantabrian (Figure 5.3(b)) coasts is 22ºC measured at the south-eastern corner of the Bay of Biscay. This maximum temperature decreases northward along the Atlantic French coast and westward along the Cantabrian one. With respect to the WIP coast, a maximum temperature of 20ºC was detected at the southern part of Portugal decreasing northward (Figure 5.3(c)). Note that although the WIP coast is south of the Atlantic French coast, the maximum coastal SST measured is 2ºC colder than the one measured in the Atlantic French coast. This is due to upwelling events which take place along the WIP coast with maximum intensity in August.

The meridional (zonal) averaging could be a source of errors in SST gradient estimates in high- gradient areas. However, in the present study, the alongshore orientation of the frontal zones near coast makes the meridional (zonal) average appropriate. The annual variability of the meridional (zonal) average of coastal SST for all coasts is represented in Figures 5.3(d-f). These panels represent the monthly average of SST (solid line), the median value for each month (line inside each box), the minimum (maximum) SST by means of the lower (upper) whisker and the first (third) quartile by means of the lower (upper) box limits. This mean annual cycle is observed to fit a sinusoidal function with a correlation coefficient higher than 0.98 for the three areas. The lowest SST values were observed from January to March with the minimum in February (10.5ºC for the Atlantic French coast, 12.5ºC for the Cantabrian coast and 14ºC for the WIP coast). The highest values were observed from June to September with the maximum in August (18.5ºC for the Atlantic French and the WIP coasts and 19.5ºC for the Cantabrian

coast). The smallest difference between maximum and minimum SST occurs along the WIP coast (Figure 5.3(f)) due to coastal upwelling, which cools surface water during summer.

5.3.3. Warming trend of coastal SST anomaly

5.3.3.1. Inter-annual trend

The trend of coastal SST anomaly along the area of study for the period 1985 - 2005 is shown in Figure 5.4.

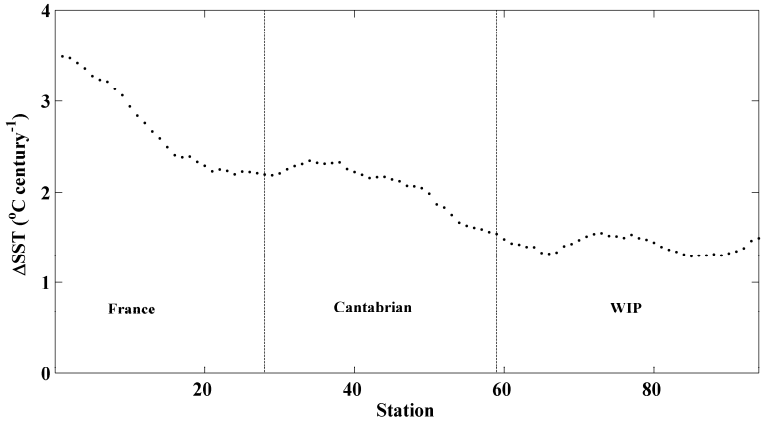

Figure 5.4. Coastal SST anomaly trend (ΔSST) along the area under study for the period 1985-2005. A running average to the 9 nearest spatial neighbours was considered for the sake of clarity. Only points with 90% significance in the T-test were computed in this running average.

ΔSST was calculated at each point along the coast by fitting the monthly anomaly to a straight line. A running average to the 9 nearest spatial neighbours was used prior to representation. Only points with 90% significance in the T-test were considered in this running average. Positive ΔSST values were observed along the coast, although with noticeable

changes both in latitude and longitude. The highest ΔSST is observed at the northernmost part of the French coast (3.5 ºC century^{-1}) and the lowest one at the southernmost part of the WIP coast (1.3 ºC century^{-1}). The mean and the standard deviation of ΔSST depicted in Table 5.I show how SST warming decreases monotonically from the French coast to the WIP coast. Results along the WIP coast are in good agreement with previous studies by Lemos et al., (2004) who found a warming trend close to 1ºC century^{-1} for the period 1941 to 2000 from weather stations placed onshore.

	<ΔSST>	*σ(ΔSST)*
France	2.7	0.5
Cantabrian	2.1	0.3
WIP	1.4	0.1

Table 5.I. Coastal increment of the SST (in ºC century^{-1}) calculated using the monthly anomaly values for the period 1985-2005. A total of 252 monthly values were linearly fitted. Only trends with significance higher than 90% from a T-test were considered in the average.

Spatial variability of coastal warming reflects the warming trend observed in the eastern North Atlantic Ocean (Figure 5.5(a)). Monthly SST data were spatially integrated in a synoptic scale of 1.5 × 1.5 degrees and then filtered with a low pass Gaussian (3 × 3 pixels) filter with standard deviation 1 (in pixels) from 1985 to 2005. Positive ΔSST values are observed in the entire area under scope, reaching maximum values over 7.0 ºC century^{-1} in the open sea.

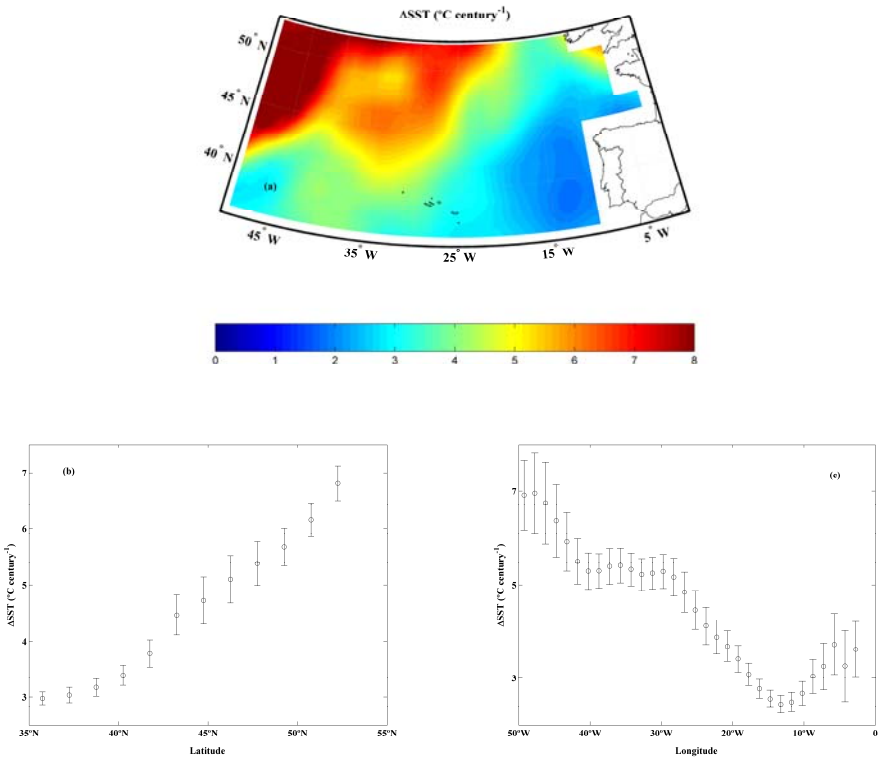

Figure 5.5. SST anomaly trend (ºC century^{-1}) of the north Atlantic area extending from 35 to 55 ºN and from 0 to 55º W for the 1985- 2005 period of time. Original data corresponding to a 4 km × 4 km × 1 week scale were averaged to 1.5º × 1.5º × 1 month scales prior to anomaly calculation (a). Data were longitudinally (b) and latitudinally averaged (c).

There is a clear increase of ΔSST with latitude as depicted in Figure 5.5(b), where ΔSST values were averaged in longitude from 50ºW to 0. On the other hand, ΔSST values were also averaged in latitude 35ºN to 55ºN. Figure 5.5(c) shows a clear decrease in longitude from 50ºW to 15ºW, with a further increase from 15ºW to 0 due to the more pronounced warming observed at

high latitudes. Some authors, Goreau et al., (2005) have hypothesized that the velocity and the total heat transport into the northwest Atlantic from the Caribbean has accelerated due to changes in the Gulf Stream. However, no relationship between the areas of high warming and the Gulf Stream was observed in the present study.

The observed rates of warming are higher than the long-term values obtained by other authors for the last half century in the ocean. For a brief summary on other studies focused on global and regional SST trends see Table 5.II in Casey and Cornillon (2001). Most of the authors observe a SST warming whose extent depends on the period, the area and the data set under scope. In addition, Levitus et al., (2000) found a warming trend close to 0.6ºC century^{-1} for the upper 300m of the world ocean for the period 1948-1998 and Arbic and Owens (2001) found values of 0.5ºC century^{-1} for the mid-depth layer (1000- 2000 db) for the Atlantic from 32ºN to 36ºN from the 1920s to 1990s. In the particular case of Mediterranean Water level, Potter and Lozier, (2004) showed a peak value of 1ºC century^{-1} for Atlantic Mediterranean Water close to the strait of Gibraltar from 1955 to 1993. However, González-Pola et al. (2005) observed that the evolution of the intermediate water masses within the south-eastern corner of the Bay of Biscay shows a warming rate between 2ºC century^{-1} and 3ºC century^{-1} from 1991 to 2003. The different warming trends depend on the considered period. For instance, the high warming rates observed in Gonzalez- Pola et al. (2005) and in the present study reflect the acceleration in climate warming observed during the last two decades of the 20th century. Notice that the 10 warmest years of the historical record have occurred after 1988 according to the Intergovernmental Panel on Climate Change (2001).

	France		*Cantabrian*		*WIP*	
	<ΔSST>	σ(ΔSST)	<ΔSST>	σ(ΔSST)	<ΔSST>	σ(ΔSST)
Winter (JFM)	0.2	0.7	0.4	0.3	0.5	0.5
Spring (AMJ)	5.1*	0.2	4.4*	0.7	3.8*	0.4
Summer (JAS)	5.0*	0.5	3.7*	0.3	2.7*	0.4
Fall (OND)	0.3	0.7	-0.5	0.2	-1.1	0.2

Table 5.II. Coastal increment of the SST (in ºC century^{-1}) calculated using the monthly anomaly values corresponding to each season for the period 1985-2005. A total of 63 monthly values were linearly fitted for each season. Asterisks correspond to trends with significance higher than 90% from a T-test.

5.3.3.2. Seasonal trends

The seasonal trends of coastal SST anomaly along the area of study for the period 1985 -2005 are shown in Figure 5.6. This figure was calculated following the protocol described for Figure 5.4. Only spring (a) and summer (b) are represented because only their significance level is higher than 90%. The observed warming trends are dependent on the season, although they are macroscopically similar to the annual trend shown in Figure 5.4. In general, spring ΔSST is higher than summer ΔSST along the entire coast and both show a trend higher than observed in the annual fitting. These results are summarized in Table 5.II, which was calculated following the protocol described in Table 5.I. Once again, the mean ΔSST shows a monotonic decrease in warming from the French coast to the WIP coast.

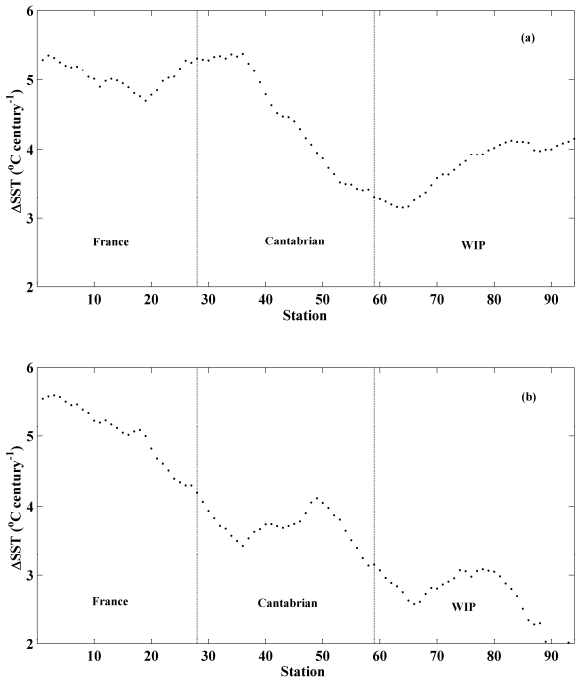

Figure 5.6. Spring (a) and summer (b) coastal SST anomaly trends (ΔSST) along the area under study for the period 1985-2005. Data treatment as in Figure 5.4.

5.4. Summary and conclusions

The inter-annual variability of coastal SST along the continental part of the Atlantic Arc shows a significant warming trend for the period 1985-2005. The following facts can be concluded:

- An inhomogeneous warming trend was observed in coastal SST increasing monotonically from the WIP coast to the French coast.
- Differences in coastal warming reflect oceanic trends observed in the north Atlantic, which is characterized by a north-western increment in ΔSST.

- Coastal warming is not constant all year long. Warming is only significant during spring and summer, following a macroscopic pattern similar to the annual one.

Coastal warming, even if lower than observed in the open ocean, can produce an important biological and economic impact in the area under scope, characterized by a high productivity. Changes that range from 1.2 to 3.5 ºC century^{-1} will presumably have a negative impact on coastal marine communities, especially in some marketable species like mussels, oysters, clams or cockles. A general increase in water temperature can alter the normal reproductive cycle of these bivalves and be involved in high summer mortalities.

Finally, the used data set only covers 21 years and can be biased by decadal oscillations. Thus, further monitoring and research should be conducted in order to determine the real extent of coastal warming.

5.5. References

Arbic, B.K., Owens, W.B., 2001. Climate warming of Atlantic intermediate waters. Journal of Climate, 14, 4091- 4108.

Beukema, J.J., 1992. Dynamics of juvenile shrimp Crangon crangon in a tidal-flat nursery of the Wadden Sea after mild and cold winters. Marine Ecology Progress Series, 83, 157–165

Bell, R.G., Goring, D.G., 1998. Seasonal Variability of Sea Level and Sea-surface Temperature on the North-east Coast of New Zealand. Estuarine Coastal and Shelf Science, 46**,** 307–318.

Cabanas, J.M., Alvarez, I., 2005. Ekman trasnport patterns in the area close to the Galician coast (NW, Spain). Journal of Atmospheric and Ocean Science, 10, 1-17.

Caires, S., Sterl, A., Komen, G., Swail, V., 2003. Global Wave Climatology Atlas, Royal Netherlands Meteorological Institute (KNMI), http://www.knmi.nl/waveatlas.

Casey, K.S., Cornillon, P., 1999. A comparison of satellite and in situ based sea surface temperature climatologies. Journal of Climate, 12**,** 1848–1863.

Casey, K.S., Cornillon, P., 2001. Global and Regional Sea Surface Temperature Trends. Journal of Climate, 14, 3801- 3818.

Chelton, D.B., Schlax, M.G., Freilich, M.H., Milliff, R.F., 2004. Satellite measurements reveal persistent small-scale features in ocean winds. Science, 303, 978-983.

Cole, J.E., Dunbar, R.B., McClanahan, T.R., Muthiga, N.A., 2000. Tropical Pacific Forcing of Decadal SST Variability in the Western Indian Ocean over the Past Two Centuries. Science, 287**,** 617-619. doi: 10.1126/science.287.5453.617

deCastro M., Gómez-Gesteira, M., Lorenzo, N., Alvarez, I., Crespo, A.J.C., 2007. Influence of atmopheric modes on coastal upwelling along the western coast of the Iberian Peninsula 1985 to 2005. Climate Research, 36, 169-179.

Diederich S., Nehls, G., van Beusekom, J.E.E., Reise, K., 2005. Introduced Pacific oyster (Crassostrea gigas) in the northern Wadden Sea: invasion accelerated by warm summers? Helgoland Marine Research, 59, 97-106.

Flohn, H., Kapala, A., Knoche, H.R., Machel, H., 1990. Recent changes of the tropical water and energy budget and of midlatitude circulations. Climate Dynamics, 4, 237- 252.

Folland, C., Parker, D., Kates, F., 1984. Worldwide marine temperature fluctuations 1856–1981. Nature, 310**,** 670–673.

Folland, C., Parker, D., Karl, T., Vinnikov, K., 1990. Observed climate variations and change, in: Houghton, J., Jenkins, G., Ephraums, J. (Eds), Climate Change: The IPCC Scientific Assessment. Cambridge University Press, pp. 195–238.

Frank, K.T, Petrie, B., Choi, J.S., Leggete, W.C., 2005. Trophic cascades in a formerly cod-dominated ecosystem. Science, 308, 1621-1623.

Gillet, N.P., Thompson, D.W.J., 2003. Simulation of recent southern hemisphere climate change. Science, 302, 273- 275.

Ginzburg, A.I., Kostianoy, A.G., Sheremet, N.A., 2004. Seasonal and interanual variability of the Black Sea surface temperature as revealed from satellite data (1982–2000). Journal of Marine Systems, 52, 33– 50.

Gómez-Gesteira, M., Moreira, C., Alvarez, I., deCastro, M., 2006. Ekman transport along the Galician coast (NW, Spain) calculated from forecasted winds. Journal of Geophysical Research, 111 C10005, doi: 10.1029/2005JC003331.

Gonzalez-Pola, C., Lavin, A., Vargas-Yañez, M., 2005. Intense warming and salinity modification of intermediate water masses in the southeastern corner of the Bay of Biscay for the period 1992- 2003. Journal of Geophysical Research, 110, C05020, doi: 10.1029/2004JC002367.

Goreau, T.J., Hayes, R.L., McAllister, D., 2005. Regional patterns of sea surface temperature rise: Implications for global ocean circulation change and the future of coral reefs and fisheries. World Resource Review, 17, 350- 374.

Gosselin, L.A., Qian, P.Y., 1997. Juvenile mortally in benthic marine invertebrates. Marine Ecology Progress Series, 146, 265-282.

Harris, L.G., Tyrrell, M.C., 2001. Changing community states in the Gulf of Maine: synergism between invaders, overfishing and climate change. Biological Invasions, 3, 9-21.

Honkoop, P.J.C., Van der Meer, J., Beukema, J.J., Kwast, D., 1998. Does temperature-influenced egg production predict the recruitment in the bivalve Macoma balthica? Marine Ecology Progress Series, 164, 229–235.

Intergovernmental Panel on Climate Change, 1996. Climate Change 1995: The Science of Climate Change, the Contribution of Working Group 1 to the Second Assessment Report of the Intergovernmental panel on Climate Change, Cambridge University Press, Cambridge.

Intergovernmental Panel on Climate Change, 2001. Climate Change 2001: The Scientific Basis: Contribution of Working Group 1 to the Third Assessment Report of the Intergovernmental Panel on Climate Change, Cambridge University Press, New York.

Koutsikopoulos, C., Le Cann, B., 1996. Physical processes and hydrological structures related to the bay of Biscay Anchovy. Scientia Marina, 60, 9-19.

Lemos, R.T., Pires, H.O., 2004. The upwelling regime off the west Portuguese coast, 1941- 2000. International Journal of Climatology, 24, 511- 524, doi: 10.1002/joc.1009.

Levitus, S., Antonov, J.I., Timothy, P.B., Stephens, C., 2000. Warming of the World Ocean. Science, 287, 2225- 2229.

Levitus, S., Boyer, T., 1994. Temperature. World Ocean Atlas 1994, NOAA Atlas NESDIS 4, pp. 117.

Nerem, S., Chambers, D.P., Leuliette, E.W., Mitchum, G.T., Giese, BS., 1999. Variations in global mean sea level associated with the 1997-1998 ENSO event. Implications for measuring long term sea level change. Geophysical Research Letters, 26, 3005- 3008.

Nykjaer, L., Van Camp, L., 1994. Seasonal and interannual variability of coastal upwelling along northwest Africa and Portugal from 1981 to 1991. Journal of Geophysical Research, 99, 14197–14208.

Occhipinti-Ambrogi, A., 2007. Global change and marine communities: alien species and climate change. Marine Pollution Bulletin, 55, 342-352.

Parmesan, C., Yohe, G., 2003. A globally coherent fingerprint of climate change impacts across natural systems. Nature, 421, 37- 42.

Paltridge, G., Woodruff, S., 1981. Changes in global surface temperature from 1880 to 1977 derived from historical records of sea surface temperature. Monthly Weather Review, 109**,** 2427–2434.

Philippart, C.J.M., van Aken, J.J., Beukema, H., Bos, O.G., Cadée, G.C., Dekker, R., 2003. Climate-related changes in recruitment of the bivalve Macoma balthica. Limnology and Oceanography, 48, 2171-2185.

Pingree, R.D., Le Cann, B., 1989. Celtic and Armorican slope and shelf residual currents. Continental Shelf Research, 23, 303-338.

Potter, R.A., Lozier, M.S., 2004. On the warming and salinification of the Mediterranean outflow waters in the North Atlantic. Geophysical Research Letters, 31, L01202, doi: 10.1029/2003GL018161.

Reynolds, R.W., Smith, T.M., 1995. A high-resolution global sea surface temperature climatology. Journal of Climate, 8**,** 1571–1583.

Reynolds, R.W., Smith, T.M., Folland, C.K., Parker, D.E., 1989. Biases in satellite-derived sea-surface-temperature data. Nature, 341**,** 728–731.

Roderick, R., Farquhar, G.D., 2002. The cause of decreased pan evaporation over the past 50 years. Science, 298, 1410- 1411.

Santos A.M.P., Kazmin, A.S., Peliz, A., 2005. Decadal changes in the Canary upwelling system as revealed by satellite observations: their impact on productivity. Journal of Marine Research, 63, 359- 379.

Strong, A., 1989. Greater global warming revealed by satellite-derived sea-surface-temperature trends. Nature, 338**,** 642–645.

Strong, A.E., Kearns, E.J., Gjovig, K.K., 2000. Sea surface temperature signals from satellite- An update, Geophysical Research Letters, 27, 1667-1670.

Thieltges, D.W., 2006. Parasite Induced Summer Mortality in the Cockle Cerastoderma edule by the Trematode Gymnophallus choledochus. Hydrobiologia, 559, 455-461.

Walther, G.R., Post, E., Convey, P., Menzel, A., Parmesan, C., Beebee, T.J.C., Fromentin, J.M., Hoegh-Guldber, O., Bairlein, F., 2002. Ecological responses to recent climate change. Nature, 416, 389-395.

Wiley, D.P., Frey, R., Zhang, H., Menzel, W.P. 2002. Extending HIRS high could trends with NODIS, NASA http://modis.gsfc.nasa.gov/sci_team/meetings/200207/presentations/menzel.pdf.

Woodruff, S., Slutz, R., Jenne, R., Steurer, P., 1987. A comprehensive ocean–atmosphere data set. Bulletin of American Meteorology Society, 68**,** 1239– 1250.

Wooster W.S., Bakun, A., McClain, D.R., 1976. The seasonal upwelling cycle along the eastern boundary of the north Atlantic. Journal of Marine Research, 34, 131-141.

Young, E., Bigg, G.R., Grant, A., 1996. A statistical study of environmental influences on bivalve recruitment in the Wash, England. Marine Ecology Progress Series, 143, 121-129.

Chapter 6

Cooling- warming cycles since 1854

Abstract

The warming trend observed during the last two decades (1985-2007) in the Bay of Biscay is put within the context of Sea Surface Temperature (SST) changes observed in the area since 1854. Macroscopically, two consecutive warming-cooling cycles were detected during this period of time: cooling from 1867 to 1910; warming from 1910 to 1945; cooling from 1945 to 1974; and warming from 1974 to nowadays. Warming rates of 0.17 and 0.22ºC per decade were measured during the warming sub- periods and cooling rates of -0.14 and -0.10 ºC per decade were measured during the cooling sub- periods. The present warming period is on the same order of magnitude although slightly more intense than the one observed from 1910 to 1945, which is consistent with previous analysis carried for the North Atlantic. Finally, the thermal amplitude defined as the difference between the maximum and minimum annual values has increased since 1974 at a rate of 0.06 ºC per decade due to the different increasing rates of the maximum (0.26 ºC per decade) and minimum (0.20 ºC per decade) SSTs.

6.1. Introduction

Ocean can play a crucial role in regulation the climate (Folland et al. 2001).The temperature of sea water mass is mainly determined by three heat fluxes: heat exchange at atmosphere- ocean interface, heat transfer by advection and turbulent diffusion and practically negligible heat exchanges on the sea bottom. In this sense, the sea surface temperature (SST) is a parameter influenced by climatic, meteorological, hydrodynamic and

topographic parameters. During the last decades, an important effort has been devoted to develop reliable surface temperature series with global coverage (for a detailed description of the state of the art see Brohan et al. (2006), Smith et al. (2008) and the references therein). In the particular case of SST, the bases merge measurements from voluntary observation ships (VOS), drifters and moored buoys and satellite data. Uncertainties in the SST data can arise due to several factors as changes in the ship routes after the opening of Panama and Suez Canals, sampling sparseness during the world wars and differences in water collection. At the end of the nineteenth century and the beginning of the twentieth century wooden and canvas buckets were used to collect seawater and around the World War II many vessels began measuring the sea temperature at the engine cooling water intake. Since the beginning of the eighties, the use of satellite derived data generated new uncertainties due both to the presence of aerosols and clouds, which can cause a cool bias, and to the fact that satellite instruments record skin temperature instead of near surface temperature (for a complete understanding of the different bias and the methods to correct bias and uncertainties see: Kushnir, 1994; Parker et al. 1994; Folland and Parker, 1995; Smith et al. 1996; Kaplan et al. 1998; Smith and Reynolds, 2002, 2003, 2004, 2005; Woodruff et al. 2003; Woorley et al. 2005; Kent and Berry, 2005; Kent and Challenor, 2006; Kent and Taylor, 2006; Brohan et al. 2006; Smith et al. 2008).

In general, the trend in SST data sets is highly dependent on spatial and temporal scales being possible to observe opposite trends when different periods of time are considered (Parker et al. 1994; Smith et al. 1994; Casey and Cornillon, 2001). Despite this fact, most of the studies carried out during the last decades conclude that a considerable global warming in SST has

occurred over the last century no matter the considered data set (Folland et al. 1984; Folland et al. 1992; Parker et al. 1994; Nicholls at al. 1996; Casey and Cornillon, 2001). This global warming is far from being uniform during the 20th century. Global SST time series show two distinct warming periods during the past 100 years according to the Intergovernmental Panel on Climate Change (2007). The first occurred during the period 1910 to 1945 and was followed by a period of cooling; the second warming period began during the 1970s. In addition, global warming is not uniformly distributed all over the world´s oceans (Paltridge and Woodruff, 1981; Folland et al. 1990; Parker et al. 1994; Smith et al. 1994; Strong et al. 2000; Casey and Cornillon, 2001). These differences among macroscopic areas (hemispheres and oceans) are even more marked at regional scales where some areas warm at higher or lower rates than the others as shown in regional studies (Cole at al. 2000; Lemos and Pires, 2004; Ginzburg et al. 2004; Santos et al. 2005; Goreau et al. 2005; Gómez-Gesteira et al. 2008).

6.1.1 Study area

The Bay of Biscay is located in the northeastern Atlantic Ocean between 0-10ºW and 43ºN- 48ºN. The northern Iberian Peninsula coast is situated at the southern part of the Bay of Biscay with an east- west orientation whilst the French coast has a north- south orientation (Figure 6.1).

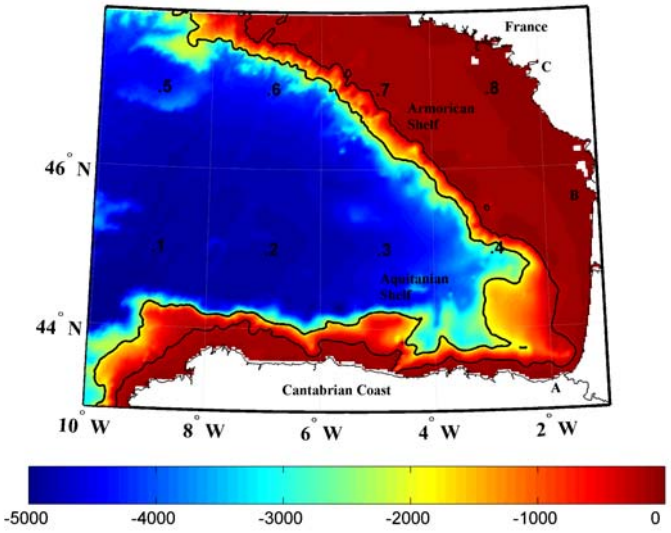

Figure 6.1. Area under scope corresponding to the Bay of Biscay. Numbers represent the points where the monthly extended reconstructed SST data were considered. A represents San Sebastian, B the Gironde river and C the Loire river. Thin (thick) line corresponds to the 200 m (2000 m) depth isobath.

This bay is bordered by three shelves: Armorican, Aquitanian and Cantabrian shelf. The continental shelf is particularly important in the northern Bay of Biscay characterized by a width ranging from 60 to over 200 km and by a very gentle slope of 0.12% (Pascual et al. 2004). In contrast, the Cantabrian shelf is characterized by its narrowness (7-20 km wide). The oceanic part of the Bay of Biscay is characterized by a weak (1–2 cm/s) and variable anti-cyclonic circulation (Saunders, 1982; Koutsikopoulos and Le Cann, 1996), as well as by cyclonic and anti-cyclonic eddies shed by the slope current (Pingree and Le Cann, 1992). The annual sequence of events generally follows the seasonal cycle of temperate seas (OSPAR, 2000). For example, wind, heating, rainfall and river run-off modify water

characteristics on the Cantabrian shelf and impose considerable spatial, seasonal and inter-annual variability. The southeastern corner of the bay has distinctive climatic and geographic characteristics with a strong continental influence over the region. The continental shelf waters are less saline, colder in winter and warmer in summer, than waters of western areas at equivalent latitudes (Valencia et al. 2003, 2004). In addition, there is a significant coupling between meteorological and oceanographic conditions over the area. Meteorological forcing drives oceanographic conditions at the sea surface (Fontan et al. 2008). In fact, air temperature explains about 88% of the SST variability, on a monthly basis, for the period 1961- 2005. Such dependence is the result of a combination of strong continental influence and relatively weak advection and transport mechanisms over the region (Valencia et al. 2004). Although, the climate regime of the Bay of Biscay is characterized by the "classical" seasonal cycle in the Atlantic climatic regime at mid- latitudes, recent studies show a "deseasonalisation" produced by the prevalence of winter- summer duality, against the establishment (in terms of values and mean duration) of spring and autumn as transitional seasons (Usabiaga et al. 2004; Fontan et al. 2008).

In spite of the marginal location of this bay, the trends over the area are consistent with the anomaly patterns described for the northeastern Atlantic Ocean. SST at San Sebastian (Figure 6.1, point A) shows the anomalies described for the North Atlantic in the 1970s (Dickson at al. 1988; Usabiaga et al. 2004). In addition, the transition period from late 1980s to early 1990s shows an increment in temperature and salinity linked to mild and dry winters in the inter-gyre area of the northeastern Atlantic (Perez et al. 1995; Perez et al. 2000). With respect to the SST trends in the area under scope, opposite trends have been observed when different periods are considered.

The SST data series in San Sebastian, from 1947 to 2001, indicates a decreasing trend in the mean annual temperature responding to the warm periods at the end of the 1940s and the 1960s (Borja et al. 2000). However, Koutsikopoulos et al. (1998) show an increasing trend of the mean SST in the Bay of Biscay during the period 1972- 1993 with a rate of about 0.64 ºC per decade. This study reveals that the warming trend was not homogenous at the scale of the bay and the adjacent sectors. The trend was recorded both in winter and in summer period with the winter slopes slightly higher but not statistically different. This pattern shows how the SST increase is more related to mild winters SST values than to warm summers (Koutsikopoulos et al. 1998). In addition, the monthly and seasonal analysis of different SST time series (ICES, 2004) indicates increasing trends for the period 1971-1998 and the most recent period 1986- 2003.

There are several biological observations that can be reasonable linked to the SST long- term changes observed (Sauriau, 1991; Junquera and Perez-Gandaras, 1993; Quero et al. 1998). In particular, some marine species whose range is thermally controlled (McMahon and Hays, 2006) can be found in areas where they have not been seen in the past, giving rise to the appearance of warm-water “exotic” marines species and, eventually, to the decline and even collapse of several marine ecosystems (Thomas et al. 2004; Diederich et al. 2005; Frank et al. 2005). In addition, coastal ecosystems have also shown to be highly vulnerable to global climate changes because warming can have impacts on biological production of coastal areas. A general increase of water temperature can produce an advancement of bivalve spawning, affecting egg production and fecundity and it can increase the number of predators affecting survival of bivalve early life state (Young et al. 1996; Honkoop et al. 1998). The key point is the fact that commercial

species as cod and tuna can be regional extinct due to rising temperature with the consequent socio-economic impact (Block et al. 2001; Righton et al. 2001; Beaugrand et al. 2003; Perry et al. 2005).

The aim of this paper is to analyze the importance of the warming trend observed during the last decades in the Bay of Biscay within the context of the different warming-cooling cycles observed since 1854. The present warming trend will be shown to be more intense than any other warming (or cooling) period observed during the last 154 years.

6.2. Data and methods

Two different but complementary SST databases have been used to characterize the temporal and spatial variability of the SST in the Bay of Biscay. The first one, which covers from 1985 to 2006, provides a high spatial resolution of SST in the area. The second one has a coarser spatial resolution but it extends back to 1854 giving the opportunity to analyze the temporal trend of SST for the last 154 years.

The first database is the weekly mean SST obtained from the Advanced Very-High Resolution Radiometer (AVHRR) onboard of NOAA series satellites (see Chapter 2).

For our purposes, the area 43ºN -48ºN, 1- 9ºW corresponding to the Bay of Biscay region was cut from the global data set for the period 1985-2006. Night-time data were used to avoid the solar heating effect.

A land mask, corresponding to the points without coverage or with low coverage was calculated as follow. The number of times each point in the study area presents valid SST values was computed for the period 1985-2006. Then, the point with the highest number of valid samples was calculated, being N_{max} the number of valid samples. Finally, all points with a

number of valid samples lower than 0.9 N_{max} were discarded from the analysis.

The following protocol was applied to the valid points. First, SST data were averaged to a monthly time scale. Then, voids due to cloud coverage or other malfunctions were interpolated from nearest neighbours by means of a weighted (Gaussian) average. The process was iterated from an initial square box of 3×3 neighbours (12×12 km) around the point up to a maximum distance of 25×25 neighbours (100×100 km). The process was automatically stopped when the number of neighbours with reliable values inside the box was higher than 5.

The second database is the extended reconstructed SST (ERSST) version 3 (ERSST.v3) data provided by the NOAA/OAR/ESRL PSD, Boulder, Colorado (see Chapter 2). SST data were considered at 8 different locations in the Bay of Biscay (Figure 6.1, points) to analyze the SST trends. The 8 points correspond to open sea locations, in order to study oceanic trends without continental influence. Point to point correlation was observed to be higher than 0.98 in all cases. This fact justifies the analysis in terms of a unique mean series which was calculated by averaging the series corresponding to the 8 points.

6.3. Results

6.3.1. Spatio- temporal characterization of SST from 1985 to 2007

Warming rates measured in the Bay of Biscay from 1985 to 2007 are analyzed in terms of the SST anomaly (SST_a) calculated from the annual cycle (Figure 6.2).

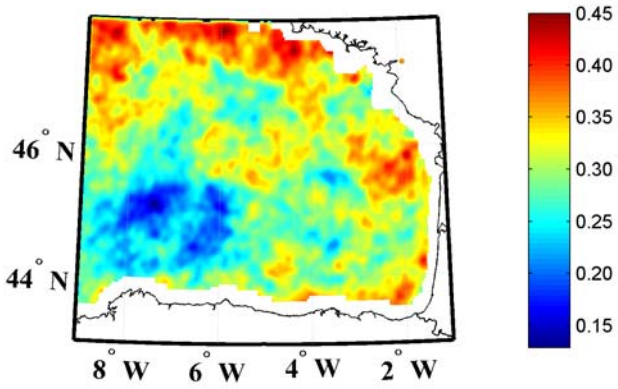

Figure 6.2. Annual warming trend (ΔSST_a in ºC per decade) for the period 1985-2006. Warming rates ranging from 0.15 ºC per decade to 0.45 ºC per decade are observed in the study area.

This figure shows an increment of SST anomaly (ΔSST_a) ranging from 0.15 ºC per decade in the southwestern part to 0.45 ºC per decade in the northwestern part and along the French coast. Voids (white areas) correspond to points with statistical significance lower than 90%.

The observed warming trend does not remain constant throughout the year, showing important seasonal variations as depicted in Figure 6.3. Seasonal warming rates measured in the Bay of Biscay from 1985 to 2007 are analyzed in terms of the SST_a calculated for every season. Only spring (AMJ) and summer (JAS) are represented since they are the only seasons with a significance level higher than 90% in most of the points.

Both spring and summer present mean warming trends higher than the annual ones (see Table 6.I). The maximum values in spring were observed in the southeastern part of the bay, reaching values on the order of 0.80 ºC per decade close to San Sebastian. Similar intensities were observed in summer in the northern part of the bay. The signal-to-noise ratio ($100\times\sigma(\Delta SST_a)/<$

ΔSST_a>) is on the order of 25% in the seasons with statistical significance and close to 15% when considering the annual period.

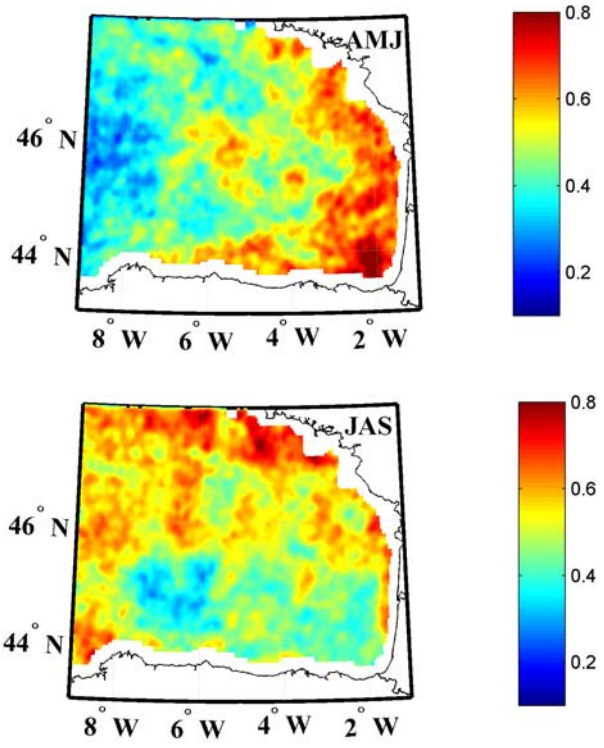

Figure 6.3. Seasonal warming trend (ΔSST_a in ºC per decade) for the period 1985-2006. Spring (AMJ) and summer (JAS) are the only seasons with a significance level higher than 90% in most of the area.

Season	$<\Delta SST_a>$	$\sigma(\Delta SST_a)$
Winter (JFM)	0.10	0.10
Spring (AMJ)	0.48*	0.13
Summer (JAS)	0.54*	0.10
Autumn (OND)	0.10	0.12
Annual	0.33*	0.05

Table 6.I. Mean seasonal and annual increment of SST anomaly (ΔSST_a; ºC decade^{-1}) in the Bay of Biscay for the period 1985-2007. Values with a significance level higher that 90% are marked with an asterisk.

6.3.2. Warming- cooling cycles from 1854 to 2007

The annual evolution of the SST was analyzed from 1854 to 2007 in order to put the intensity of the present warming trend within the context of the last two centuries.

6.3.2.1. Periodicity

The monthly evolution of SST (Figure 6.4(a)) shows a clear seasonal cycle with minimum values from January to April and maximum values from July to September. Short term fluctuations were smoothed out by means of a running average (±10 years). In spite of the smoothing imposed by the running average different modulations in SST can be observed. In particular, the width of the summer band (16.5 ºC < SST < 18.5 ºC) is observed to reach a minimum around 1910 and a maximum during the last decade. The seasonal pattern of SST can also be observed in the annual cycle of SST calculated by averaging each month from 1854 to 2007 (Figure 6.4(b)). The SST cycle shows thermal amplitude on the order of 7 ºC, with a minimum (~11 ºC) in February-March and a maximum (~18 ºC) in August. The error bars were calculated as the standard deviation of the monthly data ($\sigma(SST)$).

The signal-to-noise ratio ($100\times\sigma(SST)/\langle SST\rangle$) does not exceed 10% showing the periodic nature of the signal.

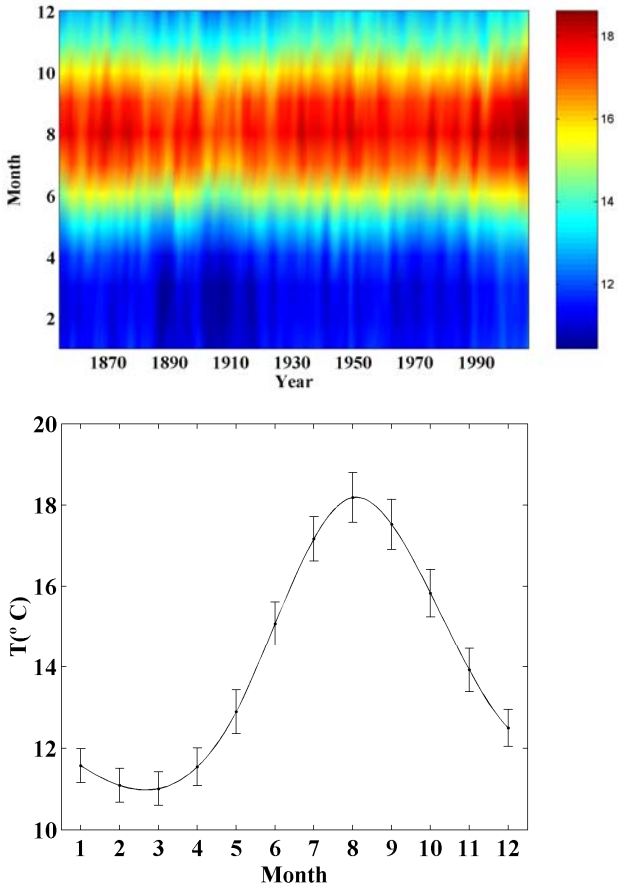

Figure 6.4. Temporal SST patterns (ºC) for the period 1854-2007. (a) Monthly evolution of SST and (b) annual cycles.

6.3.2.2. SST trends

The inter-annual variation of SST_a is calculated using the annual cycle obtained from the 154- year monthly means (Figure 6.5 light line). This monthly pattern is highly noisy, with peak values on the order of ±1.5 ºC and standard deviation of ±0.5 ºC.

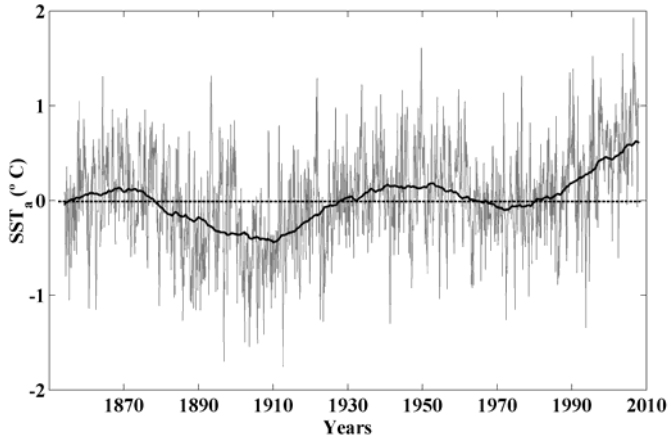

Figure 6.5. Evolution of SST_a (ºC) for the period 1854-2007. Two consecutive warming-cooling cycles can be observed.

Short term fluctuations were smoothed out (Figure 6.5 dark line) by means of a running average (±10 years) in order to highlight the macroscopic warming and cooling periods. Positive (negative) values of the SST_a mean temperature higher (lower) than the average. Two consecutive warming-cooling cycles can be observed in SST_a: (a) cooling from 1867 to 1910; (b) warming from 1910 to 1945; (c) cooling from 1945 to 1974; and (d) warming from 1974 to nowadays. The ΔSST_a -in ºC per decade- corresponding to every period is described in Table 6.II. Cooling trends, which show amplitudes on the order of -0.10 ºC per decade, are less intense

than warming trends (on the order of 0.20 ºC per decade). Extreme annual SST_a values were used to analyze different seasonal trends and thermal amplitude.

Period	ΔSST_a
1867- 1910	-0.14*
1910- 1945	+0.17*
1945- 1974	-0.10*
1974- 2007	+0.22*
1854-2007	+0.03

Table 6.II. Increment of SST anomaly (ΔSST_a; ºC decade^{-1}) for each warming-cooling period from 1854 to 2007 and for the whole period. Short term fluctuations were smoothed out by means of a running average (±10 years). Values with a significance level higher that 90% are marked with an asterisk.

The inter-annual variation of the maximum and minimum SST_a observed every year since 1854 (Figure 6.6(a) dark and light dots, respectively) reproduces, at least macroscopically, the SST_a warming-cooling cycle previously described in Figure 6.5.

Maximum values of SST_a were detected in August and minimum values in February and March, in good agreement with the annual cycle shown above (Figure 6.4(b)). Although the maximum and minimum SST_a follow a similar overall pattern, the maximum is observed to increase faster than the minimum during the last warming cycle (1974- 2007). This difference results in an increase of SST amplitude of 0.06 ºC per decade, which is much higher than the rate observed for the entire period (~0.02 ºC per decade).

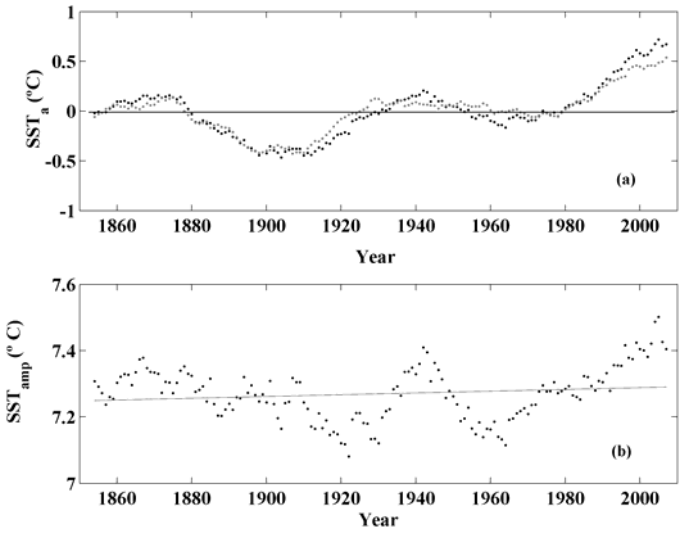

Figure 6.6. Changes in SST extremes (ºC) for the period 1854-2007. (a) Maximum and minimum SST_a (dark and light dots, respectively); (b) SST amplitude. The solid line corresponds to a linear fitting showing a trend of 0.02 ºC per decade.

6.4. Discussion

During the last decades the responses of marine ecosystems to global change have attracted the interest of the scientific community and a considerable effort has been devoted to separate anthropogenic forcing from natural variability. In this sense, the analysis of long- time SST series permits to detect past climate variations and for comparison to put in context present climate variations. In this context, the present warming trend observed in the Bay of Biscay was compared to previous warming-cooling cycles by means of a 2º×2º database from 1854 to 2007. The coarse resolution of the grid does not permit to analyze the spatial variability of SST trends in the study area. However, this database provides a suitable tool to analyze the different cycles observed during the last 154 years.

The annual SST trend observed in the present analysis is in good agreement with previous SST trends analyzed during periods of time mainly focused on the last three decades. In fact, the warming trends previously measured by Koutsikopoulos (1998) from 1972 to 1993, by the ICES (2004) for the periods 1971- 1998 and 1986- 2003 and by Gomez-Gesteira et al. (2008) for the period 1985- 2005 were reproduced in the present SST trend analysis. Although all previous studies agree in the existence of a warming trend since the seventies, there is not agreement in the warming rate. The inter-comparison among trends is a difficult task due to the use of different databases, statistical techniques and periods of reference considered by the different authors. Koutsikopoulos (1998) obtained a maximum warming rate of 0.64 ºC per decade for the period 1972- 1993 using a grid based on vessels and buoys, Planque et al. (2003) obtained a maximum warming trend of 0.6 ºC per decade in the southeastern corner of the Bay of Biscay using SST data from Meteo- France. More recently, Llope et al. (2006) obtained a warming rate of 0.5 ºC per decade using an empirical model coefficients for the period 1993- 2003 and Gomez-Gesteira et al. (2008) measured a coastal warming rate between 0.15 and 0.35 ºC per decade using satellite coastal SST data from 1985 to 2005. The satellite data corresponding to the period 1985-2007 used in the present study show a mean warming on the order of 0.33 ºC per decade. Nevertheless, this warming is neither homogeneous in space nor constant throughout the year. On the one hand, annual warming (Figure 6.2) is more intense along the French coast than along the Cantabrian coast. On the other hand, warming is especially important from April to September (Figure 6.3 and Table 6.I) in good agreement with coastal results described in Gomez-Gesteira et al. (2008). Other authors, Koutsikopoulos (1998) measured seasonal trends from 1972 to 1993 with winter slopes

slightly higher but not statistically different from the summer ones. The discrepancy between previous and present seasonal trends is probably caused for the period of time considered and the different data sources used (satellite SST data *versus* vessels and buoys). It is a well known fact that, the SST trend is highly dependent on spatial and temporal scales being sensitive to the different reference periods (Fontan et al. 2008).

The long term analysis (from 1850 to 2007) based on ERSST.v3 database shows two consecutive warming-cooling cycles with rates of 1.7 and 0.22 ºC per decade during the two warming sub- periods (1910- 1945 and 1974- 2007) and -0.14 and -0.10 ºC per decade during the cooling sub- periods (1867- 1910 and 1945- 1974) (Table 6.II). This fact seems to indicate the existence of natural oscillations as suggested Southward and Boalch (1994) and Planque et al. (2003) using the COADS records from 1844 to 2000. The present warming period is on the same order of magnitude although slightly more intense than the one observed from 1910 to 1945, which is consistent with the analysis carried out by Hobson et al. (2008) for the North Atlantic. This fact does not permit elucidating the possible anthropogenic influence on the present day warming, which still remains an open question.

In spite of the marginal location of the Bay of Biscay, the macroscopic trends observed in the area during the last 154 years (Figure 6.5 and Table 6.II) are consistent with previous studies. In fact, the two last warming trends observed in the Bay of Biscay (from 1910 to 1945 and from 1974 to nowadays) match the anomalies described in the Intergovernmental Panel on Climate Change (2007). In particular, the warming observed in the Bay of Biscay for the period 1854 to 2007 (0.03 ºC per decade, see Table 6.II) is consistent with the ones observed in the Northern Hemisphere by Rayner et al. (2006) for the period 1850-2005 (0.042 ± 0.016 ºC per decade) and by

Rayner et al. (2003) for the period 1861-2005 (0.038 ± 0.011 ºC per decade). In addition, the warming observed in the Bay of Biscay for the period 1974 - 2007 (0.22 ºC per decade, see Table 6.II) is also consistent with the values calculated in the Northern Hemisphere by other authors for the period 1979-2005 (0.190 ± 0.134 ºC per decade in Rayner et al. (2006) and 0.186 ± 0.060 ºC per decade in Rayner et al. (2003)). Our study is also consistent with the local study carried out by Goikoetxea et al. (2008) with data from the Aquarium of San Sebastian. In this study, authors found a warming of 0.23 ºC per decade for the period 1977-2007. Finally, Michel et al. (2009) observed and modeled a SST increase in the Bay of Biscay ranging from 0.22 to 0.31 ºC per decade during the period 1985-2003.

The mean warming rates obtained for the last warming period by means of both data sets considered in the present study are in good quantitative agreement. Satellite data have provided a warming rate of 0.33±0.05 ºC per decade for the period 1985-2007, which is close to the value provided for the reconstructed data corresponding to the period 1974-2007 (0.22 ºC per decade). Note that both periods do not coincide exactly and, in addition, reconstructed data correspond to oceanic values, without near coast effects as observed in satellite data.

The warming observed from 1974 to 2007 is characterized by an increment in thermal amplitude. The maximum SST has increased at a rate of 0.26 ºC per decade whilst the minimum has only increased at a rate of 0.20 ºC per decade resulting in a mean increment of thermal amplitude of 0.06 ºC per decade. Apart from these different increasing rates, the maximum starts increasing at least a decade before (~1965) the increase is detected in the minimum. The observed warming trend is due to warmer summers more than to mild winters. This result contrasts with previous research by

(Koutsikopoulos et al. 1998) who affirmed that the increasing trend was more related to mild winters than to warm summers. The different extent of both series 1972- 1993 in Koutsikopoulos et al. (1998) and 1974-2007 in our case is, possibly, the main reason of this discrepancy.

6.5. Summary and conclusions

SST variability in the Bay of Biscay has been analyzed by means of two complementary data sets. The following facts can be concluded from the present study:

1. The intense warming period observed during the last decades show both seasonal and spatial modulations. Warming rates are especially important during spring and summer. In addition, warming has been observed to be more intense in the northwestern part of the bay and along the French coast than in the Cantabrian area.
2. Two consecutive warming-cooling cycles were detected during the period 1854-2007: cooling from 1867 to 1910 (-0.14 ºC per decade); warming from 1910 to 1945 (0.17 ºC per decade); cooling from 1945 to 1974 (-0.10 ºC per decade); and warming from 1974 to 2007 (0.22 ºC per decade).
3. The present warming period (1974 to 2007) is on the same order of magnitude although slightly more intense than the one observed from 1910 to 1945 in good agreement with previous analysis carried for the North Atlantic.
4. The warming observed since 1974 also shows an increment in thermal amplitude which is mainly due to the different increasing rates of the maximum (0.26 ºC per decade) and minimum (0.20 ºC per decade) SSTs.

6.6. References

Beaugrand, G., Brender, K.M., Lindley, J.A., Souissi, S., Reid, P.C., 2003. Plankton effect on cod recruitment in the North Sea. Nature, 426, 661- 664.

Block, B.A., Dewar, H., Blackwell, S.B., Williams, T.D., Prince, E.D., Farwell, C.J., Boustany, A., Teo, S.L.H., Seitz, A., Walli, A., Fudge, D., 2001. Migratory movements, depth preferences, and thermal biology of Atlantic bluefin tuna. Science, 293, 1310- 1314.

Borja, A., Egaña, J., Valencia, V., Franco, J., Castro, R., 2000. 1947-1997, estudio y validación de una serie de datos diarios de temperatura del agua del mar en San Sebastián, procedente de su Aquarium. Ozeanografika, 3, 139-152.

Brohan, P., Kennedy, J.J., Harris, I., Tett, S.F.B., Jones, P.D., 2006. Uncertainty estimates in regional and global observed temperature changes: A new data set from 1850. Journal of Geophysical Research, 111, D21206. doi:10.1029/2005JD006548.

Casey, K.S., Cornillon, P., 2001. Global and Regional Sea Surface Temperature Trends. Journal of Climate, 14, 3801- 3818.

Cole, J.E., Dunbar, R.B., McClanahan, T.R., Muthiga, N.A., 2000. Tropical Pacific Forcing of Decadal SST Variability in the Western Indian Ocean over the Past Two Centuries. Science, 287**,** 617-619, doi: 10.1126/science.287.5453.617.

Dickson, R.R., Meincke, J., Malmberg, S.A., Leea, J., 1988. The "Great Salinity Anomaly" in the Northern North Atlantic 1968-1982. Progress in Oceanography, 20, 103-151.

Diederich S., Nehls, G., van Beusekom, J.E.E., Reise, K., 2005. Introduced

Pacific oyster (Crassostrea gigas) in the northern Wadden Sea: invasion accelerated by warm summers? Helgoland Marine Research, 59, 97-106.

Folland, C., Parker, D., Kates, F. 1984. Worldwide marine temperature fluctuations 1856–1981. Nature, 310**,** 670–673.

Folland, C., Parker, D., Karl, T., Vinnikov, K., 1990. Observed climate variations and change, in: Houghton, J., Jenkins, G., Ephraums, J. (Eds.), Climate Change: The IPCC Scientific Assessment, Cambridge University Press, pp. 195–238.

Folland, C., Nicholls, N., Nyenzi, B., Parker, B., Vinnikov, K., 1992. Observed Climate Variability and change, in: Houghton, J., Jenkins, G., Ephraums, J. (Eds.), Climate Change 1992: the supplementary Report to the IPCC Scientific Assessment, Cambridge University Press, pp. 135- 170.

Folland, C., Parker, D. ,1995. Correction of instrumental biases in historical sea surface temperature data. Quart. J. Roy. Meteor. Soc., 121, 319-367.

Folland, C.K., Rayner, N.A., Brown, S.J., Smith, T.M., Shen, S.S.P., Parker, D.E., Macadam, I., Jones, P.D., Jones, R.N., Nicholls, N., Sexton, D.M.H., 2001. Global Temperature Change and its Uncertainties Since 1861. Geophysical Research Letters, 28, 2621–2624.

Fontan, A., Valencia, V., Borja, A., Goikoetxea, N., 2008. Oceano-meteorological conditions and coupling in the southeastern Bay of Biscay, for the period 2001-2005: a comparison with the past two decades. Jounal of Marine Systems, doi:10.1016/j.jmarsys.2007.08.003

Frank, K.T, Petrie, B., Choi, J.S., Leggete, W.C., 2005. Trophic cascades in

a formerly cod-dominated ecosystem. Science, 308, 1621-1623.

Ginzburg, A.I., Kostianoy, A.G., Sheremet, N.A., 2004. Seasonal and interanual variability of the Black Sea surface temperature as revealed from satellite data (1982–2000). Journal of Marine Systems, 52, 33– 50.

Goitkoetxea, N., Borja, A., Fontan, A., Gonzalez, M., Valencia, V., 2009. Trends and anomalies of the sea surface temperature during the last 60 years within the southeastern Bay of Biscay. Continental Shelf Research, 29, 1060-1069.

Gomez-Gesteira, M., deCastro M., Alvarez, I., Gesteira, J.L.G., 2008. Coastal SST warming trend along the continental part of the Atlantic Arc (1985 – 2005). Journal of Geophysical Research, 113, C04010, doi: 10.1029/2007JC004315

Goreau, T.J., Hayes, R.L., McAllister, D., 2005. Regional patterns of sea surface temperature rise: Implications for global ocean circulation change and the future of coral reefs and fisheries. World Resource Review, 17, 350- 374.

Hobson, V.J., McMahon, C.R., 2008. Ocean surface warming: The North Atlantic remains within the envelope of previous recorded conditions. Deep- sea Research I, 55, 155-162.

Honkoop, P.J.C., Van der Meer, J., Beukema, J.J., Kwast, D., 1998. Does temperature-influenced egg production predict the recruitment in the bivalve Macoma balthica? Marine Ecology Progress Series, 164, 229–235.

ICES, 2004. The Annual ICES Ocean Climate Status Summary 2003/2004. ICES Cooperative Research Report, No. 269. 32 pp.

Intergovernmental Panel on Climate Change. 2007. Climate Change 2007:

The Physical Science Basis. Contribution of Working Group 1 to the Fourth Assessment Report of the Intergovernmental panel on Climate Change, Cambridge University Press, Cambridge.

Junquera, S., Perez- Gandaras, G., 1993. Polpulation diversity in Bay of Biscay anchovy (Engraulis encrasicolus L. 1758) as revealed y multivariate analisys of morphometric and meristic characters. ICES Journal of Marine Science, 50, 383- 391.

Kaplan, A., Cane, M.A., Kushnir, Y., Clement, A.C., Blumenthal, M.B., Rajagopalan, B., 1998. Analyses of global sea surface temperature 1850- 1991. Journal of Geophisical Research, 103, 18567- 18589.

Kent, E., Berry, D.I., 2005. Quantifying random measurement errors in voluntary observing ships' meteorological observations. International Journal of Climatology, 25, 843- 856. doi: 10.1002/joc.1167.

Kent, E., Challenor, P.G., 2006. Toward estimating climatic trends in SST. Part II: random errors. Journal of Atmospheric and Oceanic Technology, 23, 476- 486.

Kent, E., Taylor, P.K., 2006. Toward estimating climatic trends in SST. Part I: methods of measurements. Journal of Atmospheric and Oceanic Technology, 23, 464- 475.

Koutsikopoulos, C., Le Cann, B., 1996. Physical processes and hydrological structures related to the Bay of Biscay Anchovy. Scientia Marina, 60, 9–19.

Koutsikopoulos, C., Beillois, P., Leroy, C., Taillefer, F., 1998. Temporal trends and spatial structures of the sea surface temperature in the Bay of Biscay. Oceanologica Acta, 21, 335-344.

Kushnir, Y., 1994. Interdecadal variations in North atlantic Sea Surface

Temperature and Associated Atmospheric Conditions. American Meteorological Society, 141- 157.

Lemos, R.T., Pires, H.O., 2004. The upwelling regime off the west Portuguese coast, 1941- 2000. International Journal of Climatology, 24, 511- 524, doi: 10.1002/joc.1009.

Llope, M., Anadon, R., Viesca, L., Quevedo, M., Gonzalez- Quiros, R., Stenseth, N.C., 2006. Hydrography of the Southern Bay of Biscay shelf- break region: Interacting the multiscale physical variability over the period 1993- 2003. Journal of Geophysical Research, 111, C09021, doi: 10.1029/2005JC002963.

McMahon, C.R., Hays, G.C., 2006. Thermal niche, large-scale movements and implications of climate change for a critically endangered marine vertebrate. Global Change Biology, 12, 1330- 1338.

Michel, S., Treguier, A.M., Vandermeirsch, F., 2009. Temperature variability in the Bay of Biscay during the past 40 years, from an in situ analysis and a 3D global simulation. Continental Shelf Research, 29, 1070-1087.

Nicholls, N., Gruza, G.V., Jouzel, J., Karl, T., Ogallo, L., Parker, D., 1996. Observed Climate Variability and change, in: Houghton, J., Jenkins, G., Ephraums, J. (Eds.), Climate Change 1995: the science of climate change, Cambridge University Press, pp. 133- 192.

OSPAR Commission, 2000. Quality Status Report 2000: Region IV – Bay of Biscay and Iberian Coast. OSPAR Commission, London. 134 + xiii pp.

Paltridge, G., Woodruff, S., 1981. Changes in global surface temperature from 1880 to 1977 derived from historical records of sea surface temperature. Mon. Wea. Rev., 109**,** 2427–2434.

Parker, D.E., Jones, P., Folland, C., Bevan, A., 1994. Interdecadal changes of surface temperature since the late nineteenth century. Journal of Geophysical Research, 99, 14 373- 14 339.

Pascual, A., Cearreta, A., Rodríguez-Lázaro, J., Uriarte, A., 2004. Geology and Palaeoceanography, in: Borja, A., Collins, M. (Eds.), Oceanography and Marine Environment of the Basque Country, Elsevier Oceanography Series nº 70, Elsevier, pp. 53-73.

Perry, A.L., Low, P.J., Ellis, J.R., Reynolds, J.D., 2005. Climate change and distribution shifts in marine fishes. Science, 308, 1912- 1915.

Planque, B., Beillois, P., Jegou, A.M., Lazure, P., Petitgas, P., Puillat, I., 2003. Large- scale hydroclimatic variability in the Bay of Biscay: the 1900s in the context of interdecadal changes. ICES Marine Science, 219, 61- 70.

Pérez, F.F., Ríos, A.F., King, B.A., Pollard, R.T., 1995. Decadal changes of the θ-S relationship of the Eastern North Atlantic Central Water. Deep-Sea Research I, 42, 1849-1864.

Pérez, F.F., Pollard, R.T., Read, J.F., Valencia, V., Cabanas, J.M., Ríos, A.F., 2000. Climatological coupling of the thermohaline decadal changes in Central Water of the Eastern North Atlantic. Scientia Marina, 64, 347-353.

Pingree, R.D., Le Cann, B., 1992. Three anticyclonic Slope Water Oceanic eDDIES (SWODDIES) in the southern Bay of Biscay in 1990. Deep- Sea Research I, 39, 1147–75.

Quero, J.C., Du Buit, M.H., Vayne, J.J., 1989. Les poissones du golfe de Gascogne. Oceanological Acta, 21, 345- 351.

Rayner, N.A., Parker, D.E., Horton, E.B., Folland, C.K., Alexander, L.V., Rowell, D.P., Kent, E.C., Kaplan, A., 2003. Global analyses of sea

surface temperature, sea ice, and night marine air temperature since the late nineteenth century. Journal of Geophysical Research, 108, 4407, doi: 10.1029/2002JD002670.

Rayner, N.A., Brohan, P., Parker, D.E., Folland, C.K., Kennedy, J.J., Vanicek, M., Ansell, T.J., Tett, S.F.B., 2006. Improved analyses of changes and uncertainties in sea surface temperature measured in situ since the mid-nineteenth century: the HadSST2 dataset. Journal of Climate, 19, 446–469.

Righton, D., Metcalfe, J.D., Connolly, P., 2001. Different behavior of North and Irish Sea cod. Nature, 411, 156.

Santos, A.M.P., Kazmin, A.S., Peliz, A., 2005. Decadal changes in the Canary upwelling system as revealed by satellite observations: their impact on productivity. Journal of Marine Research, 63, 359- 379.

Saunders, P.M., 1982. Circulation in the eastern North Atlantic. Journal of Marine Reseasrch, 40, 641–57.

Sauriau, P.G., 1991. Spread of Cyclope neritea (Mollusca:Gastropoda) along the north- eastern Atlantic coasts in relation to oyster culture and to climatic fluctuations. Marine Biology, 109, 199- 309.

Smith, T.M., Reynolds, R.W., Ropelewski, C.F., 1994. Optimal averaging of seasonal sea surface temperatures and associated confidence intervals (1860- 1989). Journal of Climate, 7, 949- 964.

Smith, T.M., Reynolds, R.W., Livezey, R.E., Stokes, D.C., 1996. Reconstruction of of historical sea surface temperatures using empirical orthogonal functions. Journal of Climate, 9, 1403- 1420.

Smith, T.M., Reynolds, R.W., 2002. Bias corrections for historic sea surface temperatures based on marine air temperatures. Journal of Climate, 15, 73- 87.

Smith, T.M., Reynolds, R.W., 2003. Extended reconstruction of global sea surface temperatures based on COADS data (1854- 1997). Journal of Climate, 16, 1495- 1510.

Smith, T.M., Reynolds, R.W., 2004. Improved extended reconstruction of SST (1854- 1997). Journal of Climate, 17, 2466- 2477.

Smith, T.M., Reynolds, R.W., 2005. A global merged land- air- sea surface temperature reconstruction based on historical observations (1880- 1997). Journal of Climate, 18, 2021- 2036.

Smith, T.M., Reynolds, R.W., Peterson, T.C., Lawrimore, J., 2008. Improvements to NOAA's Historical Merged Land- Ocean Surface Temperature Analysis (1880- 2006). Journal of Climate, 21, 2283- 2296.

Southward, A.J., Boalch, G. T., 1994. The effects of changing climate on marine life: Past events and future predictions, in: Man and the Maritime Environment, Exeter Mar. Stud., 9, 101- 143. University of Exeter Press, Exeter, U. K.

Strong, A.E., Kearns, E.J., Gjovig, K.K., 2000. Sea surface temperature signals from satellite- An update, Geophysical Research Letters, 27, 1667-1670.

Thomas, C.D., Cameron, A., Green, R.E., Bakkenes, M., Beaumont, L.J., Collingham, Y.C., Erasmus, E.F.N., de Siqueira, M.F., Grainger, A., Hannah, L., Hughes, L., Huntley, B., van Jaarsveld, A.S., Midgley, G.F., Miles, L., Ortega- Huerta, M.A., Townsend Peterson, A., Philips, O.L., Williams, S.E., 2004. Extinction risk from climate change. Nature, 427, 145- 148

Usabiaga, J.I., Sáenz-Aguirre, J., Valencia, V., Borja, A., 2004. Climate and Meteorology, variability and its influence on the Ocean. In: Borja,

A., Collins, M. (Eds.), Oceanography and Marine Environment of the Basque Country. Elsevier Oceanography Series nº 70, Elsevier, Amsterdam, 75-96.

Valencia, V., Borja, A., Fontán, A., Pérez, F.F., Ríos, A.F., 2003. Temperature and salinity fluctuations in the Basque Coast (SE Bay of Biscay) from 1986 to 2000 related to the climatic factors. ICES Marine Science, 219, 340-342.

Valencia, V., Franco, J., Borja, A., Fontán, A., 2004. Hydrography of the southeastern Bay of Biscay. In: Borja, A., Collins, M. (Eds.), Oceanography and Marine Environment of the Basque Country. Elsevier Oceanography Series nº 70, Elsevier, Amsterdam, 159-194.

Woodruff, S.D., Worley, S.J., Arnott, J.A., Diaz, H.F., Elms, J.D., Jackson, M., Lubker, S.J., Parker, D.E., 2003. COADS updates and the blend with the UK Met Office Marine Data Bank, in Advances in the Applications of Marine Climatology- The Dynamic part of the WMO Guide of the Applications of Marine Meteorology. WMO/TD- No. 1081 (JCOMM Technical Report Nº. 13), 3-10 (CD-ROM)

Worley, S.J., Woodruff, S.D., Reynolds, R.W. Lubker, S.J., Lott, N., 2005. ICOADS release 2.1 data and products. International Journal of Climatology, 25, 823- 842.

Young, E., Bigg, G.R., Grant, A., 1996. A statistical study of environmental influences on bivalve recruitment in the Wash, England. Marine Ecology Progress Series, 143, 121-129.

Conclusiones

Inicialmente se ha analizado la influencia de los eventos de afloramiento a lo largo de la costa oeste Cantábrica en diferentes escalas espacio- temporales. Por un lado, se ha caracterizado la frecuencia e intensidad de eventos de afloramiento desde 1967 hasta 2007 a partir de datos del transporte de Ekman y de la temperatura superficial del mar. Por otro lado, se ha analizado la dependencia de la temperatura del mar con las condiciones de afloramiento para un periodo continuo (Junio- Septiembre 2008) en la zona inter- mareal de la Ría do Barqueiro. De este estudio se han extraído las siguientes conclusiones:

1. El índice de afloramiento (UI) muestra un marcado ciclo anual con valores máximos (favorables al afloramiento) en Julio y Agosto y valores mínimos en Enero y Diciembre. Durante la estación de invierno los patrones de teleconexión EA/WR y EA explican mayoritariamente la variabilidad de UI mientras que durante la estación de verano, la variabilidad de UI se explica en términos del patrón EA. El patrón NAO también muestra alguna influencia en UI.
2. El número medio de días bajo condiciones favorables para el desarrollo de eventos de afloramiento de Junio a Septiembre es de entre 12 y 14 días por mes. La probabilidad de encontrar condiciones favorables es de ~ 17% cuando los eventos de afloramiento duran al menos 5 días consecutivos. Los datos de temperatura superficial del

mar también revelaron la presencia de agua fría cerca de costa asociada a vientos favorables al afloramiento.

3. El análisis de la relación entre la temperatura de del agua en la zona inter-mareal de la Ría do Barqueiro y el afloramiento de Junio a Septiembre de 2008 muestra que cuando UI era máximo la temperatura del agua del estuario disminuye unos días después. Ambas variables demostraron tener una correlación negativa con un valor máximo de -0.8 correspondiente a un desfase de 5 días entre el valor máximo de UI y la disminución de la temperatura en el estuario.

4. Finalmente, este estudio ha demostrado que se han observado eventos de afloramiento intensos y duraderos en la parte oeste de la plataforma continental Cantábrica aunque son menos comunes que a lo largo de la costa Atlántica. Este hecho produce unas condiciones favorables para el desarrollo dentro de estos estuarios de especies extranjeras invasoras que provienen de aguas más cálidas.

A continuación, se han caracterizado evidencias de eventos de afloramiento en la plataforma norte gallega en febrero de 2008 y sus implicaciones en los patrones biológicos y químicos de la columna de agua de las Rías Gallegas del Norte. También se ha analizado la recurrencia de esos eventos de afloramiento invernales en la costa norte gallega desde 1967 hasta 2007. De este estudio se han extraído las siguientes conclusiones:

1. La distribución de salinidad y temperatura de la columna de agua aflorada en la Ría do Barqueiro corresponde a agua sub-superficial de la plataforma. Este hecho contrasta con el tipo de agua que aflora

en los estuarios de la costa oeste gallega en invierno que es ENACW o IPC.

2. Las concentraciones de sales nutrientes y los niveles de nitratos no sufren variaciones durante el episodio de afloramiento invernal y son característicos de la mezcla invernal a través de la columna de agua.

3. La biomasa plantónica no mostró grandes cambios debido al evento de afloramiento, únicamente se observó que pequeños flagelados y ciliatos plantónicos duplicaron su abundancia. Además, los dinoflagelados aumentaron un orden de magnitud su presencia indicando la intrusión de agua de la plataforma en el estuario.

4. Finalmente, se ha demostrando que la posibilidad de observar eventos de afloramiento invernales en las Rías Norte Gallegas no es despreciable y no deben ser considerados como episodios aislados ya que el número de días por mes bajo condiciones favorables al afloramiento es de entre 8 y 19.

Posteriormente, se ha analizado la variabilidad inter- anual de la temperatura superficial del mar costera a lo largo de la parte continental del Arco Atlántico para el periodo 1985- 2005. De este análisis se pueden concluir los siguientes hechos:

1. Se ha observado una tendencia al calentamiento inhomogénea en la temperatura superficial del mar en la costa aumentando monótonamente desde la costa oeste de la Península Ibérica hasta la costa francesa.

2. Las diferencias en el calentamiento a lo largo de la costa refleja las tendencias observadas en el Atlántico Norte, las cuales se

caracterizan por un incremento norte- oeste de la temperatura superficial del mar.

3. El calentamiento es significativo durante la primavera y el verano, siguiendo un patrón macroscópico similar al calentamiento anual.

4. El calentamiento costero, aunque menor que el oceánico, tiene importantes implicaciones biológicas y económicas. Variaciones de la temperatura superficial del mar en la costa del orden de 1.2 a 3.5 ºC por siglo pueden alterar considerablemente los ciclos biológicos de especies como: mejillones, ostras, almejas… que son vitales para el desarrollo económico de la zona.

Finalmente, se ha analizado la importancia de la actual tendencia al calentamiento observada durante las últimas décadas en el Golfo de Vizcaya en el contexto de los diferentes ciclos de calentamiento- enfriamiento observados desde 1854.

De este estudio se han extraído las siguientes conclusiones:

1. El intenso periodo de calentamiento observado durante las últimas décadas muestra modulaciones estacionales y espaciales. Las velocidades de calentamiento son especialmente importantes en primavera y verano. Además se ha observado que son también más intensas en la parte noroeste del Golfo de Vizcaya y a lo largo de la costa francesa que en el área del Cantábrico.

2. Se han detectado dos ciclos de calentamiento- enfriamiento durante el periodo 1854- 2007: enfriamiento de 1867 a 1910 (-0.14ºC por década); calentamiento de 1910 a 1945 (0.17ºC por década); enfriamiento de 1945 a 1974 (-0.10ºC por década); y un calentamiento desde 1974 a 2007 (0.22ºC por década).

3. El actual periodo de calentamiento es del mismo orden de magnitud aunque ligeramente más intenso que el observado de 1910 a 1945, lo cual coincide con previos estudios llevado a cabo en el Atlántico Norte.

4. El calentamiento observado desde 1974 muestra un aumento en la amplitud térmica producido por las diferentes velocidades de calentamiento de los máximos (0.26ºC por década) y de los mínimos (0.20ºC por década) de la temperatura superficial del mar.